Title
Deciphering trophoblast identity, specification, and communication in the developing placenta

Author
Marsh, Bryan Patrick

Publication Date
2022

Peer reviewed|Thesis/dissertation

Deciphering trophoblast identity, specification, and communication in the developing placenta

by
Bryan Marsh

DISSERTATION
Submitted in partial satisfaction of the requirements for degree of
DOCTOR OF PHILOSOPHY

in

Developmental and Stem Cell Biology

in the

GRADUATE DIVISION
of the
UNIVERSITY OF CALIFORNIA, SAN FRANCISCO

Approved:

DocuSigned by:
Susan Fisher
3D7FD5EAA89E411...

Susan Fisher
Chair

DocuSigned by:
Alex Pollen
DocuSigned by:
Robert Blelloch
91DFF4C4A2FF4FC...

Alex Pollen

Robert Blelloch

Committee Members

For my parents, Susan and Barry

Acknowledgements

Many people require thanks for their generous support, guidance, and patience throughout my Ph.D. First, I thank my mentor Robert for his relentless and infectious optimism and excitement. His optimism was necessary throughout this process to present an apparent failure into a nascent opportunity, turn unhelpful pessimism into useful skepticism, and, for lack of better words, turn a frown upside down. He also demonstrated how to explore science broadly and provided the excitement and tools to perform interdisciplinary and rigorous science.

I thank my thesis committee Susan Fisher and Alex Pollen for the generous gift of their time, support, and expertise. They probed the foundations of my hypotheses and data, corrected my misconceptions, and elevated these studies tremendously.

I thank the current and former members of the Blelloch Lab for a fun and rigorous training environment. Lab meetings each week probably did the most to mold me as a scientist. I thank the senior graduate students when I joined the lab – Amy Chen, TJ Hu, and Jake Freimer – for contributing fun, philosophy, and technical knowledge in equal measure. I thank the postdocs in the lab – Brian DeVeale, Deniz Goekbuget, and Carolyn Sangokoya – for guidance, instruction, and plain talk when data/reasoning just didn't make sense. I thank Ryan Boileau for his scientific ideas, his jokes, and scientific ideas that were jokes, and for jokes that turned into halfway decent scientific ideas. Having someone in the lab with which to weather the graduate school was invaluable.

Our conversations did as much, if not more, to shape my science philosophies as any formal instruction.

I thank the members of the Fisher lab for accepting me as a part of the lab. I especially thank Yan Zhou who provided essential knowledge, guidance and enthusiasm throughout multiple projects. Without her technical skills, none of the human work would have been possible. I also thank Mirhan Kapidzic for his expertise, time, and effort in isolating many sets of trophoblast for me.

I thank the mentors who gave me early opportunities and prepared me so well for graduate school. I thank Professor Ann Burke for giving me my first opportunity to work in a lab, teaching me to run a mouse colony, and instilling a long-lasting interest in evolutionary and developmental biology. I thank Dr. Stan Artap for being a fantastic mentor, for teaching me all my technical skills, how to break down a paper, how to present, and how to advocate for myself. I truly would not be here without his teaching, time, and effort. Finally, I thank Professor Carla Kim for taking me into her lab despite knowing I would only be there for a short period of time and for providing an awesome and supportive lab environment from which to launch into graduate school.

I thank the former and current members of the UCSF DSCB/BMS programs for orientation, guidance, venting, and many Yosemite, ski, and bar trips.

I thank friends near and far – Matt, Nick, Jess, Matthew, Eliza, Anna, Ebb, Seth, Shims, Drew, Roth, Ruth – for their love and support, visits to SF, and for hosting me when I needed to get away.

Finally, I thank my parents for their constant love, support, and patience.

Contributions

The research that comprises this thesis was conducted under the supervision of Dr. Robert Blelloch at the University of California, San Francisco. This work was supported by the NIH P50 HD055764 and the Fletcher Jones Fellowship.

Chapter 2 describes work published in eLife in 2020 with the following authors: Bryan Marsh and Robert Blelloch. I performed all the experiments and analyzed the data. Robert Blelloch and I wrote the manuscript.

Chapter 3 describes work summarized in a preprint and posted on BioRxiv in 2022 with the following authors: Bryan Marsh, Yan Zhou, Mirhan Kapidzic, Susan Fisher, and Robert Blelloch. Yan Zhou and Mirhan Kapidzic collected the human placenta samples, performed tissue dissections, and isolated cells from the villous chorion and the smooth chorion. Yan Zhou assisted in the single cell RNA-seq profiling of all samples and immunofluorescence staining. I performed all other experiments. I analyzed the data with input from Yan Zhou, Susan Fisher, and Robert Blelloch. Robert Blelloch, Susan Fisher, and I wrote the manuscript.

I wrote this thesis with input from Robert Blelloch, Susan Fisher, and Alex Pollen.

Deciphering trophoblast identity, specification, and communication in the developing placenta

Bryan Marsh

Abstract

The placenta is the first organ to develop and establishes the essential connection between embryonic/fetal and maternal cells, protects the embryo/fetus, mediates exchange of all nutrients with maternal blood, and instructs its development. Often an afterthought to embryonic development, the molecular determinants of trophoblast identity and function remain incomplete. Here we use single cell RNA sequencing methods to profile distinct aspects of placental development in mouse and human.

The placenta is the interface between mother and embryo/fetus in all eutherian species. However, our understanding of this essential organ remains incomplete. A substantial challenge has been the syncytial cells of the placenta, which have made dissociation and independent evaluation of the different cell types of this organ difficult. In Chapter 2, we address questions concerning the ontogeny, specification, and function of the cell types of a representative hemochorial placenta by performing single nuclei RNA sequencing (snRNA-seq) at multiple stages of mouse embryonic development focusing on the exchange interface, the labyrinth. Timepoints extended from progenitor-driven expansion through terminal differentiation. Analysis by snRNA-seq identified transcript profiles and inferred functions, cell trajectories, signaling interactions, and transcriptional drivers of all but the most highly polyploid cell types of the placenta. These data profile placental

development at an unprecedented resolution, provide insights into differentiation and function across time, and provide a resource for future study.

The human placenta contains two specialized regions: the villous chorion where gases and nutrients are exchanged between maternal and fetal blood, and the smooth chorion which surrounds more than 70% of the developing fetus but whose cellular composition and function are poorly understood. In chapter 3, we use single cell RNA sequencing to compare the cell types and molecular programs between these two regions in the second trimester human placenta. Each region consists of progenitor cytotrophoblasts (CTBs) and extra-villous trophoblasts (EVTs) with similar gene expression programs. While CTBs in the villous chorion differentiate into syncytiotrophoblasts, they take an alternative trajectory in the smooth chorion producing a previously unknown CTB population, which we term smooth-chorion-specific CTBs (SC-CTBs). Marked by expression of region-specific cytokeratins, the SC-CTBs form a stratified epithelium above a basal layer of progenitor CTBs. They express epidermal and metabolic transcriptional programs consistent with a primary role in defense against physical stress and pathogens. Additionally, we show that SC-CTBs closely associate with EVTs and secrete factors that inhibit the migration of the EVTs. This restriction of EVT migration is in striking contrast to the villous region where EVTs migrate away from the chorion and invade deeply into the decidua. Together, these findings add an important new dimension to our understanding of CTB differentiation in these distinct regions of the human placenta. This knowledge has broad implications for studies of the development, functions, and diseases of the human placenta.

Together these studies further our understanding of lineage specification and trophoblast communication in placental development and all data are publicly available as a resource for future scientific inquiry.

Table of Contents

List of Figures

Chapter 1: Introduction

The placenta, the first organ to develop, is the necessary bridge between maternal and embryonic/fetal tissues (Turco and Moffett, 2019; Knöfler et al., 2019). This remarkable organ must develop shortly after conception to perform myriad functions for the embryo/fetus that will eventually be carried out by multiple organ systems in the adult. These functions include gas exchange (lung), nutrient exchange (intestine), filtration (liver), waste excretion (intestine/kidney), and hormone production (various endocrine organs)[Burton and Fowden, 2015]. The placenta is also incredibly dynamic over the course of gestation, performing distinct roles specific to developmental stages. These roles require the specification, maturation, and coordination of numerous cell types, which must be robust in identity but adaptable to developmental timing and environmental challenges. A foundational understanding of the placenta rooted in its cellular components is essential for a complete understanding of the organ's role during development and dysfunction during disease.

The placenta is a defining feature of, and specific to, eutherian mammals (Maltepe and Fisher, 2015; Wildman et al., 2006). The evolutionary history and anatomical organizations of the placenta among species paint a portrait of an organ that is highly mutable but always in service of the same goals – construct and maintain an environment for embryonic/fetal development, enable and facilitate maternal-fetal exchange, and protect from pathogenic, immunological, and physical insults. Over the last 140 million years, the eutherians have evolved rapidly resulting in four clades of placental mammals (Afrotheria, Xenartha, Laurasiatheria, Euarchontaglires), four

distinct placental gross morphologies (Diffuse, Cotyledonary, Zonary, Discoid), and at least four different organizations of the maternal-fetal exchange interface (Epitheliochorial, Synepitheliochorial, Endotheliochorial, Hemochorial)[Roberts et al., 2016; Wildman et al., 2006]. The structural variation among eutherian placentas is greater than that of any other organ and raises numerous exciting theoretical questions concerning the selective pressures on a short-lived organ, the influence of retroviral elements on gene expression, and convergent evolution (Griffith and Wagner, 2017; Chuong, 2013). This variation poses a challenge in a practical experimental sense concerning the applicability of knowledge from studies of the placenta in model organisms to the human organ. Several recent reviews have compared placental development in mouse and humans. They conclude that despite striking differences, data from the mouse provides an important perspective on human placental development (Hemberger et al., 2020; Woods et al., 2018). However, several aspects of human development remain poorly modeled in other species. Therefore, mouse and human represent important independent but complementary models for studying placental development.

This introduction will cover placental development in the mouse (the most common mammalian model organism), placental development in the human, and single cell RNA profiling technologies that have aided in the understanding of these organs at a molecular level.

Placental development in mouse

Placental development in the mouse begins at the blastocyst stage with trophectoderm specification from the inner cell mass, definitively and irreversibly separating the extraembryonic and embryonic lineages (Rossant and Tam, 2009; Maltepe et al., 2010). The trophectoderm gives rise to all extraembryonic lineages, including the placenta (Hemberger et al., 2020). Implantation of the blastocyst at E4.5 begins the process of decidualization of the maternal endometrial stroma cells, beginning the coordinated development of the maternal-fetal interface (Hemberger et al., 2020). By E5.5 the extraembryonic cells are specified into two lineages, the extraembryonic ectoderm and the ectoplacental cone (Rossant and Tam, 2009). Each lineage, which gives rise to spatially restricted and functionally distinct regions of the mature mouse placenta, contains highly specialized trophoblast populations (Maltepe and Fisher, 2015). The extraembryonic ectoderm is located proximal to the developing embryo and gives rise to the placental labyrinth, the expansive area for exchange of gases, nutrients and waste between the maternal blood and the fetal circulation (Simmons et al., 2008a; Ueno et al., 2013; Maltepe and Fisher, 2015).

The ectoplacental cone is located distal to the embryo and in close proximity to the decidua. The cells of this region give rise to the junctional zone, an exocrine region important for metabolism and hormone secretion, and invasive trophoblasts that remodel maternal arteries to allow maternal blood to contact the placenta (Woods et al., 2018; Simmons et al., 2007). The fusion of the allantois with the chorion at E8.5 triggers cascades of differentiation in each lineage (Watson and Cross, 2005). This fusion event

establishes the mature structure of the placenta. Thereafter, the mesoderm-derived fetal blood vessels of the allantois intercalate with the trophoblasts of the extraembryonic ectoderm leading to differentiation and expansion of the labyrinth from E9.5-E14.5 (Watson and Cross, 2005; Hemberger et al., 2020; Ueno et al., 2013), and subsequently, the maturation and expansion of the junctional zone ending at parturition between E18-21 (Simmons et al., 2007).

Development of the labyrinth

Development of the placental labyrinth requires tight coordination of trophoblast differentiation with the invasion and branching of the fetal vasculature (Watson and Cross, 2005). By E9.5, immediately after chorioallantoic fusion, multipotent labyrinth trophoblast progenitors (LaTPs) can be identified in the nascent labyrinth. LaTPs are marked by elevated expression of Epcam and are localized to the basal chorionic plate and in clusters throughout the developing labyrinth. LaTPs are present and proliferating at E9.5-10.5, before decreasing in number by E12.5 and ceasing to exist by E14.5 (Ueno et al., 2013). This timeline correlates with the development, expansion, and maturation of the labyrinth. Clonal analysis using fluorescent reporters established that LaTPs contribute to the three terminally differentiated lineages of the labyrinth—Syncytiotrophoblast layer I (SynTI), Syncytiotrophoblast layer II (SynTII), and sinusoidal trophoblast giant cells (S-TGC)[Ueno et al., 2013]. While LaTP are accepted as the sole progenitor cells of the labyrinth, the factors required for their specification remain unknown. Hgf/c-Met signaling is required for LaTP proliferation and also for expression of Gcm1, a transcription factor required for labyrinth formation (Ueno et al., 2013;

Anson-Cartwright et al., 2000). Clusters of Gcm1 positive cells initiate branching morphogenesis of the labyrinth at E8.5 and are strong candidates for LaTP precursors, though this has not been proven (Anson-Cartwright et al., 2000; Simmons and Cross, 2005). Genetic deletion of *Gcm1* reduces the proliferation rate and total number of LaTP but does not block specification (Ueno et al., 2013). This suggests that *Gcm1* is important for LaTP function but is not required for LaTP specification. The spatiotemporal dynamics of LaTP specification, especially with respect to chorioallantoic fusion, remains an exciting and open area of investigation.

The trophoblast component of the maternal-fetal exchange interface in the mouse placenta is a trilaminar structure comprised of each of the lineages derived from LaTP—SynTIs, SynTIIs, and S-TGCs (Simmons and Cross, 2005; Simmons et al., 2008a). S-TGCs reside in the maternal blood space, farthest from the fetal vasculature. Termed ‘giant cells’ because of their increased ploidy, these large cells line the maternal blood sinuses with long perforated projections, which allow maternal blood to pass through and contact the trophoblasts beneath (Coan et al., 2005). S-TGCs are an important source of placental lactogens, which suggests a primary role as the endocrine cells of the labyrinth. S-TGC uniquely express *Ctsq* from E11.5 onward, but no earlier unique markers have been identified. Thus, little is known about the specification and maturation of these cells (Simmons et al., 2007).

Beneath the S-TGC is the SynTI layer. As the name suggests, SynTI are multinucleate syncytial cells that form through repeated cellular fusion events. SynTI contact maternal

blood and comprise the outermost continuous trophoblast layer of the labyrinth (Woods et al., 2018). Because numerous vesicular proteins, transporters, and receptors such as CD71 are localized to their apical surfaces, SynTI is considered to be important for uptake from maternal blood (Ueno et al., 2013, Simmons et al., 2008a).

Beneath the SynTI layer is SynTII, another multinucleate syncytial layer. An important distinction between the two syncytial layers is that SynTII does not contact maternal blood and instead is opposed to the fetal vasculature, separated only by a shared basal lamina (Cross, 2000; Simmons et al., 2008a). Together, SynTI and SynTII facilitate uptake from maternal blood and export to fetal circulation, respectively. In contrast to S-TGC and SynTI, much is known about the specification of SynTII from trophoblast progenitors. *Gcm1* is required for formation of this syncytium *in vivo* and is highly expressed in mature SynTII (Anson-Cartwright et al., 2000; Ueno et al., 2013). Additionally, SynTII have been derived *in vitro*, with specification relying on canonical Wnt signaling (Zhu et al., 2017). While the spatial orientation and basic functions of each layer are known, a detailed understanding of the molecular determinants of the specification of each lineage from LaTPs remains lacking.

Development of the junctional zone

The cells of the ectoplacental cone give rise to the junctional zone, which occupies the interstitial space between the labyrinth and the decidua (Woods et al., 2018; Simmons et al., 2007). The junctional zone contains several specialized cell types, including spongiotrophoblasts (SpTs), glycogen trophoblasts (GCs), and several subtypes of

trophoblast giant cells (TGCs)[Simmons and Cross, 2005]. Each of these cell types has exocrine functions and is located near the maternal blood sinus enabling secretion directly into maternal circulation (Adamson et al., 2002). Lineage tracing alone, and in combination with scRNA-seq, demonstrate a common progenitor, derived from the ectoplacental cone and marked by *Prdm1*, for the three cell types (Mould et al., 2012; Nelson et al., 2016). However, the factors required for establishment of this progenitor remain elusive as data from mouse mutants is complex and our knowledge of potential regulators is incomplete (Simmons et al., 2005).

The SpT layer is located directly above the labyrinth and secretes antiangiogenic factors, including Flt1 and Plfr (Cross et al., 2002). This layer is in direct contact with the TGCs that overlie the SpT and secrete angiogenic factors (Proliferin), vasodilators (Adrenomedullin), and anticoagulants (Thrombomodulin) to promote the remodeling of maternal arteries and the flow of maternal blood to the labyrinth below (Lee et al., 1988; Yotsumoto et al., 1988; Weiler-Guettler et al., 1996). These opposing signals may establish a barrier against the expansion of the maternal endothelium into the SpT and labyrinth regions (Cross et al., 2002). TGCs are a heterogenous group of cells that are all highly polyploid and mononuclear. TGCs are endocrine cells and are the largest producer of placental hormones, including the prolactins, a family that has undergone repeated genomic expansion in the mouse (Simmons et al., 2007; Wiemers et al., 2003). Several subtypes of TGC have been defined, including parietal TGC – that overlie the SpT – and spiral artery TGCs – that invade into the decidua and remodel the maternal arteries. The molecular markers and determinants of TGC sub-specification

remain unclear, but combinatorial expression of the prolactin genes can be used to identify certain subpopulations (Simmons et al., 2007; Simmons et al., 2008b). The third cell type in the junctional zone is the glycogen trophoblast, which first appears interspersed in the SpT layer at approximately E12.5 (Simmons et al., 2005). The name derives from the glycogen-rich deposits in their cytoplasm and they are uniquely marked by *Pcdh12* expression (Rampon et al., 2005; Bouillot et al., 2006). However, few additional markers or molecular determinants of this lineage have been identified. In sum, the junctional zone represents a complex structure whose development, components, functions, and interactions must still be elucidated.

Morphological studies and genetic evidence from mouse mutants have generated a detailed description of the developmental milestones, cellular components, and key regulators of murine placenta development. However, a molecular accounting of the determinants of cell fate and function does not yet exist.

Placental development in humans

Placental development in human, as in mouse, begins with the separation of trophectoderm and inner cell mass at the blastocyst stage (Hemberger et al., 2020; Turco and Moffett, 2019). After implantation, human placenta development proceeds rapidly as trophectoderm-derived primary syncytiotrophoblast (STBs; multinucleate cells) and diploid cytotrophoblasts (CTBs) form a shell surrounding the developing embryo. The placental villi – the functional units for gas, nutrient, and waste exchange – are established within the first 2-3 weeks of gestation (Knöfler et al., 2019; Turco and

Moffett, 2019). The villi are formed by CTB invasion into the primary syncytial layer and followed by the migration of stromal and endothelial cells (Knöfler et al., 2019; Hemberger et al., 2020). The result is a stromal core that houses and supports the fetal vessels, covered by a CTB monolayer and an outer STB layer. To maximize surface area, the villi undergo extensive branching morphogenesis and arborization (Knöfler et al., 2019). The tips of villi in contact with the decidual stroma invade into the decidua and form permanent structures called anchoring villi (Turco and Moffett, 2019; Maltepe and Fisher, 2015). Upon migrating out from the anchoring villi, CTBs differentiate into extravillous trophoblasts (EVTs) that invade deeply into the decidua, home to the maternal arteries, and remodel them allowing blood to flow to the underlying villi (Maltepe and Fisher, 2015; Knöfler et al., 2019). This forms the mature structure of the villous placenta, also known as the villous chorion (VC).

At approximately 6-7 weeks of gestation, the villi opposite the site of implantation begin to degenerate (Knöfler et al., 2019; Hamilton and Boyd, 1960; Benirschke et al., 2006). This process spreads radially, restricting villi to the mature discoid organization of the human placenta (Knöfler et al., 2019). The causes of degeneration are not well understood. The most parsimonious explanation is mechanical. The ballooning of the amnion separates the overlying villi from the decidua and maternal blood supply, which triggers atrophy. While degeneration eliminates the arborized villi (SCTs and a vascularized stroma), an epithelial-like cytotrophoblast layer atop a connective tissue layer persists until parturition. The term smooth chorion (SC) denotes the absence of villi (Benirschke et al., 2006; Genbacev et al., 2015). Although EVTs are found in the

SC, they fail to invade the adjacent decidua (Genbacev et al., 2015; Garrido-Gomez et al., 2017; Pique-Regi et al., 2017). The distinct morphological and cellular composition of the SC and the VC suggests these two regions have different functions. While considered vestigial, lacking the STBs and vascularization and villous organization required for nutrient transfer, the SC makes up more than 70% of the extraembryonic surface area surrounding the developing embryo/fetus (Benirschke et al., 2006). As gestation proceeds, the fetus grows and forces the amnion, associated fetal stroma, SC, and decidual stroma into contact, leading to fusion of these layers (Genbacev et al., 2015; Boyd and Hamilton, 1967). Therefore, the human placenta becomes separated into two regionally distinct regions by mid-second trimester.

The ontogeny, differentiation trajectories, and relationships between the mature lineages of the VC trophoblast – CTBs, STBs, and EVTs – have been studied and reviewed extensively (Hemberger et al., 2020; Knöfler et al., 2019; Turco and Moffett et al., 2019). CTBs, often termed villous CTBs, function as a multipotent progenitor for all trophoblast lineages in the developing VC (Knöfler et al., 2019; Okae et al., 2018). In the villi, CTBs self-renew to maintain a monolayer separating the stromal villous core and the overlaying STB. At seemingly sporadic spatial intervals CTBs differentiate and fuse with the STB layer (Knöfler et al., 2019). Differentiation to STB requires cell cycle exit, as P21 and GCM1 complex to drive transcription of endogenous retroviral genes that mediate membrane fusion (Lu et al., 2017). STB can also be generated *in vitro*, with canonical WNT signaling and elevation of cAMP being essential for this process (Okae et al., 2018; Haider et al., 2018). Further maturation then occurs as STB function

as the main source of fetal derived hormones, including CGA and CSH1 (Liu et al., 2018; Maltepe et al., 2010). STB are the conduit for nutrient uptake from maternal blood and to which they return spent materials (Maltepe and Fisher, 2015). As such, STB are highly polarized, with an apical surface covered with microvilli and optimized for both diffusion and active transport (Burton and Fowden, 2015). CTBs at the tips of anchoring villi do not differentiate to STB and instead migrate outward into the decidua through the cell column, which connects the villi and the uterus. During this migration, CTBs in the cell column undergo a final mitotic cycle and differentiate into EVTs (Genbacev et al., 1997; Knöfler et al., 2019). This process entails a dramatic remodeling of adhesion, immune and vascular molecules, which, necessary for EVT migration into maternal tissue and blood vessels. For example, CTBs in the cell column switch numerous integrin heterodimers (e.g., ITGA5 to ITGA1) and vasculogenic/angiogenic molecules (e.g., VEGF family members) and upregulate various matrix metalloproteinases (e.g., MMP9) and immunomodulatory factors such (e.g., HLA-G) (Fisher et al., 1989; Kovats et al., 1990; Zhou et al., 1997; Genbacev et al., 1997; McMaster et al., 1995; Knöfler et al., 2019).

It is accepted that the SC and VC contain similar CTB populations (Benirschke et al., 2006; Pique-Regi et al., 2019; Genbacev et al., 2015). Immunolocalization demonstrates the expression of CTB markers (KRT7) and EVTs stage-specific antigens (HLA-G and ITGA4) in both locations (Genbacev et al., 2015; Garrido-Gomez et al., 2017). Single cell RNA-sequencing of tissue samples, including the SC, identifies EVTs isolated from this region as clustering with EVT isolated from the VC. Because this

analysis did not identify CTBs in the SC, the similarities between CTBs across regions could not be addressed (Pique-Regi et al., 2019). Similarity between EVTs from the VC and SC has been described previously, but remains in contrast with the divergent behavior of these cells (Genbacev et al., 2015). Unlike their counterparts in the VC, EVTs in the SC do not invade deeply into the decidua or remodel maternal arteries (Genbacev et al., 2015; Garrido-Gomez et al., 2017). However, whether SC-derived EVT lack inherent invasive capacity and if this capacity changes over time or as a result of disease is unclear (Genbacev et al., 2015; Garrido-Gomez et al., 2017). Therefore, unanswered questions about SC-CTBs concern their role as EVT progenitors and whether invasion is under autocrine or paracrine control.

Despite the paucity of molecular markers distinguishing SC from VC trophoblasts or identifying SC trophoblast subtypes, several morphological studies provide insight into cellular heterogeneity and potential functions of SC-CTBs. Yeh et al., identify two distinct populations defined as vacuolar and eosinophilic (Yeh et al., 1989). An additional study notes variability in SC-CTBs morphology, including their nuclei and organelles (Bou-Resli et al., 1981). It has been hypothesized that the cells of the SC are in varying stages of degeneration. However, three pieces of evidence contradict this theory (Benirschke et al., 2006). First, strong staining for alkaline phosphatase shows that SC-CTBs are metabolically active (Yeh et al., 1989). Second, these cells incorporate tritiated thymidine, which shows they are replicating and dividing (Benirscke et al., 2006). Finally, SC-CTBs are connected by gap junctions, which allow passage of ions, signaling molecules, and metabolites between cells (Bartels and Wang, 1983).

Taken together, these results suggest a level of activity, growth, and coordination that is not characteristic of a degenerating tissue.

Single cell profiling methodologies

Single cell RNA-sequencing (scRNA-seq) has become an important and commonplace technique for profiling mRNA expression of organs, tissues, or systems, which are made up of heterogeneous collections of cells. Cataloguing and quantifying the transcripts in each cell enables identification of broad types, estimation of their proportions, and generation of hypotheses about their functions at scale (Kharchenko, 2021). Improvements in the throughput of scRNA-seq allow for the profiling of large numbers of cells, permitting the robust identification of rare populations and/or the capture of all cells in an organ or organism (Stuart and Satija, 2019).

The ability to perform unbiased profiling of large numbers of cells has motivated three common types of scRNA-seq experiments. The first is broad surveys of cell types in a particular environment. Generally termed ‘atlases’, these experiments begin with the premise of identifying and characterizing the cell types in a particular system and inferring their behavior. Chapter 2 of this thesis is an example of this type of experiment. We determined the transcriptional features of hard to isolate cell types in the mouse placental labyrinth. The second category is comparative studies that use scRNA-seq to identify differences between two conditions such as wildtype vs. mutant, healthy vs disease, or – as exemplified in Chapter 3 of this thesis – the differences between CTBs in two spatially distinct regions of the human placenta. The third type is the use of

scRNA-seq in combination with molecular perturbations or recording systems. Examples include scRNA-seq in combination with CRISPR perturbations, lineage recorders, and other high throughput single cell genomic measurements (Dixit et al., 2016; Datlinger et al., 2017; Wagner et al., 2018; Chan et al., 2019). At the time of writing, no examples of this type of experiment have been published in the placenta. Future applications of this experimental framework in placental research are discussed in Chapter 4.

Premise of these studies

At the outset of the experiments presented in this thesis, only one publication had applied scRNA-seq to the mouse placenta (Nelson et al., 2016) and only two had used the technique to profile the human placenta (Pavlicev et al., 2017; Tsang et al., 2017). Inspired by the recent profiling of nuclei instead of whole cells (Grindberg et al., 2013; Lacar et al., 2016; Habib et al., 2017), in Chapter 2 we describe experiments in which we applied single nuclei RNA-sequencing (snRNA-seq) to address outstanding questions about the ontogeny and differentiation of the mouse labyrinth. Building on previous work implicating changes the human SC coordinated with severe pre-eclampsia (Garrido-Gomez et al., 2017), in work summarized in Chapter 3 we sought to establish a baseline for the cellular composition, molecular identities, and developmental trajectories of the SC trophoblasts in the context of their VC counterparts. Both studies provide public resources for generating hypotheses. They will also be valuable for comparing new datasets, including the molecular changes

associated with placental pathologies that are the result of genetic alterations in mice or associated with pregnancy diseases in humans.

References

Adamson, S. L., Lu, Y., Whiteley, K. J., Holmyard, D., Hemberger, M., Pfarrer, C., & Cross, J. C. (2002). Interactions between trophoblast cells and the maternal and fetal circulation in the mouse placenta. *Developmental Biology*. https://doi.org/10.1016/S0012-1606(02)90773-6

Anson-Cartwright, L., Dawson, K., Holmyard, D., Fisher, S. J., Lazzarini, R. A., & Cross, J. C. (2000). The glial cells missing-1 protein is essential for branching morphogenesis in the chorioallantoic placenta. *Nature Genetics*. https://doi.org/10.1038/77076

Bartles, H., & Wang, T. (1983). Intercellular Junctions in the Human Fetal Membranes. *Anatomy and Embryology*, 103–120.

Benirschke, K., Kaufmann, P., & Baergen, R. (2006). Pathology of the Human Placenta. In *Pathology* (Vol. 38, Issue 2). https://doi.org/10.1016/s0031-3025(16)39684-2

Bou-Resli, M. N., Al-Zaid, N. S., & Ibrahim, M. E. A. (1981). Full-term and prematurely ruptured fetal membranes. In *Cell and Tissue Research* (Vol. 220, Issue 2). https://doi.org/10.1007/bf00210508

Bouillot, S., Rampon, C., Tillet, E., & Huber, P. (2006). Tracing the Glycogen Cells with Protocadherin 12 During Mouse Placenta Development. *Placenta*, *27*(8), 882–888. https://doi.org/10.1016/j.placenta.2005.09.009

Boyd, J. D., & Hamilton, W. J. (1967). Development and Structure of the Human Placenta From the End of the 3Rd Month of Gestation. *BJOG: An International Journal of Obstetrics & Gynaecology*, *74*(2), 161–226. https://doi.org/10.1111/j.1471-0528.1967.tb14864.x

Boyd, J. D., & Hamilton, W. J. (1967). Development and Structure of the Human Placenta From the End of the 3Rd Month of Gestation. *BJOG: An International Journal of Obstetrics & Gynaecology*, *74*(2), 161–226. https://doi.org/10.1111/j.1471-0528.1967.tb14864.x

Burton, G. J., & Fowden, A. L. (2015). The placenta: A multifaceted, transient organ. *Philosophical Transactions of the Royal Society B: Biological Sciences*, *370*(1663). https://doi.org/10.1098/rstb.2014.0066

Chan, M. M., Smith, Z. D., Grosswendt, S., Kretzmer, H., Norman, T. M., Adamson, B., Jost, M., Quinn, J. J., Yang, D., Jones, M. G., Khodaverdian, A., Yosef, N., Meissner, A., & Weissman, J. S. (2019). Molecular recording of mammalian embryogenesis. *Nature*, *570*(7759), 77–82. https://doi.org/10.1038/s41586-019-1184-5

Chuong, E. B. (2013). Retroviruses facilitate the rapid evolution of the mammalian placenta. *BioEssays : News and Reviews in Molecular, Cellular and Developmental Biology*, *35*(10), 853–861. https://doi.org/10.1002/bies.201300059

Coan, P. M., Ferguson-Smith, A. C., & Burton, G. J. (2005). Ultrastructural changes in the interhaemal membrane and junctional zone of the murine choriollantoic

placenta across gestation. *Journal of Anatomy*, *207*(6), 783–796. https://doi.org/10.1111/j.1469-7580.2005.00488.x

Cross, J. C., Hemberger, M., Lu, Y., Nozaki, T., Whiteley, K., Masutani, M., & Adamson, S. L. (2002). Trophoblast functions, angiogenesis and remodeling of the maternal vasculature in the placenta. *Molecular and Cellular Endocrinology*, *187*(1–2), 207–212. https://doi.org/10.1016/S0303-7207(01)00703-1

Cross, J. C. (2000). Genetic insights into trophoblast differentiation and placental morphogenesis. *Seminars in Cell & Developmental Biology*, *11*(2), 105–113. https://doi.org/10.1006/SCDB.2000.0156

Datlinger, P., Rendeiro, A. F., Schmidl, C., Krausgruber, T., Traxler, P., Klughammer, J., Schuster, L. C., Kuchler, A., Alpar, D., & Bock, C. (2017). Pooled CRISPR screening with single-cell transcriptome readout. *Nature Methods*, *14*(3), 297–301. https://doi.org/10.1038/nmeth.4177

Dixit, A., Parnas, O., Li, B., Chen, J., Fulco, C. P., Jerby-Arnon, L., Marjanovic, N. D., Dionne, D., Burks, T., Raychowdhury, R., Adamson, B., Norman, T. M., Lander, E. S., Weissman, J. S., Friedman, N., & Regev, A. (2016). Perturb-Seq: Dissecting Molecular Circuits with Scalable Single-Cell RNA Profiling of Pooled Genetic Screens. *Cell*, *167*(7), 1853-1866.e17. https://doi.org/10.1016/j.cell.2016.11.038

Fisher, S. J., Cui, T., Zhang, L., Hartman, L., Grahl, K., Guo-Yang, Z., Tarpey, J., & Damsky, C. H. (1989). Adhesive and degradative properties of human placental

cytotrophoblast cells in vitro. *Journal of Cell Biology*, *109*(2), 891–902. https://doi.org/10.1083/jcb.109.2.891

Genbacev, O., Zhou, Y., Ludlow, J. W., & Fisher, S. J. (1997). Regulation of human placental development by oxygen tension. *Science*, *277*(5332), 1669–1672. https://doi.org/10.1126/science.277.5332.1669

Genbacev, O., Zhou, Y., Ludlow, J. W., & Fisher, S. J. (1997). Regulation of human placental development by oxygen tension. *Science*, *277*(5332), 1669–1672. https://doi.org/10.1126/science.277.5332.1669

Griffith, O. W., & Wagner, G. P. (2017). The placenta as a model for understanding the origin and evolution of vertebrate organs. *Nature Ecology and Evolution*, *1*(4), 1–10. https://doi.org/10.1038/s41559-017-0072

Grindberg, R. V., Yee-Greenbaum, J. L., McConnell, M. J., Novotny, M., O'Shaughnessy, A. L., Lambert, G. M., Araúzo-Bravo, M. J., Lee, J., Fishman, M., Robbins, G. E., Lin, X., Venepally, P., Badger, J. H., Galbraith, D. W., Gage, F. H., & Lasken, R. S. (2013). RNA-sequencing from single nuclei. *Proceedings of the National Academy of Sciences of the United States of America*, *110*(49), 19802–19807. https://doi.org/10.1073/pnas.1319700110

Habib, N., Avraham-Davidi, I., Basu, A., Burks, T., Shekhar, K., Hofree, M., Choudhury, S. R., Aguet, F., Gelfand, E., Ardlie, K., Weitz, D. A., Rozenblatt-Rosen, O., Zhang, F., & Regev, A. (2017). Massively parallel single-nucleus RNA-seq with DroNc-seq. *Nature Methods*. https://doi.org/10.1038/nmeth.4407

Haider, S., Meinhardt, G., Saleh, L., Kunihs, V., Gamperl, M., Kaindl, U., Ellinger, A., Burkard, T. R., Fiala, C., Pollheimer, J., Mendjan, S., Latos, P. A., & Knöfler, M. (2018). Self-Renewing Trophoblast Organoids Recapitulate the Developmental Program of the Early Human Placenta. *Stem Cell Reports*, *11*(2), 537–551. https://doi.org/10.1016/j.stemcr.2018.07.004

Haider, S., Meinhardt, G., Saleh, L., Kunihs, V., Gamperl, M., Kaindl, U., Ellinger, A., Burkard, T. R., Fiala, C., Pollheimer, J., Mendjan, S., Latos, P. A., & Knöfler, M. (2018). Self-Renewing Trophoblast Organoids Recapitulate the Developmental Program of the Early Human Placenta. *Stem Cell Reports*, *11*(2), 537–551. https://doi.org/10.1016/j.stemcr.2018.07.004

Hemberger, M., Hanna, C. W., & Dean, W. (2020). Mechanisms of early placental development in mouse and humans. *Nature Reviews Genetics*, *21*(1), 27–43. https://doi.org/10.1038/s41576-019-0169-4

Kharchenko, P. V. (2021). The triumphs and limitations of computational methods for scRNA-seq. *Nature Methods*, *18*(7), 723–732. https://doi.org/10.1038/s41592-021-01171-x

Knöfler, M., Haider, S., Saleh, L., Pollheimer, J., Gamage, T. K. J. B., & James, J. (2019). Human placenta and trophoblast development: key molecular mechanisms and model systems. In *Cellular and Molecular Life Sciences*. https://doi.org/10.1007/s00018-019-03104-6

Kovats, S., Main, E. K., Librach, C., Stubblebine, M., Susan, J., Demars, R., Wang, J., Res, O., Kovats, S., Main, E. K., Librach, C., Stubblebine, M., Fisher, S. J., & Demars, R. (1990). A Class I Antigen , HLA-G , Expressed in Human Trophoblasts Published by : American Association for the Advancement of Science Stable URL : http://www.jstor.org/stable/2873939 A Class I Antigen , HLA-G , Expressed in Human Trophoblasts. *Science*, *248*(4952), 220–223.

Lacar, B., Linker, S. B., Jaeger, B. N., Krishnaswami, S., Barron, J., Kelder, M., Parylak, S., Paquola, A., Venepally, P., Novotny, M., O'Connor, C., Fitzpatrick, C., Erwin, J., Hsu, J. Y., Husband, D., McConnell, M. J., Lasken, R., & Gage, F. H. (2016). Nuclear RNA-seq of single neurons reveals molecular signatures of activation. *Nature Communications*, *7*. https://doi.org/10.1038/ncomms11022

Lee, S. J., Talamantes, F., Wilder, E., Linzer, D. I. H., & Nathans, D. (1988). Trophoblastic giant cells of the mouse placenta as the site of proliferin synthesis. *Endocrinology*, *122*(5), 1761–1768. https://doi.org/10.1210/endo-122-5-1761

Liu, Y., Fan, X., Wang, R., Lu, X., Dang, Y. L., Wang, H., Lin, H. Y., Zhu, C., Ge, H., Cross, J. C., & Wang, H. (2018). Single-cell RNA-seq reveals the diversity of trophoblast subtypes and patterns of differentiation in the human placenta. *Cell Research*. https://doi.org/10.1038/s41422-018-0066-y

Lu, X., Wang, R., Zhu, C., Wang, H., Lin, H. Y., Gu, Y., Cross, J. C., & Wang, H. (2017). Fine-Tuned and Cell-Cycle-Restricted Expression of Fusogenic Protein Syncytin-2

Maintains Functional Placental Syncytia. *Cell Reports*, *21*(5), 1150–1159. https://doi.org/10.1016/j.celrep.2017.10.019

Maltepe, E., Bakardjiev, A. I., & Fisher, S. J. (2010). The placenta: Transcriptional, epigenetic, and physiological integration during development. *Journal of Clinical Investigation*, *120*(4), 1016–1025. https://doi.org/10.1172/JCI41211

Maltepe, E., & Fisher, S. J. (2015). Placenta: The Forgotten Organ. *Annual Review of Cell and Developmental Biology*. https://doi.org/10.1146/annurev-cellbio-100814-125620

Mould, A., Morgan, M. A. J., Li, L., Bikoff, E. K., & Robertson, E. J. (2012). Blimp1/Prdm1 governs terminal differentiation of endovascular trophoblast giant cells and defines multipotent progenitors in the developing placenta. *Genes and Development*, *26*(18), 2063–2074. https://doi.org/10.1101/gad.199828.112

Nelson, A. C., Mould, A. W., Bikoff, E. K., & Robertson, E. J. (2016). Single-cell RNA-seq reveals cell type-specific transcriptional signatures at the maternal–foetal interface during pregnancy. *Nature Communications*. https://doi.org/10.1038/ncomms11414

Nelson, A. C., Mould, A. W., Bikoff, E. K., & Robertson, E. J. (2016). Single-cell RNA-seq reveals cell type-specific transcriptional signatures at the maternal-foetal interface during pregnancy. *Nature Communications*, *7*. https://doi.org/10.1038/ncomms11414

Pavličev, M., Wagner, G. P., Chavan, A. R., Owens, K., Maziarz, J., Dunn-Fletcher, C., Kallapur, S. G., Muglia, L., & Jones, H. (2017). Single-cell transcriptomics of the human placenta: Inferring the cell communication network of the maternal-fetal interface. *Genome Research*, *27*(3), 349–361. https://doi.org/10.1101/gr.207597.116

Rampon, C., Prandini, M. H., Bouillot, S., Pointu, H., Tillet, E., Frank, R., Vernet, M., & Huber, P. (2005). Protocadherin 12 (VE-cadherin 2) is expressed in endothelial, trophoblast, and mesangial cells. *Experimental Cell Research*. https://doi.org/10.1016/j.yexcr.2004.08.024

Roberts, R. M., Green, J. A., & Schulz, L. C. (2016). The evolution of the placenta. *Reproduction (Cambridge, England)*, *152*(5), R179-89. https://doi.org/10.1530/REP-16-0325

Rossant, J., & Tam, P. P. L. (2009). Blastocyst lineage formation, early embryonic asymmetries and axis patterning in the mouse. *Development*, *136*(5), 701–713. https://doi.org/10.1242/dev.017178

Simmons, D. G., & Cross, J. C. (2005). Determinants of trophoblast lineage and cell subtype specification in the mouse placenta. *Developmental Biology*, *284*(1), 12–24. https://doi.org/10.1016/j.ydbio.2005.05.010

Simmons, D. G., Fortier, A. L., & Cross, J. C. (2007). Diverse subtypes and developmental origins of trophoblast giant cells in the mouse placenta.

Developmental Biology, *304*(2), 567–578. https://doi.org/10.1016/J.YDBIO.2007.01.009

Simmons, D. G., Natale, D. R. C., Begay, V., Hughes, M., Leutz, A., & Cross, J. C. (2008). Early patterning of the chorion leads to the trilaminar trophoblast cell structure in the placental labyrinth. *Development*. https://doi.org/10.1242/dev.020099

Simmons, D. G., Rawn, S., Davies, A., Hughes, M., & Cross, J. C. (2008). Spatial and temporal expression of the 23 murine Prolactin/Placental Lactogen-related genes is not associated with their position in the locus. *BMC Genomics*. https://doi.org/10.1186/1471-2164-9-352

Stuart, T., & Satija, R. (2019). Integrative single-cell analysis. *Nature Reviews Genetics*, *20*(5), 257–272. https://doi.org/10.1038/s41576-019-0093-7

Tsang, J. C. H., Vong, J. S. L., Ji, L., Poon, L. C. Y., Jiang, P., Lui, K. O., Ni, Y. B., To, K. F., Cheng, Y. K. Y., Chiu, R. W. K., & Lo, Y. M. D. (2017). Integrative single-cell and cell-free plasma RNA transcriptomics elucidates placental cellular dynamics. *Proceedings of the National Academy of Sciences of the United States of America*, *114*(37), E7786–E7795. https://doi.org/10.1073/pnas.1710470114

Turco, M. Y., & Moffett, A. (2019). Development of the human placenta. *Development (Cambridge)*, *146*(22), 1–14. https://doi.org/10.1242/dev.163428

Ueno, M., Lee, L. K., Chhabra, A., Kim, Y. J., Sasidharan, R., VanHandel, B., Wang, Y., Kamata, M., Kamran, P., Sereti, K. I., Ardehali, R., Jiang, M., & Mikkola, H. K. A. (2013). C-Met-Dependent Multipotent Labyrinth Trophoblast Progenitors Establish Placental Exchange Interface. *Developmental Cell*, *27*(4), 373–386. https://doi.org/10.1016/j.devcel.2013.10.019

Wagner, D. E., Weinreb, C., Collins, Z. M., Briggs, J. A., Megason, S. G., & Klein, A. M. (2018). Single-cell mapping of gene expression landscapes and lineage in the zebrafish embryo. *Science*, *360*(6392), 981–987. https://doi.org/10.1126/science.aar4362

Watson, E. D., & Cross, J. C. (2005). Development of structures and transport functions in the mouse placenta. *Physiology*, *20*(3), 180–193. https://doi.org/10.1152/physiol.00001.2005

Weiler-Guettler, H., Aird, W. C., Rayburn, H., Husain, M., & Rosenberg, R. D. (1996). Developmentally regulated gene expression of thrombomodulin in postimplantation mouse embryos. *Development*, *122*(7), 2271–2281. https://doi.org/10.1242/dev.122.7.2271

Wiemers, D. O., Shao, L. J., Ain, R., Dai, G., & Soares, M. J. (2003). The mouse prolactin gene family locus. *Endocrinology*, *144*(1), 313–325. https://doi.org/10.1210/en.2002-220724

Wildman, D. E., Chen, C., Erez, O., Grossman, L. I., Goodman, M., & Romero, R. (2006). Evolution of the mammalian placenta revealed by phylogenetic analysis.

Proceedings of the National Academy of Sciences of the United States of America, *103*(9), 3203–3208. https://doi.org/10.1073/pnas.68.4.866

Woods, L., Perez-Garcia, V., & Hemberger, M. (2018). Regulation of Placental Development and Its Impact on Fetal Growth—New Insights From Mouse Models. *Frontiers in Endocrinology*. https://doi.org/10.3389/fendo.2018.00570

Yeh, I. T., O'Connor, D. M., & Kurman, R. J. (1989). Vacuolated Cytotrophoblast: A subpopulation of trophoblast in the chorion laeve. *Placenta*, *10*(5), 429–438. https://doi.org/10.1016/0143-4004(89)90053-2

Yotsumoto, S., Shimada, T., Cui, C. Y., Nakashima, H., Fujiwara, H., & Ko, M. S. H. (1998). Expression of adrenomedullin, a hypotensive peptide, in the trophoblast giant cells at the embryo implantation site in mouse. *Developmental Biology*, *203*(2), 264–275. https://doi.org/10.1006/dbio.1998.9073

Zhou, Y., Fisher, S. J., Janatpour, M., Genbacev, O., Dejana, E., Wheelock, M., & Damsky, C. H. (1997). Human cytotrophoblasts adopt a vascular phenotype as they differentiate: A strategy for successful endovascular invasion? *Journal of Clinical Investigation*, *99*(9), 2139–2151. https://doi.org/10.1172/JCI119387

Zhu, D., Gong, X., Miao, L., Fang, J., & Zhang, J. (2017). Efficient Induction of Syncytiotrophoblast Layer II Cells from Trophoblast Stem Cells by Canonical Wnt Signaling Activation. *Stem Cell Reports*, *9*(6), 2034–2049. https://doi.org/10.1016/j.stemcr.2017.10.014

Zhu, D., Gong, X., Miao, L., Fang, J., & Zhang, J. (2017). Efficient Induction of Syncytiotrophoblast Layer II Cells from Trophoblast Stem Cells by Canonical Wnt Signaling Activation. *Stem Cell Reports*. https://doi.org/10.1016/j.stemcr.2017.10.014

Chapter 2: Single nuclei RNA-seq of mouse placental labyrinth development

Abstract

The placenta is the interface between mother and fetus in all eutherian species. However, our understanding of this essential organ remains incomplete. A substantial challenge has been the syncytial cells of the placenta, which have made dissociation and independent evaluation of the different cell types of this organ difficult. Here, we address questions concerning the ontogeny, specification, and function of the cell types of a representative hemochorial placenta by performing single nuclei RNA sequencing (snRNA-seq) at multiple stages of mouse embryonic development focusing on the exchange interface, the labyrinth. Timepoints extended from progenitor driven expansion through terminal differentiation. Analysis by snRNA-seq identified transcript profiles and inferred functions, cell trajectories, signaling interactions, and transcriptional drivers of all but the most highly polyploid cell types of the placenta. These data profile placental development at an unprecedented resolution, provide insights into differentiation and function across time, and provide a resource for future study.

This study was published in eLife in 2020 (Marsh and Blelloch, 2020).

Introduction

The placenta links maternal tissues and the embryo, providing necessary support and instructing the development of the embryo. The placenta performs many essential functions including transport of nutrients and exchange of gasses and waste between maternal and fetal blood, production and uptake of hormones, and regulation of the

maternal immune system (Maltepe et al. 2015; Woods et al. 2018). The mouse placenta is separated into three main regions – the decidua, the junctional zone (JZ), and the labyrinth. Select fetal trophoblast invade into the maternal decidua and remodel and line maternal arteries, facilitating maternal blood to flow into the fetal portion of the placenta (Adamson et al. 2002; Maltepe et al. 2015). The JZ lies directly beneath the decidua and is comprised of parietal trophoblast giant cells, spongiotrophoblast, and glycogen cells that largely function in hormone secretion and metabolism (Simmons et al. 2007; Woods et al. 2018). Beneath the JZ, closest to the embryo, is the labyrinth, which is specially designed to maximize surface area for gas and nutrient exchange between maternal and fetal blood (Figure 2.1A) (Simmons et al. 2008; Soncin et al. 2015;Woods et al. 2018).

The development of the labyrinth structure begins with fusion of the allantois with the chorion at E8.5 (Cross et al. 2003). This begins a process of invasion and branching morphogenesis resulting in an expansive surface area for gas and nutrient exchange by E10.5 (Soncin et al. 2015). The gas exchange interface in the mouse contains three layers of differentiated trophoblast separating maternal blood from the endothelial cells of the fetal vasculature (Simmons et al. 2008; Maltepe et al 2015; Coan et al. 2005). Sinusoidal trophoblast giant cells (S-TGC) reside in the maternal blood space, have demonstrated exocrine functions, and are a source of placental lactogens (Simmons et al. 2008). S-TGC are attached to the outermost syncytiotrophoblast layer (SynTI) but are perforated allowing maternal blood to contact SynTI (Coan et al. 2005; Woods et al. 2018). Next, are the two SynT layers which together transport gasses and nutrients from the maternal blood to the fetal vasculature (Giorgiades et al. 2002; Woods et al. 2018). SynTI is the

outer layer in direct contact with maternal blood forming the barrier between maternal blood and fetal tissue. Beneath, is SynTII which functions as an intermediary between SynTI on its apical membrane and the fetal endothelium on its basal side. Proper patterning of each cell type ensures efficient transport of nutrients and waste between maternal and fetal blood, and is necessary for embryonic growth, development, and viability.

Investigating the cells of the placental labyrinth is difficult due to their size and an expansion in the number or ploidy of nuclei. SynT cells are multinucleate and are not amenable to standard dissociation and isolation procedures. As a reference, human SynT are 80-200uM in diameter and contain 5-15 nuclei meaning their size and fragility do not allow for profiling by FACS or passage through microfluidic channels for droplet based single cell RNA sequencing (Liu et al. 2018). Therefore, questions remain about how each cell type is specified, how essential placental functions are distributed between cell types, and how each cell type changes throughout developmental time.

Single cell RNA sequencing has become the preferred method for understanding the composition of a complex tissue at the transcriptional level. Several studies in both mouse (Nelson et al. 2016; Home et al. 2019) and human (Vento-Tormo et al. 2018; Suryawanishi et al. 2018) have profiled the placenta using scRNA-seq, however, syncytiotrophoblast are greatly underrepresented in these data. Studies in mouse have either avoided profiling the labyrinth trophoblast, or are unable to distinguish between the two SynT layers (Nelson et al. 2016; Home et al. 2019). Recently, application of droplet-

based transcriptome profiling to nuclei has been shown to provide high quality data and results which recapitulate those from whole cell scRNA-seq (Habib et al. 2017; Lake et al. 2017; Bakken et al. 2018; Ding et al. 2020). To circumvent complications with single cell dissociation and capture of placental cells, we applied single nuclei RNA-seq (snRNA-seq) to the mouse placenta.

In this study, we used snRNA-seq to profile the murine placental development at four time points spanning placental cell type specification, differentiation, and maturation (E9.5, E10.5, E12.5, and E14.5). We resolve all populations of the labyrinth at single nucleus resolution and identify distinct markers and transcript signatures for each population. We are able to separate each SynT layer, furthering the understanding of the independent roles of each cell type at the gas exchange interface. Mapping differentiation from stem/progenitor cells to terminal differentiation, we capture novel intermediates and identify putative regulators. We predict signaling interactions between populations of the labyrinth to understand crosstalk between these populations, revealing factors guiding concerted development of SynT and fetal endothelium. Finally, we identify transcription factor (TF) driven gene regulatory networks active in each placental population, uncovering candidate regulators of fate and function in the placenta. By separating and characterizing placental cell types, specifically those in the labyrinth, these data provide a resource for understanding development *in vivo*, generation of molecular tools *in vitro* and *in vivo*, and for future modeling of prenatal pathologies.

Results

Nuclear Isolation and snRNA-seq of mouse placental cells (E9.5-E14.5)

To gain a better understanding of the constitution of cell types and developmental trajectories in the mouse placenta, we performed single nuclei droplet-based sequencing of their transcriptomes at four embryonic time points: E9.5, E10.5, E12.5, and E14.5. Given the largely syncytial nature of the placenta, we reasoned that sequencing of nuclei would bypass the problems inherent in using a single cell RNA sequencing approach. To decrease contribution from maternal tissues, the placenta was carefully dissected at the boundary between the fetal junctional zone and the maternal decidua (Figure 2.1A). On the labyrinth side of the placenta, the placenta was separated from embryo proper at the point of attachment with the allantois on the basal side (embryo facing). Nuclei were isolated and sorted for DNA content by FACS enabling the removal of doublets and contaminating cytoplasmic RNA (Figure 2.1B). Isolated nuclei were subjected to droplet-based sequencing using the 10x Genomics platform.

A total of 27,326 nuclei passed quality control (between 500 and 4000 unique genes identified and fewer than 0.25% mitochondrial reads), ranging from 4124 to 9485 nuclei across the embryonic days (Figure 2.1C, Table S1). Clustering of nuclei using the Seurat package identified 26 clusters, then projected in UMAP expression space allowing for an understanding of the relationship among populations as visualized by proximity (Figure 2.1D, Figure 2.2A-C) (Satija et al. 2015; Butler et al. 2018). Based on general markers, these populations were separated into 5 broad groups: Trophoblast, Decidual Stroma, Blood Cells, Endothelial Cells, and Fetal Mesenchyme.

The maternal decidual stroma was identified by the absence of Xist expression in male embryonic tissue (Figure 2.1E). Marker genes further subdivided the five broad groups into subgroups (Figure 2.2D). The fetal mesenchyme group consisted of two distinct subgroups. One (clusters 6, 10, and 24) expressed markers of pericytes (e.g. *Acta2*) and several growth factors including *Wnt5b* and *Pdgfrb* that are critical for development and maintenance of vascular populations (Eaton et al. 2020). The other (clusters 15 and 19) expressed *Gata4*, *Kit,* and *Pdpn.* The nature of the cells in this subgroup is unclear, but immunofluorescence for PDPN showed the cells to be interstitial with long projections that appear to make contact with PECAM positive fetal endothelial cells (Figure 2.2E). The endothelial group consisted of cells expressing markers of vascular endothelium (Cluster 3 - *Pecam1*, *Kdr*, *Tek*), lymphatic endothelium (cluster 26 - *Flt4*/*Vegfr3*), and pro-angiogenic and lymphogenic lineages (Clusters 20 and 25 - *Vegfc* and *Igf1*, respectively) (Cao et al. 1998; Björndahl et al. 2005). The identification of cells expressing lymphatic markers is intriguing because the placenta is not thought to contain lymphatics. However, lymphatic endothelium has been discovered in human and it is possible a similar cell type exists in mouse (*Pique-Regi et al. 2019).* The blood cell group consisted of putative erythrocytes (Cluster 13 - *Hbb-y*, *Hba-x*), macrophages (Cluster 17 - *Mrc1+; Martinez and Gordon, 2014*), B-cells (Cluster 21 - *Bank1*, *Btla; Aiba et al. 2006*), T-cells (Cluster 22 – Gzmc, *Slamf1, Cd84; Griewank et al. 2007, Veillette 2006*), and natural killer cells (Cluster 23 - *Cd244; Lee et al. 2004*). Together, these data show that snRNA-seq has the sensitivity and specificity to identify the multitude of cell types in the developing placenta.

Sub-clustering identifies the trophoblast subpopulations of the labyrinth and junctional zone

Trophoblast cells are unique to the placenta and perform the majority of its specialized functions. Unsurprisingly, they also make up the largest of the five broad groups of nuclei (Figure 2.1D). To gain a deeper understanding of the trophoblast populations, we used Seurat to cluster only trophoblast nuclei. Nuclei collected at each individual timepoint were analyzed separately and those assigned a trophoblast identity were then integrated and visualized on a single UMAP. This analysis resulted in 13 clusters consisting of 16,386 nuclei, with clusters ranging in size from 159 to 2906 nuclei (Figure 2.3A, Figure 2.4A). The clusters formed five appendages arising from a central body.

The central body consisted of 4 clusters. One of these clusters highly expressed the receptor tyrosine kinase *Met* (Figure 2.3B), which was previously described as a marker of labyrinth trophoblast progenitor (LaTP) cells with trilineage potential: SynTI, SynTII, and S-TGC (Ueno et al. 2013). The snRNA-seq data places these cells as most closely related to SynTII. Notably, the LaTP shared expression of the Wnt signaling pathway members *Ror2*, *Lgr5*, and *Tcf7l1* with presumptive SynTII precursors. Interestingly, the clustering identified a second subpopulation of cells in the central body that shared relatively high expression of *Tcf7l1* and the long non-coding RNA *Pvt1* with LaTPs, but expressed low levels of *Met*, *Ror2*, and *Lgr5* and high levels of *Egfr* (Figure 2.3B). These cells were more closely related to SynTI and S-TGC. We designated this subpopulation as LaTP2. Correlative analysis of RNA levels for Met and Egfr in individual cells confirmed that for the most part these markers were uniquely expressed in LaTP and LaTP2 cells

respectively (Figure 2.4B). Previously described LaTPs were also shown to express high levels of the adhesion protein EPCAM (Ueno et al. 2013). EPCAM mRNA and protein was mostly limited to the MET+ LaTP cells, although rare EPCAM/EGFR double positive cells were also present (Figure 2.4C-D). Positionally, MET expressing LaTP cells were more basal than the EGFR expressing LaTP2 cells, suggesting that LaTP may be giving rise to LaTP2 (Figure 2.4D). Consistent with this interpretation, immunofluorescence staining of E8.5 embryos identified a large number of EPCAM/MET double positive cells, but few EGFR positive cells in the developing chorion plate (Figure 2.4E). Together, these data show that LaTPs can be separated into two populations based both on mRNA and protein expression. The developmental relationship between these two populations will require future lineage tracing.

The remaining two clusters within the central body appeared to represent precursors of the differentiated cells of the junctional zone – glycogen cells (GCs) and spongiotrophoblasts (SpT) [Junctional zone precursors (JZPs) 1 and 2 (Figure 2.3A)]. JZP1 exclusively expressed high levels of *Cdh4*, whereas *Prune2* and *Ncam1* showed a continuum of expression, increasing from JZP 1 to 2 and finally specified GCs (Fig2B and Figure 2.5A). Markers such as *Igfbp7*, *Pla2g4d*, *Plac8, and Pcdh12* marked later stages of GC specification. In contrast to GCs, the SpT arm separated from late JZP2/ early GCs, with increasing expression of *Mitf*, *Flt1*, *Prl8a9*, and *Slco2a1* as they transitioned from precursors to differentiated cells. The relationship between LaTPs and JZPs is unclear as they shared few markers. One shared marker was *Pvt1*, a target and enhancer of expression of the oncogene *Myc* and, therefore, may reflect the shared proliferative

nature of these two populations, explaining their juxtaposition in UMAP space (Tseng et al. 2014).

The arms extending from the central body showed a transition from progenitors through precursors to fully differentiated cells representing five previously described cell types of the mouse placenta: SynTI, SynTII, S-TGCs, GCs, and SpTs. SynTI was easily identified based on the expression of known markers of SynTI function including the transferrin receptor *Tfrc* and monocarboxylase transporter *Mct1* (Walentin et al. 2016), but also expressed previously unknown markers such as the transcription factor (TF) *Glis1* and the retinol receptor *Stra6* (Figure 2.3B). SynTI precursors also expressed these markers, albeit at lower levels, while additionally expressing high levels of the signaling molecules *Epha4* and *Tgfa*, which decreased with further differentiation. SynTII was annotated by expression of the TF *Gcm1* and fusion gene *Synb* (Maltepe et al 2015, Simmons et al 2008), but also expressed many previously unknown cell specific genes such as the glucagon receptor *Gcgr* and vascular endothelial growth factor *Vegfa*. SynTII precursors showed elevated expression of *Ror2* and *Lgr5* relative to the LaTP. In contrast, *Tcf7l1* decreased throughout the process of differentiation from LaTP to SynTII. S-TGCs were easily identified by the expression of the canonical marker *Ctsq* (Simmons et al 2007; Simmons et al 2008), but also uniquely expressed the leptin receptor *Lepr* and the Nitric Oxide Synthase 1 adaptor *Nos1ap* among other genes. Marker genes for all populations are included in supplementary information (Figure 2 – source data 1).

We further probed the transition from multipotent LaTP through precursors to each of the differentiated labyrinth cell types (SynTII, SynT1, and S-TGC) using pseudotime analysis. The pseudotime analysis program Slingshot aligned cells along a 2D trajectory from the most transcriptionally similar LaTP population (LaTP-SynTII; LaTP2-SynTI; LaTP2-STGC) to each of the mature populations (Figure 2C-E). Pseudotime analysis expanded upon the marker genes for each population by defining the timing of expression of genes through the differentiation process and identifying distinct signaling pathways in each lineage. Expression of Wnt regulated TF *Tcf7l1* along with Wnt receptor *Ror2* were maintained from LaTP through commitment to a SynTII precursor state. Upon commitment to the SynTII lineage, the TF *Zfhx3* and growth factor receptor *Igf1r* are newly expressed while canonical markers *Gcm1* and *Synb* are among the later transcript changes (Figure 2.3C). SynTI Precursor cells maintain *Pvt1* expression but uniquely upregulate the ephrin receptor *Epha4*, the Egf-related ligand *Tgfa*, and the Egf receptor substrate *Eps8*. Only mature SynTI express the kinase *Prkce* and clathrin coat assembly protein *Snap91* (Fig 2D). S-TGC Precursor cells activate the receptors *Pparg* and *Lifr* as well as the hypoxia induced TF *Epas1* upon lineage commitment. Expression of the canonical marker *Ctsq* occurs only in mature S-TGC along with *Lepr* and the Glucocorticoid signaling effector *Tsc22d3* (Fig 2E). These data are consistent with distinct signaling pathways (e.g. SynTII – WNT, IGF; SynTI – EGF, EPH; S-TGC – LIF, PPAR) driving differentiation of LaTP into the three main cell types of the placental labyrinth. Interestingly, the S-TGC appear to differentiate from the junction of LaTP2 and JZP1 (Figure 2.3A), potentially suggestive that S-TGC arise from ectoplacental cone cells (Simmons et al. 2007; Simmons et al. 2011) as well as from chorion derived LaTP (Ueno

et al. 2013). It is also possible the location of the S-TGC near JZP1 reflects the shared prolactin expression between S-TGC and other junctional zone populations. Again, lineage tracing will be required to address their developmental relationships.

As described above, the remaining two arms were consistent with differentiation of the JZ populations: SpT and GC cells. Immunofluorescence of the representative markers NCAM1 and SLCO2A1 confirmed their expression in the JZ (Figure 2.3F). Furthermore, staining of juxtaposed sections confirmed their mutually exclusive expression (Figure 2.5B). Co-staining with the known GC marker PCDH12 (Rampon et al. 2005), verified the GC identity of the NCAM1+ cells (Figure 2.5C). Previous work has identified differential expression of prolactin genes between GC and SpT (Simmons et al. 2008). Therefore, we analyzed the expression of these genes in our dataset. Expression analysis of prolactin genes showed both distinct and overlapping expression of this large gene family between the SpT and GC cells, and confirmed the identities of these clusters (Figure 2.6A and B). Of important note, parietal TGC nuclei were not identified in our snRNA-seq data, likely due to their very large size precluding their passage through the FACS pre-filter, which removes nuclei greater than 35 microns (Figure 2.5D). Our data also did not identify invasive trophoblast giant cells (spiral artery and canal TGCs) that invade the decidua, which was dissected away. Still, this analysis of the trophoblast snRNA-seq was able to clarify the cell types and their relationships for a predominance of the lineages of the mouse placenta identifying novel intermediate states and markers of the different cell populations.

Developmental time course and trajectory inference reveal details of lineage dynamics and commitment

Next, we asked how the trophoblast cell populations changed over developmental time by separating the conglomerate data into its individual timepoints (Figure 2.7A). This visualization clearly showed the rapid diminishment of the LaTP populations over time, resulting in few progenitors remaining by E14.5 (Figure 2.7A and B). The precursor populations also decreased over time, presumably maturing into terminally differentiated cells, which dramatically increased during the time course (Figure 2.7A and B). To determine which populations were primarily responsible for the expansion of the number of cells in the placenta, we evaluated expression of the cell cycle marker *Mki67* which is lost when cells exit the cell cycle (Gerdes et al. 1984). The majority of *Mki67* expressing nuclei were among the progenitor and precursor cell populations (Figure 2.8A). However, at E9.5 and E10.5, a substantial number of nuclei at the distal tips of each arm also expressed *Mki67*, suggesting ongoing proliferation even after cells have transitioned to a more mature-like expression state. Very few nuclei expressed *Mki67* at E14.5 consistent with the expansion in placental cell number happening prior to E14.5, with later growth occurring through cellular hypertrophy rather than cell division (Ueno et al. 2013; Paikari et al. 2017).

Cellular dynamics can be tracked not only by collecting samples at different developmental time points, but also by leveraging splicing information inferred through comparisons of intron vs. exonic reads of genes within individual cells, termed RNA velocity. We performed RNA velocity using the scVelo package to produce vectors

representing both the direction and speed of cellular maturation (Bergen et al. 2019). In the scVelo visualization, each nucleus is identified by
an arrow representing the inferred direction and rate of cellular change projected in UMAP space. The data was visualized separately for each different developmental timepoint to discern the dynamics of cell transitions and how these dynamics change over time (Figure 2.7C). In addition, the velocity magnitude was summarized for each cell population at each developmental timepoint (Figure 2.7D).

These analyses uncovered a number of interesting properties associated with placental development. Progenitor vectors (LaTP and LaTP2) showed little directionality and small magnitudes, likely reflecting a maintenance of multipotency and self-renewal. In contrast, the cells within each precursor population showed uniform directionality and large magnitudes, especially at E10.5 and E12.5, the period of greatest placental expansion. Surprisingly, the differentiated cell populations also showed vectors of great magnitude and uniform directionality at the early timepoints, suggesting ongoing transcriptional maturation, before diminishing by E14.5. To evaluate ongoing changes in the mature populations, we selected the S-TGC population and performed differential expressional analysis between each timepoint and E9.5. Consistent with the vectors, the number of differentially expressed genes at each consecutive timepoint increased from 143 to 700 genes (adj. P-value <0.05; Figure 2.7E, Figure 2.8B).

Gene ontology analysis showed that genes up at E9.5 were highly enriched for ontology groups concerning cell division, while those at E14.5 were enriched for Ras GTPase

signaling and various developmental processes (Figure 2.8C). Examples of genes that increased over developmental time include *Ctsq*, the Cathepsins (*Ctsj*, *Ctsr*, *Ctsm*, *Cts3*, and *Cts6*), and several genes involved in hormone signaling and response (*Lepr*, *Tsc22d3*, and *Ghrh*) (Figure 2.8B, D, E, F). In contrast, *Podxl* is expressed from the very early stages of S-TGC specification through E14.5. *Podxl* is a highly charged membrane protein which, in a different context, has been implicated in luminogenesis in early embryos (Shahbazi et al. 2017). While the formation of maternal blood spaces in the placental is distinct from the early embryo, the early expression of Podxl in S-TGCs might function in maintaining open maternal blood spaces within the placental labyrinth. The differential dynamics of PODXL and LEPR in S-TGCs was confirmed by immunohistochemistry (Figure 2.7F). Similar ongoing maturation processes were seen in the SynTII, SynTI, GC, and SpT populations (Figure 2.8G). Together these data support a model of early expansion by self-renewing progenitor cells and committed precursors followed by ongoing maturation of all five differentiated cell types of the placenta proper.

Defining distinct roles of the trophoblast subtypes at the gas exchange interface

The labyrinth is the site of transport between fetal and maternal blood in the mouse placenta. Fetal and maternal blood are separated by a thin membrane consisting of four cell layers starting with the fetal endothelial cells, then SynTII, followed by SynTI, and finally S-TGCs (Simmons et al. 2008) (Figure 2.9A). A basal lamina separates the fetal endothelial cells from SynTII cells. The expression programs and functions of the three trophoblast cell layers have been difficult to dissect due to the syncytial nature of the SynTI and SynTII cells. Isolation of nuclei followed by snRNA-seq overcomes this barrier

enabling the determination of the unique expression programs of each trophoblast layer. Immunohistochemistry for the marker genes PECAM1, IGF1R, STRA6, and PODXL demonstrate each cluster corresponds to Endothelial, SynTII, SynTI, and S-TGC populations respectively *in vivo* (Figure 2.9A). Each layer could be distinguished by high resolution image analysis with nucleated erythrocytes residing in the PECAM1+ fetal vessels and large polyploid S-TGC residing in the maternal blood sinuses. PODXL+ cytoplasmic extensions of the S-TGCs spread over the perimeter of the maternal blood space forming a permeable lining (Figure 2.9A).

SynTII, SynTI, and S-TGCs were distinguished from one another based on their transcript profiles (Figure 2.9B). Furthermore, gene ontology analysis of differentially expressed genes between populations suggested highly distinct functions (Figure 2.9C-E and Figure 2.10). SynTII differentially expressed genes were highly enriched for cell-cell and cell-matrix interactions such as those encoding cell junction and cell adherens proteins consistent with a role as a basal permeability barrier between maternal and fetal blood. SynTII also expressed collagens and laminin subunits (Figure 2.9E) which likely form the basal lamina separating SynTII from the fetal endothelium. Also identified in SynTII differentially expressed genes was the stem cell population maintenance GO category, which included several genes known to be important for placental function though not specific to stem cells (Bcl9, Gata2, and Tbx3).

In contrast, SynTI differentially expressed genes were enriched for intracellular transport and cell signaling including genes encoding for vesicular organization and transport,

protein localization to membranes, and Ras signaling. These data are consistent with SynTI layer playing a critical role in the transport of materials between maternal and fetal blood. SynTI is also enriched for genes involved in neuron projection development, driven by expression of canonical axonal pathfinding genes (Plxna2, Plxnd1) and synapse genes (Snap91). The exact function of these genes in SynTI is unclear and would be of interest for future study.

Although more generally understood as an exocrine cell type, the S-TGC were enriched for GTPase and Ras signaling and receptors including Kras, Grb2, and Pdgfrb, suggesting these cells also transduce signals from maternal blood. S-TGC differentially expressed genes were strikingly enriched for those encoding for migration factors. Such expression could explain the long thin cellular extensions from these cells, which form the only non-syncytial trophoblast at the interface (Coan et al. 2005). S-TGCs are connected to SynTI by desmosomes, which are known to undergo constant remodeling and have additional functions in signaling and migration (Simmons et al 2008; Johnson et al. 2014). These S-TGC specific programs along with the high expression of *Podxl*, likely underlie a central role for these cells in the function of the maternal sinuses. S-TGC are also enriched for the placental development category which includes several genes important for giant cell function including *Hand1* (regulation of giant cell lineage), *Hsd17b2* (steroid hormone production), and *E2F7* (endoreduplication).

Given that the labyrinth represents the site of exchange of nutrients, minerals, metabolites, ions, gases, and regulatory factors, between the mother and fetus, we next

wanted to better understand how these functions are distributed across the different trophoblast layers. We focused on two large functional categories: solute transporter and cholesterol/vitamin transport. All genes in these categories that were found to be differentially expressed between one of the interface populations (SynTI, SynTII, S-TGC) compared to all other trophoblast populations were included in this analysis. The results suggested a striking separation of functions between the layers (Figure 2.10B and C). For example, genes responsible for carboxylate transport were highly enriched in SynTII, while organic anion transporters were enriched in SynTI. Even within specific transport pathways, functions were often separated; for example, factors important in Zinc transport were distributed across, yet distinctly expressed between the populations. Cholesterol transporters are enriched in SynTII (*Scarb1*, *Vldlr*) and S-TGC (*Hdlbp*, *Ldlr*), while Folate receptors (*Folr1*, *Folr2*) are uniquely expressed in SynTI. Together, these data show a highly evolved separation of functions between the three trophoblast layers that separate maternal from fetal blood.

Predicting cell signaling within the placental labyrinth

Single cell RNA-seq has been used to predict signaling between different cell types of a tissue or organ (Efremova et al. 2020; Vento-Tormo et al. 2018). Here, we asked whether we could do the same with snRNA-seq to provide insight into the developmental signals driving mouse placental development. We used the package CellPhoneDB (Efremova et al. 2020) which applies a data base of annotated receptor-ligand pairs to the single cell expression data evaluating all possible combinations of cell types (i.e. identified clusters). We focused our analysis on the populations of the developing labyrinth (LaTP, LaTP2,

SynTI Precursor, SynTI, SynTII, S-TGC Precursor, S-TGC, and fetal endothelium). Given that CellPhoneDB receptor-ligand database was developed for human cells, we only included orthologous genes from our mouse snRNA-seq data. The results are summarized as a heatmap of the predicted strength (average log 2 expression of ligand-receptor pair) in Figure 2.12 with receptor-ligand interactions shown on the rows and each cluster pair shown as columns. A total of 139 unique ligand–receptor interactions reaching significance (adj. p-value < 0.05) were uncovered.

CellPhoneDB predicted an interaction between *Rspo3* in the endothelium with *Lgr5* in the LaTP/SynTII lineage (Figure 2.11A). *Rspo3* is required *in vivo* for the maintenance of *Gcm1* expression (Kazanskaya et al. 2008; Aoki et al. 2007) and canonical Wnt signaling is essential for differentiation of SynTII (Zhu et al. 2017, Matsuura et al. 2011). Predicted signaling in the opposite direction included *Vegfa* secreted by SynTII to the receptors *Kdr*, *Flt1*, *Nrp1*, *Nrp2* located only on endothelial cells. Immunostaining confirmed SynTII and SynTI as the sources of VEGFA in the labyrinth (Figure 2.11B, Figure 2.13). These data suggest a feedback loop where *Rspo3*-*Lgr5* supports SynTII differentiation and function, while *Vegfa*-*Kdr*/*Flt1* drives vascular maintenance and remodeling, thereby coordinating lineage differentiation with development of tissue structure.

Analysis of marker genes suggested Egf signaling as a regulator of LaTP differentiation to SynTI (Figure 2.3D). CellPhoneDB analysis was consistent with that interpretation as it predicted an interaction between the EGFR ligands *Tgfa*, *Hbegf* and *Nrg1* produced by SynTI with *Egfr* on both LaTP2 and SynTI precursor populations. However, it also

predicted an interaction with *Egfr on* LaTP, SynTII, and S-TGCs (Figure 2.11C). We confirmed protein expression HBEGF alone in SynTI, and colocalization of HBEGF and EGFR in SynTII (Figure 2.11D; Figure 2.13B and C). Therefore, SynTI appears to be a hub of EGF signaling that impacts the majority of the cell populations in the labyrinth. Loss of *Egfr in vivo* results in decreased placental size, disorganized labyrinth, and a reduction in the SpT layer (Du et al 2003; Miettinen et al. 1994; Strunk et al. 2004). Depletion of Egf ligands yields a variety of phenotypes (Liu et al. 2019; Luetteke et al. 1993). Taken together, these data suggest a complex regulation of Egfr signaling being coordinated by SynTI that is critical for proper development of the labyrinth.

Numerous ligand-receptor interactions between *Bmp8a* and several receptors, including *Acvr1*, *Bmpr1*, and *Bmpr2* were predicted in the labyrinth. The source of *Bmp8a* is LaTP and SynTII and the receptors are located on all labyrinth populations, including LaTP and SynTII (Figure 2.11E). Additional Bmp 60A subfamily members, *Bmp6* and *Bmp7*, were highly secreted. *Bmp7* is secreted by LaTP and *Bmp6* by the endothelium (Figure 2.11E and F). In addition to BMP ligand and receptors, the pathway's downstream effectors, the *Smad* TFs, also showed striking differential expression between the cell types of the labyrinth. *Smad2/4/7* were relatively uniformly expressed in trophoblasts, while *Smad1/3/5/6* displayed varied levels of expression across trophoblast populations (Figure 2.11G and Figure 2.13D). Previous work has shown that while *Bmp8a* is largely redundant with *Bmp8b*, loss of *Smad1* and combined knockout of *Bmp5/7* exhibit severe placental defects (Zhao et al. 1996; Tremblay et al. 2001; Solloway et al. 1999). Cell type specific perturbation of elements of the Bmp pathway has not been performed; however,

ligand-receptor modeling with CellPhoneDB combined with snRNA-seq expression data provides insight into how the pathway likely functions *in vivo*.

Modeling transcription factor regulon activity identifies new candidate regulators of SynTII

Transcription factors (TFs) are the most direct regulators of cell fate and can be used to reprogram cells to new cell fates (Kubaczka et al. 2015). Our snRNA-seq data contained many well-studied TFs, but expression alone is not necessarily a good indicator of function. TFs typically act cooperatively with other TFs and numerous factors influence their activity. Therefore, we sought to identify active TFs based on both expression of the TF and its downstream targets within the same cells. To do so, we used the SCENIC package (Aibar et al. 2017) which uses a database of TFs and their annotated motifs to identify enrichment of a TF motif within or near the promoter regions of co-expressed genes within each cell to define “regulon activity”. As such SCENIC infers activity of a transcriptional network rather than considering expression of the TF alone.

Application of SCENIC to the trophoblast dataset recovered 200 transcription factor regulons with activity in at least one cluster. To ensure that the regulon activity data maintained the variation of the transcript expression data, we projected the nuclei in UMAP space using regulon activity transcript expression as the underlying variable. The resulting plot was color coded based on a cluster identity as defined by Seurat analysis of transcript expression (Figure 2.14A). There was overall strong agreement in the two approaches to separate nuclei by cell type both in UMAP space and hierarchical

clustering of Pearson correlations between populations (Figure 2.3A vs. Figure 2.14A, Figure 2.15A). These data show that TF regulon activity provides an alternative means to identify the different cell types of the placenta.

The identified regulons with differential activity across the populations included both known and unknown TF regulators of placental development. Known factors include *Gcm1* in SynTII specification, *Grhl2* in S-TGC, and *Ets2* in JZ development (Figure 2.14B) (Anson-Cartwright et al 2000; Walentin et al. 2015; Yamamoto et al. 1998). Examples of the many unknowns include *Tbx15* in LaTP, *Gata1* in SynTII, *Pax2* in SynTI, and *Meis1* in S-TGC. The power of the regulon approach is further supported by comparing the distribution of TF expression alone versus that of their regulon (Figure 2.14C). While expression of *Gcm1* and *Pax8* correlated the distribution of their regulon activity, *Ets2* and *Esrrg* did not. *Ets2* was broadly expressed, yet its regulon activity was highly enriched among differentiating S-TGCs and GCs. *Esrrg*, on the other hand, was lowly expressed throughout, yet showed strong regulon active among SpT cells. *Esrrg* is not well studied in the mouse placenta, but has known roles in steroid hormone production and metabolism in human trophoblast, functions also important in the mouse placenta (Poidatz et al. 2012; Luo et al. 2014).

Given that most of the TFs underlying cluster specific regulons have not been studied in the placenta, we next researched the Mouse Genome Informatic database for any phenotypes associated with the knockout of TFs driving the uncovered regulons. Only 17 of the 200 TFs had annotated placental phenotypes, while 124 are lethal during

development (defined as until weaning) (Figure 2.14D). Many of these developmental lethal phenotypes likely are associated with placental defects given that 68% of 103 intrauterine lethal and subviable mouse knockout lines also have placental defects (Perez-Garcia et al. 2018). Unfortunately, few of knockouts evaluated in the Perez-Garcia et al paper were for transcription factors, making comparisons to our regulon data impossible. However, we did see robust and cell type specific expression of several factors uncovered in their paper as having placental phenotypes, including *Fryl* in GCs, *Atp11a* in the SynTI lineage, and *Adcy9* in SynTII (Figure 2.15B and C). Together, these analyses suggest likely important roles for the uncovered regulons in placental development.

Next, we asked if we could uncover networks among the TFs themselves focusing on the SynTII lineage. In particular, the regulon data was evaluated for evidence of coexistence of paired regulon activity with associated high confidence annotations (defined by either direct annotation or inferred by orthology) of binding sites for one or both of the TFs in the other TF's promoter region (Figure 2.14E). *Gcm1*, the master regulator of the SynTI lineage, and *Zhfx3* have reciprocal high confidence motif in their promoter regions, suggestive of a positive feedback loop. *Zfhx3* and *Tcf7l2* also show mutual regulation of one another, and *Tcf7l2* also has a high confidence binding site in the promoter of *Gcm1*. Thus, these 3 TFs establish what appears to be an autoregulatory loop. *Zfhx3* (*Atbf1*) does not have known functions in the placenta. However, two independent genetic disruptions of *Zfhx3* result in embryonic to pre-weaning lethality with surviving pups exhibiting severe growth defects (Sun et al. 2012; Parsons et al. 2015). While *Tcf7l2*

knockout mice do not have a placental phenotype, we identify high confidence motifs in the promoter regions of many genes important for SynTII differentiation and function including *Lgr5*, *Vegfa*, *Slc43a2*, and *Gcm1* (Perez-Garcia et al. 2018; Kazanskaya et al. 2008; Guetg et al. 2014). It is possible that redundancy with *Tcf7l1* underlies the lack of *Tcf7l2* knockout placental phenotype (Nguyen et al. 2009).

Zfhx3 also appears to be in a positive regulatory loop with the two TFs *Zmiz1* and *Mxi1*. *Zmiz1* and *Mxi1* in turn both have high confidence binding sites in the promoter of *Gata1*. While *Gata1* has not been studied in the context of the mouse placenta, transcript expression, regulon activity, and high confidence motifs suggest it regulates multiple genes with important functions in SynTII including *Vegfa*, *Slc40a1* (ferroportin), and the basal epithelial transcription factor *Trp63*. Immunofluorescence showed the colocalization of GATA1 with IGFR1, thereby confirming its expression in SynTII (Figure 2.14F). In particular, strong GATA1 protein expression was visible in the SynTII nuclei abutting the basal membrane (Figure 2.14F and Figure 2.15D – white arrowheads), but not in SynTI nuclei closest to maternal blood spaces (Figure 2.14F – yellow arrowhead). Strong GATA1 staining was also obvious in the nuclei of fetal erythrocytes with vascular lumen. Therefore, GATA1 appears to be expressed exclusively in SynTII population of trophoblasts and likely has important regulatory functions specific to SynTII.

Discussion

This study profiles the development of the mouse placenta by transcriptome capture of nuclei, rather than whole cells, resulting in a high-resolution map of labyrinth

differentiation and allowing for the first independent analyses of the two SynT populations. In contrast to previous studies where SynT comprise fewer than 10% of cells identified, almost 30% of trophoblast nuclei captured in this study originate from SynT cells. Profiling four developmental stages from E9.5 to E14.5 allowed for the capture of stem/progenitor and terminally differentiated populations including previously unknown intermediate states and new putative regulators of cell identity. Modeling receptor-ligand interactions predicted how SynTII and endothelial cells coordinate spatial proximity and development through growth factor secretion. In addition, network inference predicted gene regulatory networks defined by TFs and feedback loops among the TFs, including novel candidate regulators of placental development. All together, these data represent a high-resolution map of placental labyrinth development providing insights into the cell autonomous and non-autonomous molecular events underlying the formation and function of this remarkable organ.

Understanding the development of any tissue begins with the progenitor populations. Previous work uncovered a population of EPCAM and MET expressing progenitors that give rise to the three trophoblast populations of the labyrinth (SynTI, SynTII, and S-TGC) (Ueno et al. 2013). Clustering analysis of the snRNA-seq data separated these cells into two closely related clusters, LaTP and LaTP2. Both expressed *Epcam*, but only LaTP expressed *Met*. The relationship between these populations is unclear. Both LaTP populations had low RNA velocities and there was no coordinated directionality to indicate differentiation from one population to the other. However, the relative positions of the two populations in the developing labyrinth and the earlier presence of EPCAM/MET double

positive cells (i.e. at E8.5) suggest that LaTP2 arise from LaTP. Alternatively, the two populations may arise from progenitors that separate earlier in development resulting in distinct lineage biases. LaTP is more similar to SynTII, while LaTP2 is more similar to SynTI and S-TGC. Understanding the specification and heterogeneity of labyrinth progenitors will be an important undertaking given that early defects are likely to have large effects in proportion of terminally differentiated trophoblast resulting in embryonic defects and ultimately reduced viability.

Tracking differentiation from the LaTP populations identified previously unknown precursor populations along differentiation to SynTI and S-TGC. Profiling differentiation to SynTII confirmed previous work demonstrating the role of Wnt signaling in specification and efficient differentiation of SynTII, both *in vivo* and *in vitro* (Zhu et al. 2017; Matsuura et al. 2011). However, such detailed information and derivation protocols did not exist for SynTI or S-TGC. SynTI precursor cells strongly upregulated Egf signaling members *Tgfa* and *Eps8*. Additionally, expression of Egf ligands by mature SynTI and *Egfr* by LaTP 2, SynTII, and S-TGC underscore the centrality of Egf signaling to labyrinth development and function. While Egfr loss or mutation *in vivo* causes labyrinth disorganization, the deciphering of mechanism has been confounded by defects in junctional zone cells and strain specific variation (Du et al. 2003; Strunk et al. 2004; Dackor et al. 2009, Lee et al. 2009). In human trophoblast, EGF has been shown to stimulate differentiation to SynT *in vitro* and decreased EGFR phosphorylation is associated with intrauterine growth restriction (Morrish et al. 1987; Fondacci et al. 1994). Given the redundancy of Egf ligands, a careful temporal and cell type specific dissection of the loss of *Egfr* will be

necessary to separate the multiple functions of Egf signaling in placental development and health.

Pseudotemporal ordering along the S-TGC trajectory implicated Lif-Stat3 signaling evidenced by increasing expression of *Lifr* and supported by high activity of the predicted *Stat3* regulon by SCENIC. Loss of *Lifr* results in disorganization of the labyrinth and dramatically enlarged non-functional maternal blood sinuses lined by multinuclear aggregates, and not S-TGC (Ware et al. 1995). While Lif-Stat3 is also active in the junctional zone, this striking labyrinth phenotype is likely explained by a necessity for Lif signaling in the differentiation, patterning, and/or function of S-TGC. Deciphering how *Lifr* is necessary for S-TGC and the regulation of maternal blood spaces will require genetic manipulation specific to S-TGC. This will be important to understand establishment and maintenance of functional maternal blood spaces which are at the core of common placental diseases like preeclampsia, fetal growth restriction, and diabetic complications (Ware et al. 1995; Roberts et al. 2012).

This study represents the first independent transcript profiling of each SynT layer *in vivo*. This was achieved by the isolation of nuclei prior to transcriptome capture. These data demonstrate the utility of snRNA-seq in profiling syncytial placental cells without damaging and lengthy enzymatic digestion or single cell dissociation. Mouse is the most common model for human placentation, even though the species differ in organ morphology, especially with respect to the gas exchange interface. Human placentas have villi that float in a pool of maternal blood. The villi are covered by a single syncytial

layer and have no clear S-TGC equivalent. Comparing the transcript profiles of the interface populations in mouse and human will help to understand how the functions of SynTI, SynTII, and S-TGC are distributed across the fewer trophoblast populations of the human placenta. Such information is also likely to provide important insight into how the different structures arose during evolution and which human developmental processes can be effectively modeled in mouse.

In our study of the mouse labyrinth, specific marker genes identified in each layer provide insight into the functions of SynTI versus SynTII. Gene Ontology analysis of SynTI indicates enrichment for membrane associated proteins, including numerous transporters, receptors, and GTPase signaling factors. Many of these proteins, like STRA6, are localized to the apical surface where they transduce signals and uptake nutrients from maternal blood. However, SynTII also expressed many classes of solute transporters and signaling receptors, reflecting the export of molecules to the fetal endothelium. SynT layer specific expression indicates which transporters are likely involved in uptake from maternal blood (SynTI enriched), export to fetal blood (SynTII enriched), or both (SynTI and SynTII enriched). Transcript data represent the first step in understanding the chain of nutrient transport and inform the critical cell type for targeted therapies for nutrient deficiencies.

Surprisingly, SynTII display unique enrichment for adhesion and junctional proteins, likely necessary to support frequent gap junctions on the border with SynTI and robust attachment to the basal lamina, respectively. Notably, several laminin, integrin, and

collagen subunits are highly expressed. Electron microscopy has demonstrated only one basal lamina exists, which is between SynTII and fetal endothelial cells (Coan et al. 2005). Endothelial cells express a complementary set of extracellular matrix protein subunits (*Col4a1*, *Col5a*2, *Col18a1*), suggesting deposition of this membrane is a coordinated process between these two cell types. Coordinated development between SynTII and the endothelium is also found in a positive feedback loop of necessary growth factors (Wnt and Vegf). These data support an additional role for SynTII as a vascular support cell and likely cell type of origin for many placental vascular abnormalities.

Recent work identified that a surprising proportion of developmental lethal mouse mutants had unidentified placental phenotypes (Perez-Garcia et al. 2018). At least 200 TF defined regulatory networks are active in trophoblast during development. Over 62% of these TFs exhibit developmental lethal phenotypes upon homozygous loss of function but only 8.5% have published placental phenotypes (according to MGI). Candidate regulators were identified in all cell types, including *Zfp110* in LaTP, *Pax2* in SynTI, *Gata1* in SynTII, *Meis1* in S-TGC, and *Etv6* in GCs. For some TFs with strong phenotypes in other organ systems, a methodical analysis of placental morphology may not have been performed or published. For example, *Zfhx3* is predicted to form an autoregulatory loop with *Gcm1* and regulate several genes important to SynTII function. While loss of *Zfhx3* results in developmental lethality and severe growth defects, its role in placental development has not been examined (Sun et al. 2012; Parsons et al. 2015). Several TFs may have not been identified due to overlapping or compensatory roles with other proteins. One such example is *Tcf7l1* and *Tcf7l2*. While highly active in the SynTII, *Tcf7l2* exhibits no

placental abnormalities upon knockout. *Tcf7l1*, which is also highly active in LaTP, has demonstrated redundancy with *Tcf7l2* in the skin and it is likely each factor compensates for loss of the other (Nguyen et al. 2009). As the knockout of both factors is lethal prior to the genesis of the labyrinth, conditional deletion in only extraembryonic tissues would be required to investigate their function in the placenta. While conditional or temporal control over deletion may be necessary for other factors inducing early lethality (*Klf5*) or confounding defects in other organ systems (*Gata1*), genetic deletions for almost all identified TFs exist and represent a large resource for immediate study of their effects in placental development.

In summary, this study represents a compendium of mouse placental labyrinth development from E9.5 through E14.5. These data provide a lens through which to better understand congenital defects, environmental and nutrient deficiencies, and species-specific differences in development and function.

Figures

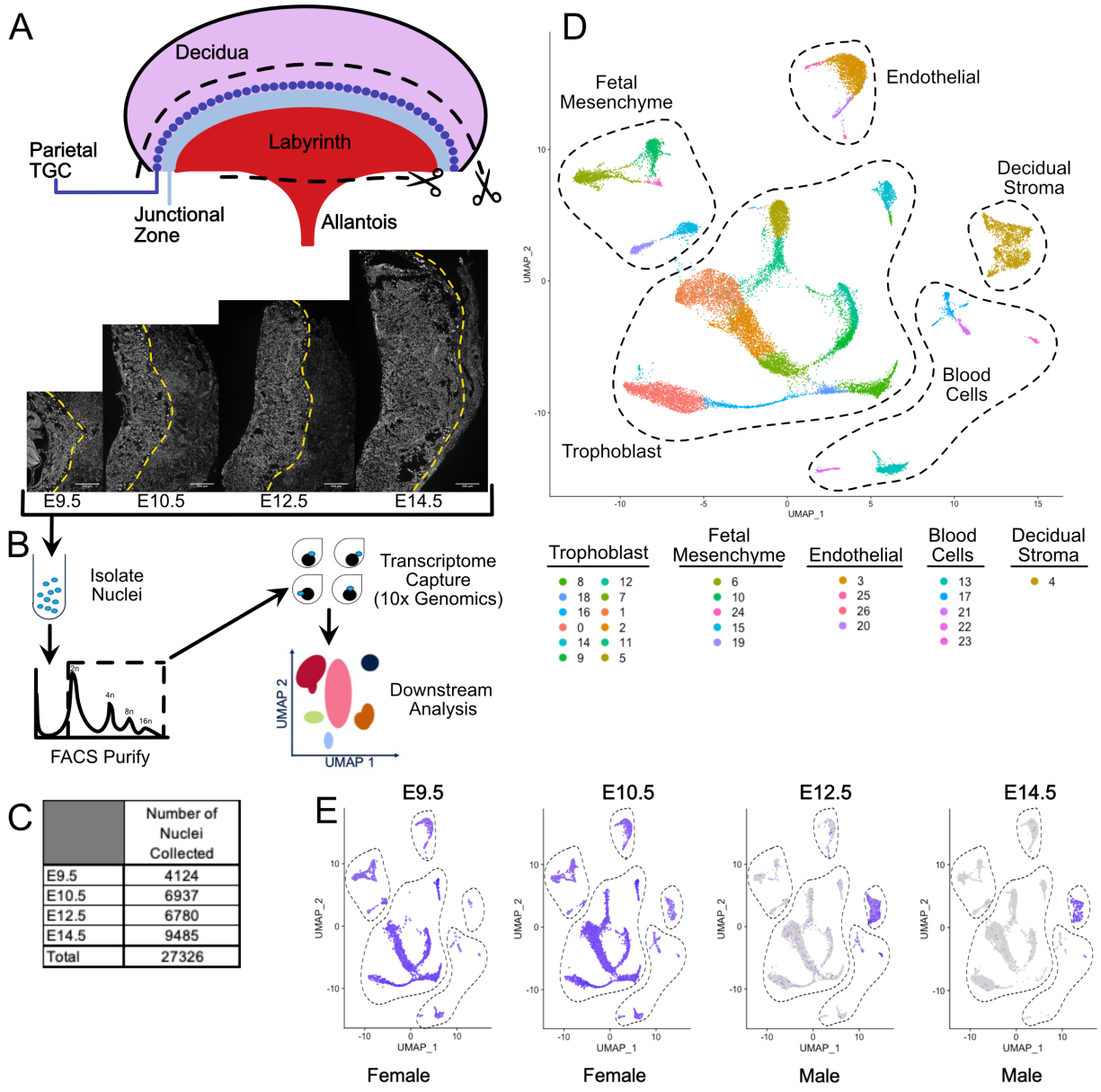

Figure 2.1 - Nuclear isolation and snRNA-seq of mouse placental cells (E9.5-E14.5).

(A) Schematic showing the main regions of the placenta – Labyrinth, Junctional Zone, Parietal TGC, and Decidua. Removal of the decidual stroma and the allantois is marked by scissors and cut lines. Sections of placentas at E9.5-14.5 stained with DAPI to label nuclei and reveal tissue architecture. The dotted line is drawn at the interface between the junctional zone (left of the line) and the maternal decidual stroma (right) to demonstrate the growth occurring during this time span. (B) Schematic outlining nuclei isolation from tissue, purification using FACS, transcriptome capture, and downstream analysis. (C) Number of nuclei collected at each gestational age and in total. (D) Visualization of the 27,326 nuclei included in the analysis plotted in two dimensions by

transcriptome similarity using uniform manifold approximation and projection (UMAP). Each dot represents one nucleus colored according to assignment by clustering analysis (see Methods). Dotted lines encircle clusters with common properties. (E) Expression of *Xist* in each sample. Female placenta samples express *Xist* in all nuclei. Male placental samples express *Xist* only in maternally derived nuclei. The main cell type groupings from D are outlined here also.

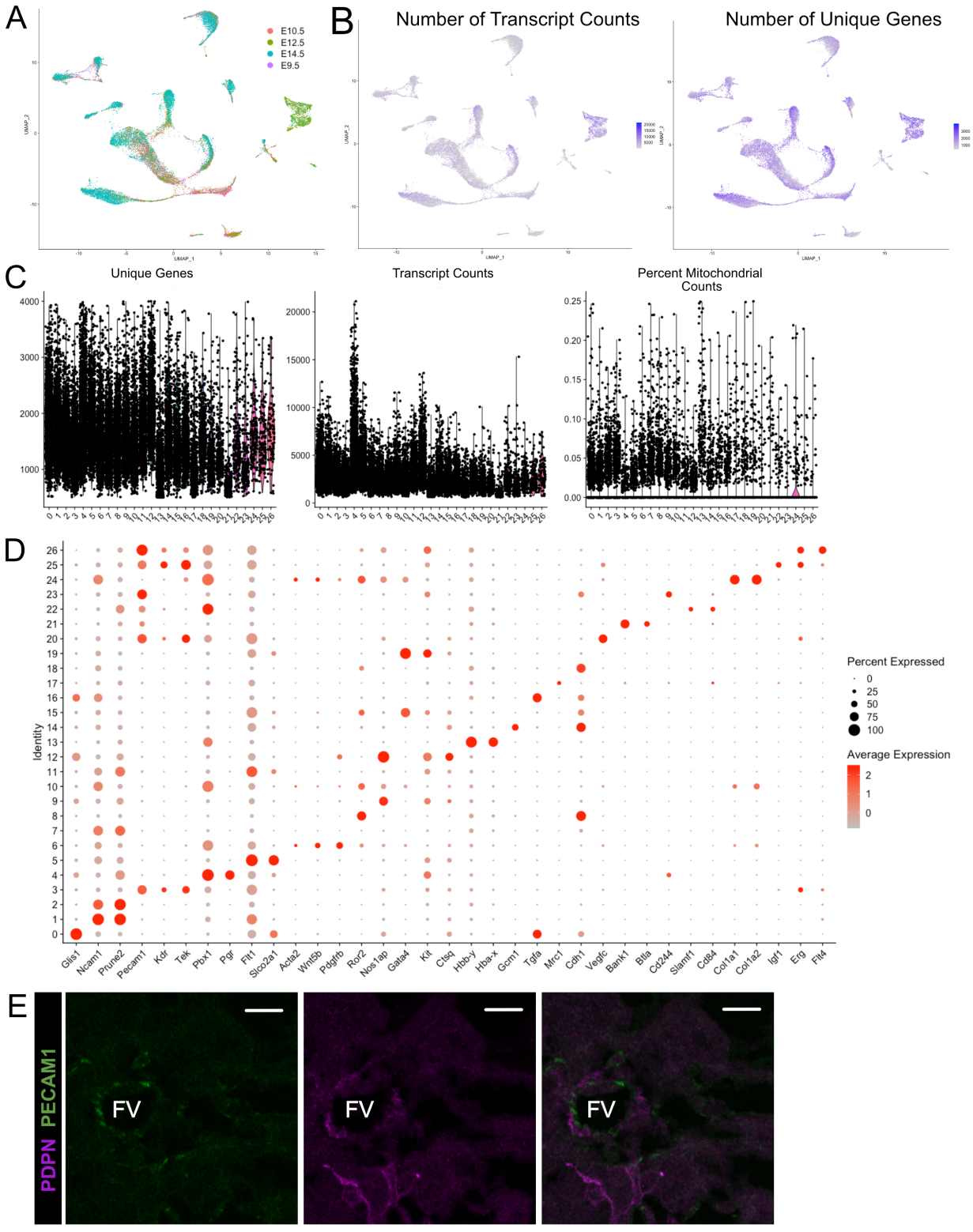

Figure 2.2 - snRNA-seq (E9.5-E14.5) dataset metrics and annotations.
(A) UMAP projection of all nuclei color coded by timepoint from which they were collected. (B) The number of transcripts identified per nucleus (left) and the number of

unique genes identified (right) per cell projected in UMAP space. (C) Violin plots showing the number of unique genes (left), number of transcripts (middle), and the percent of reads mapping to mitochondrial genes (right) for each cluster identified in Figure 2.1D. (D) Dot plot showing the average expression per cluster and percent of nuclei in each cluster expressing select marker genes. Genes are listed on the x-axis and clusters on the y-axis. (E) Immunofluorescence staining of PDPN and PECAM1 at E10.5 showing PDPD+ cells mesenchymal cells and contacts with fetal PECAM+ endothelial cells (Scale Bar – 20um; FV – Fetal Vessel).

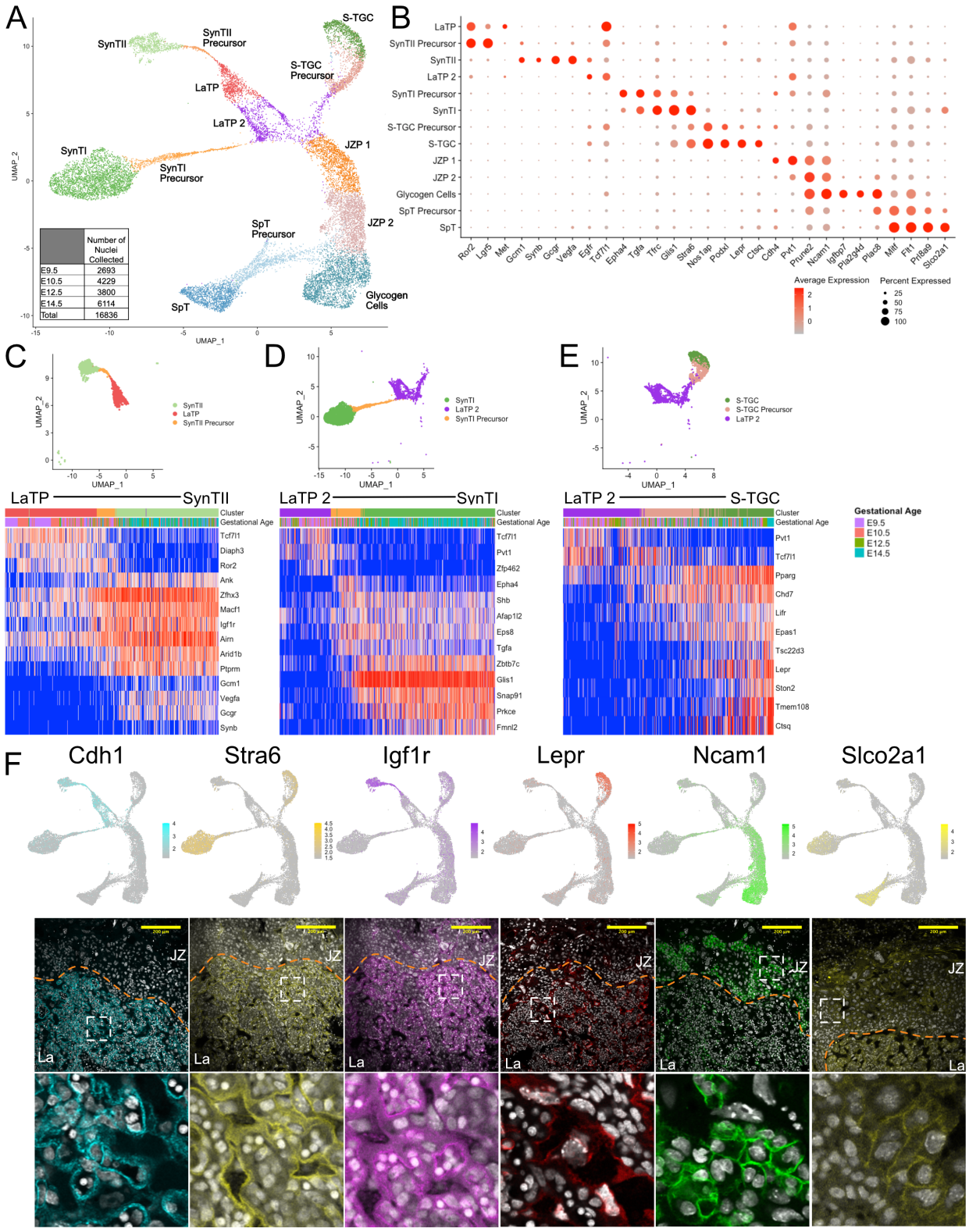

Figure 2.3 - Sub-clustering of the trophoblast nuclei identifies the cell types of the labyrinth and junctional zone.

(A) UMAP showing the 16,836 nuclei included in the trophoblast subset, clustered and plotted according to transcriptome similarity. Clusters were annotated according to canonical marker genes and named below. Inset shows the number of nuclei collected at each gestational age. (B) Dot plot showing average expression and percent of nuclei in each cluster expressing canonical and novel marker genes identified for each cluster. Genes listed on the x-axis and clusters on the y-axis. (C-E) Nuclei along the differentiation from LaTP to SynTII, SynTI, and S-TGC were ordered by pseudotime using Slingshot. The nuclei included along each pseudotime axis shown at top. The expression of select genes (y-axis) representing each differentiation are shown in each heatmap. Each column represents a nucleus organized in pseudotime proceeding from left to right along the x-axis. (F) Expression of genes unique to several trophoblast populations projected in UMAP space (top) and localization of corresponding protein in E12.5 mouse placenta sections by immunofluorescence staining (Middle – 20x, Scale Bar = 200uM; Bottom – high magnification inset area shown by white dashed line). Separation of labyrinth (La) and junctional zone (JZ) shown by the orange dashed line.

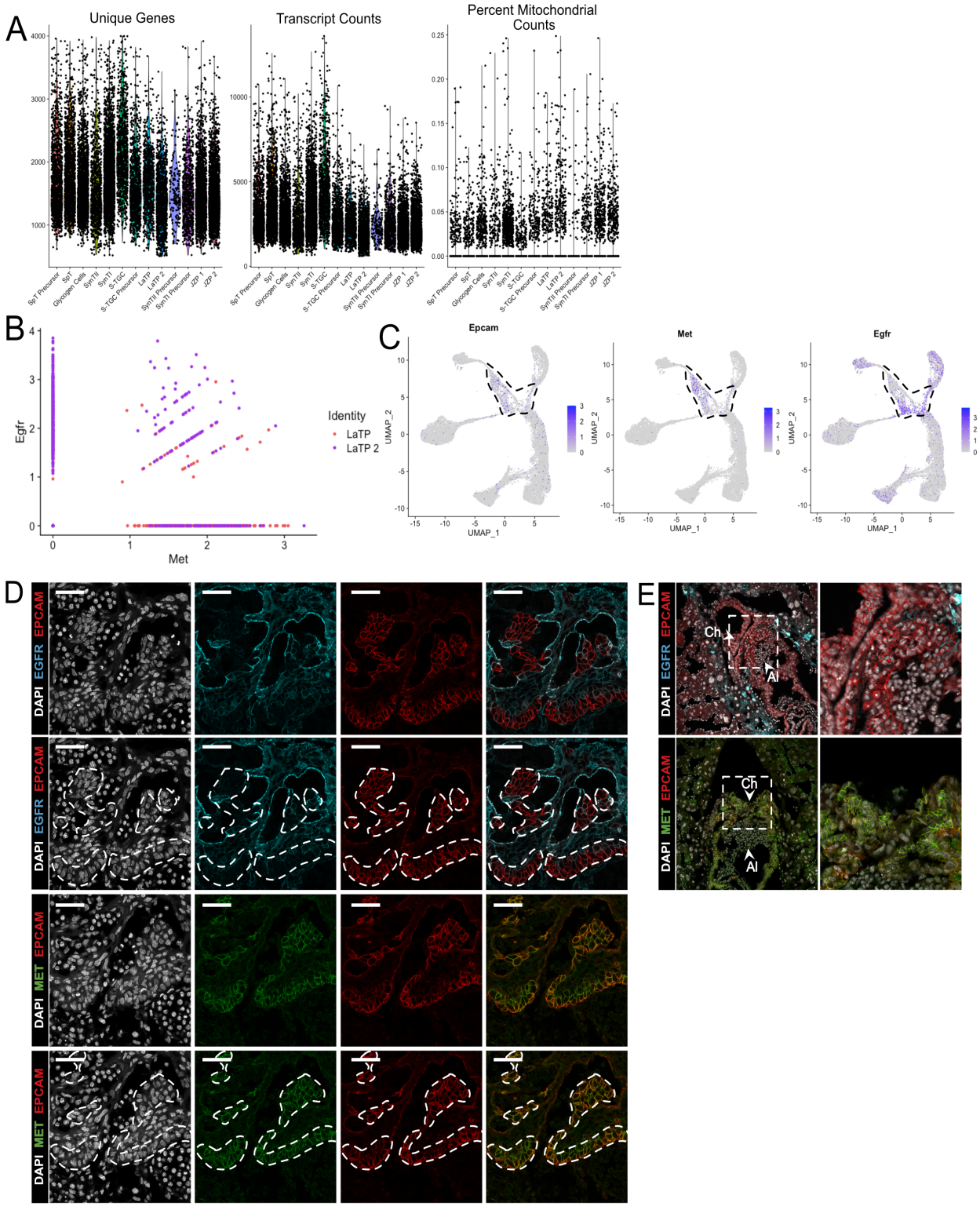

Figure 2.4 - Trophoblast subset metrics and LaTP subcluster localization.
(A) Violin plots showing the number of unique genes (left), number of transcripts (middle), and the percent of reads mapping to mitochondrial genes (right) for each cluster identified in the trophoblast dataset in Figure 2.2A. (B) Scatter plot of expression

of *Egfr* and *Met* in LaTP and LaTP2 clusters showing *Egfr* expression to be highly enriched in LaTP2. (C) Expression of *Epcam* RNA projected in trophoblast nuclei. LaTP and LaTP 2 clusters are outlined by the dotted line. (D) Immunofluorescence staining of EPCAM and EGFR (top two rows) or EPCAM and MET (bottom two row). White dashed lines outline EPCAM expression as a marker of canonical LaTPs. MET expression colocalizes with EPCAM and represent the LaTP cluster. EGFR and EPCAM domains are largely non-overlapping, with EGFR expressing cells representing the distinct LaTP2 cluster. EGFR is also expressed in mature SynTII. (E) Immunofluorescence staining of EPCAM and EGFR or EPCAM and MET at E8.5. Arrows denote the allantois (Al) and the chorion (Ch). The white box denotes the inset at right.

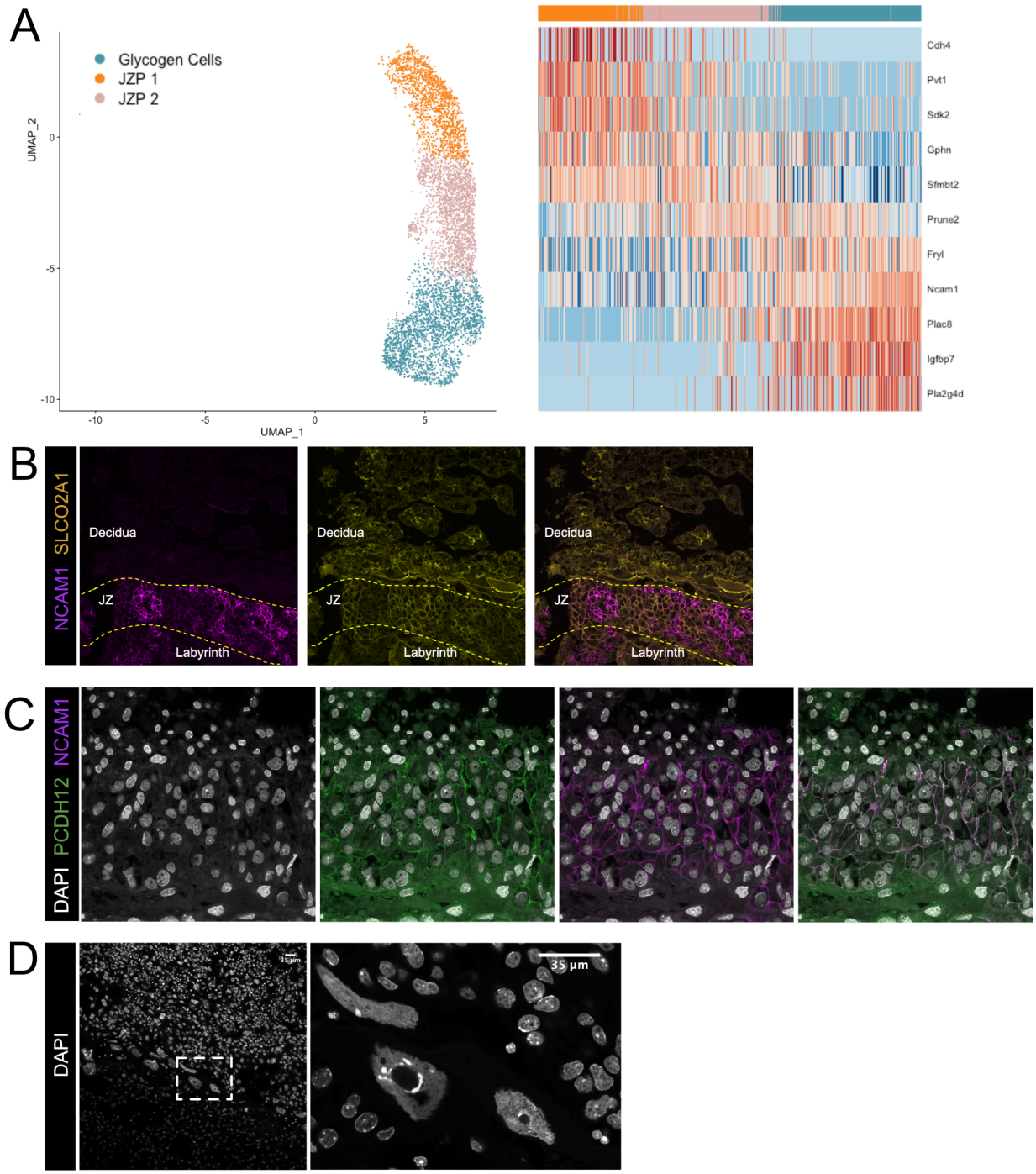

Figure 2.5 - Localization of JZ clusters.
(A) Nuclei along the differentiation from JZP1 to GCs were ordered by pseudotime using Slingshot. The nuclei included along each pseudotime axis shown at left. The expression of select genes (y-axis) representing differentiation are shown in heatmap (right). Each column represents a nucleus organized in pseudotime proceeding from left to right along the x-axis. (B) Immunofluorescence staining of sections from E12.5 placentas for Ncam1

(Purple) and Slco2a1 (Yellow). Dashed lines separate boundaries between placental regions (Labyrinth, JZ – Junctional Zone, and Decidua). (C) Immunofluorescence staining of sections from E12.5 placentas for Pcdh12 (Green) and Ncam1 (D) DAPI staining in E12.5 placental sections. Dashed box outlines the magnified region shown at left.

A

Genes	Expression (Simmons et al. 2008)	Expression in this study
Prl3b1	Spongiotrophoblast	Both (higher in SpT)
Prl2c	Spongiotrophoblast	SpT (low expression - Prl2c2)
Prl8a1	Spongiotrophoblast	SpT
Prl8a6	Spongiotrophoblast	SpT
Prl8a8	Spongiotrophoblast	Both
Prl7a2	Spongiotrophoblast	Both (higher in SpT)
Prl3a1	Spongiotrophoblast	SpT
Prl2b1	Spongiotrophoblast	Both
Prl5a1	Spongiotrophoblast	Not detected
Pcdh12	Glycogen Cell	Glycogen Cell
Prl6a1	Glycogen Cell	Glycogen Cell (low expression)
Prl2a1	Glycogen Cell	Glycogen Cell (low expression)
Prl7b1	Glycogen Cell	Glycogen Cell (low expression)
Prl7c1	Glycogen Cell	Glycogen Cell (low expression)
Tpbpa	Both	Both
Prl4a1	Both	Not detected
Prl8a9	Both	Both (higher in SpT)
Prl7d1	Both	Both

B

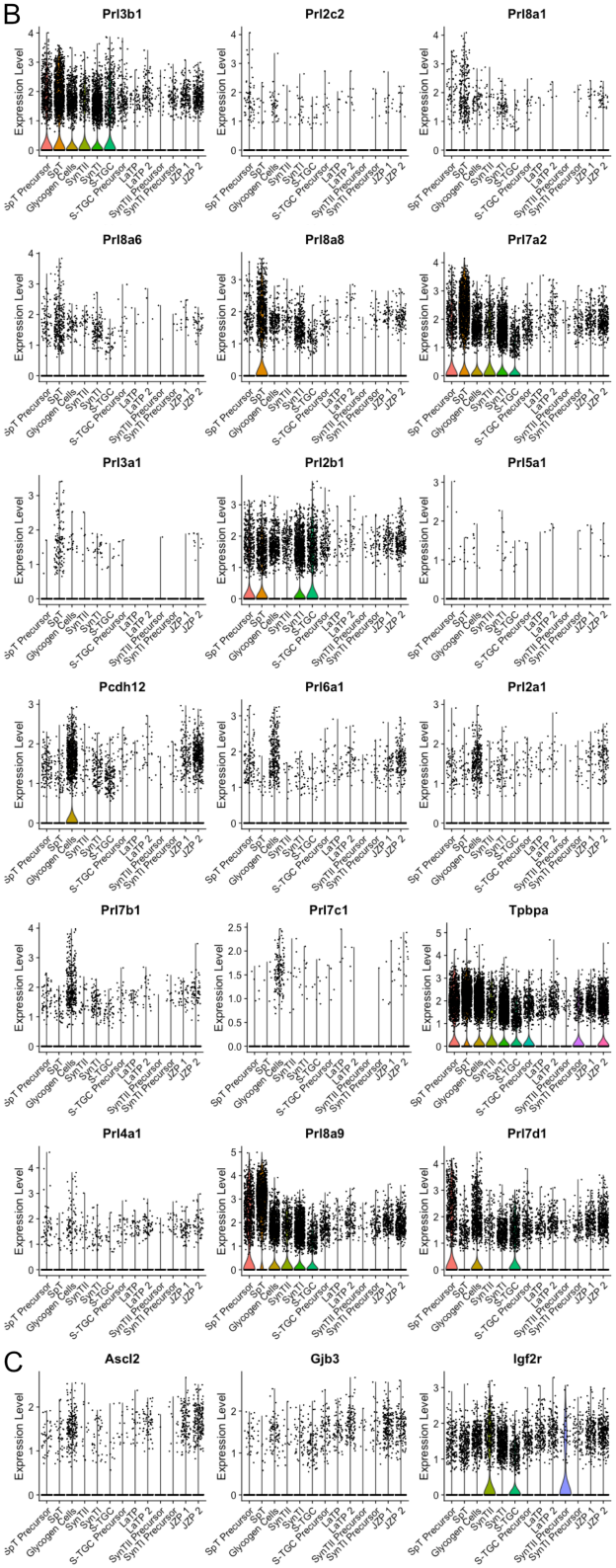

C

Figure 2.6 - Junctional Zone Markers

(A) Table of Prolactin gene expression in either Spongiotrophoblast or Glycogen Cells from Simmons et al. 2008 and their expression in the snRNA-seq data. (B) Violin plots showing the expression of the prolactin genes in (A). (C) Violin plots showing the expression of additional canonical markers Pcdh12, Tpbpa, Ascl2, Gjb2, and Igf2r.

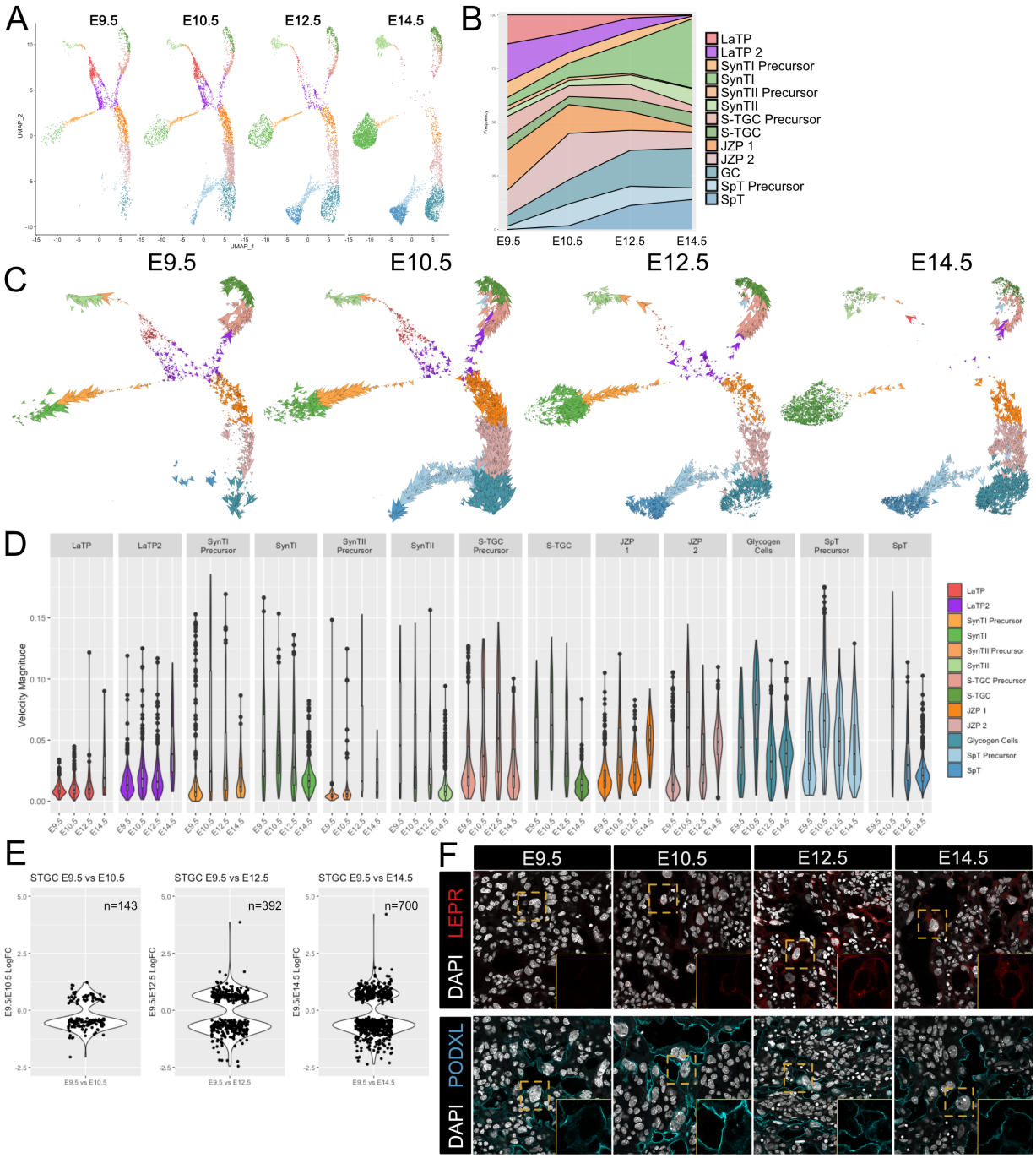

Figure 2.7 - Developmental time course and trajectory inference reveal details of lineage dynamics and commitment in trophoblast.
(A) UMAP projection of all nuclei captured at each gestational age. (B) Quantification of the proportion of each cluster captured at each developmental time point. (C) RNA velocity vectors of the trophoblast nuclei at each time point. Arrows show the estimated magnitude and direction of each nucleus in pseudotime. (D) The magnitude of velocity vectors shown in D summarized as violin plots, with nuclei split by cluster identity and

developmental time point. (E) Violin plots showing the log2 fold change of differentially expressed genes between nuclei from S-TGC at E9.5 vs. each other timepoint. (F) Immunofluorescence staining of LEPR (top) and PODXL (bottom) in the placental labyrinth at each developmental timepoint at 63x. Insets, magnification of area surrounding a S-TGC indicated by dotted line, DAPI stain removed to highlight protein expression.

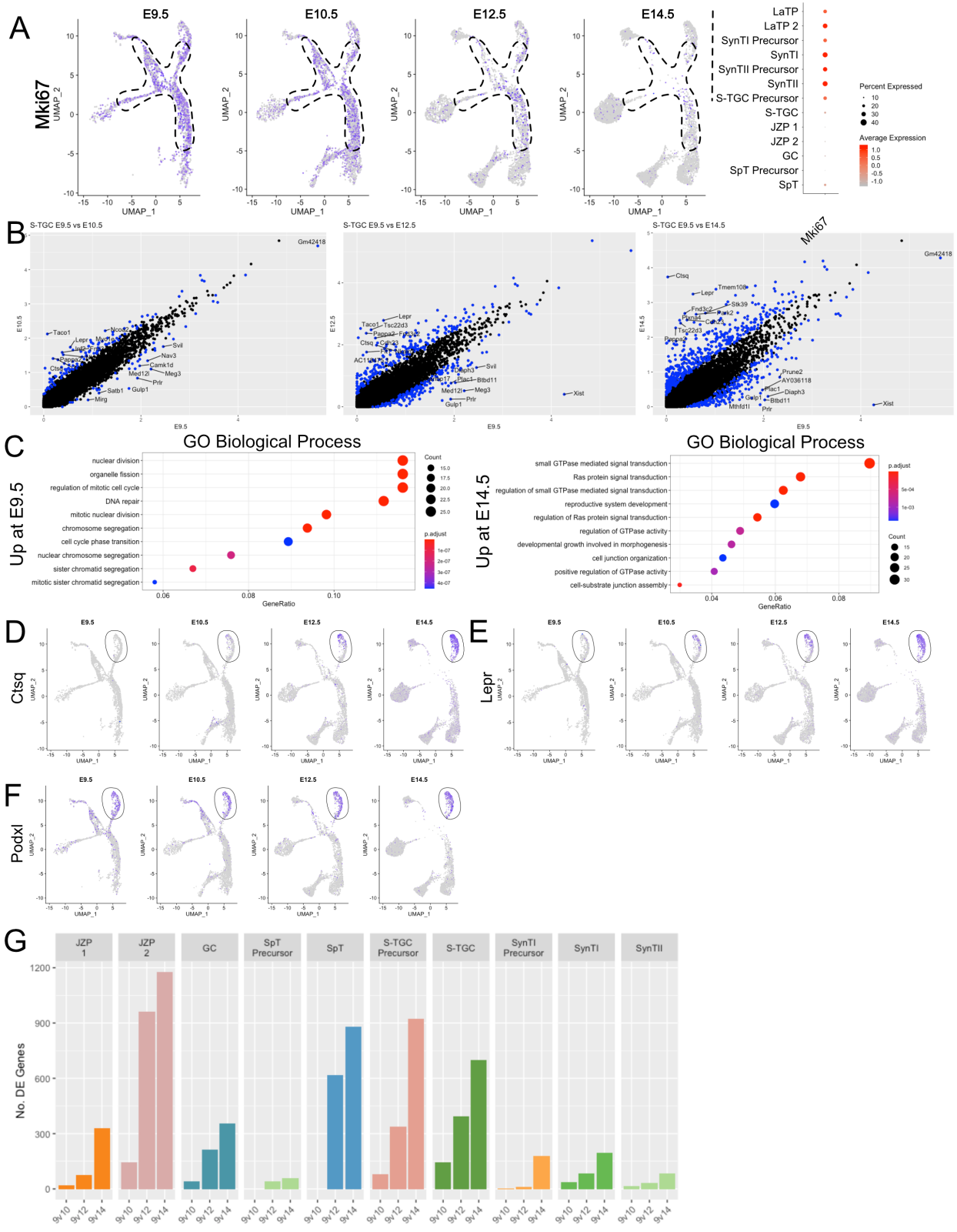
A
E9.5
E10.5
E12.5
E14.5
Mki67
UMAP_1
UMAP_2
LaTP
LaTP 2
SynTI Precursor
SynTI
SynTII Precursor
SynTII
S-TGC Precursor
S-TGC
JZP 1
JZP 2
GC
SpT Precursor
SpT
Percent Expressed
Average Expression
B
S-TGC E9.5 vs E10.5
S-TGC E9.5 vs E12.5
S-TGC E9.5 vs E14.5
Mki67
Gm42418
Xist
C
GO Biological Process
Up at E9.5
nuclear division
organelle fission
regulation of mitotic cell cycle
DNA repair
mitotic nuclear division
chromosome segregation
cell cycle phase transition
nuclear chromosome segregation
sister chromatid segregation
mitotic sister chromatid segregation
GeneRatio
Count
p.adjust
GO Biological Process
Up at E14.5
small GTPase mediated signal transduction
Ras protein signal transduction
regulation of small GTPase mediated signal transduction
reproductive system development
regulation of Ras protein signal transduction
regulation of GTPase activity
developmental growth involved in morphogenesis
cell junction organization
positive regulation of GTPase activity
cell-substrate junction assembly
GeneRatio
p.adjust
Count
D
Ctsq
E
Lepr
F
Podxl
G
JZP 1
JZP 2
GC
SpT Precursor
SpT
S-TGC Precursor
S-TGC
SynTI Precursor
SynTI
SynTII
No. DE Genes
9v10
9v12
9v14

Figure 2.8 - Time resolved differences in S-TGC
(A) Expression of Mki67 projected in UMAP space at each time point (left). The dotted line outlines the progenitor populations LaTP, LaTP2, SynTI Precursor, SynTII Precursor, and JZP 1/2. Quantification, shown as a dot blot representing percent cells expressing (increasing with dot size) and average expression (increasing with red color) of *Mki67* in each cell population combined across all timepoints (right). (A) Scatter plot of differential expression (log2 fold change) in S-TGC nuclei comparing expression at E9.5 on the x-axis with E10.5 (left), E12.5 (middle), and E14.5 (right). Each dot represents a gene and significantly differentially expressed genes are colored blue (adj. P-value <0.05, 100 permutations). The top 10 differentially expressed genes by log2FC in either direction are labeled. (B) Gene Ontology (Biological Process) of genes upregulated at E14.5 vs E9.5 (left) and genes upregulated at E9.5 vs E14.5 (right) (adj. P-value < 0.05, logFC > 0.5). GeneRatio is the of the number of genes in the given ontology divided by the number of genes found in any ontology. (D-F) Expression of *Ctsq* (D), *Lepr* (E), *Podxl* (F) across trophoblast cells represented on UMAP plot at each developmental time point. The S-TGC population is circled by a solid line. (G) The number of differentially expressed genes (y-axis) between each timepoint for each cluster (with greater than 50 nuclei captured at each timepoint).

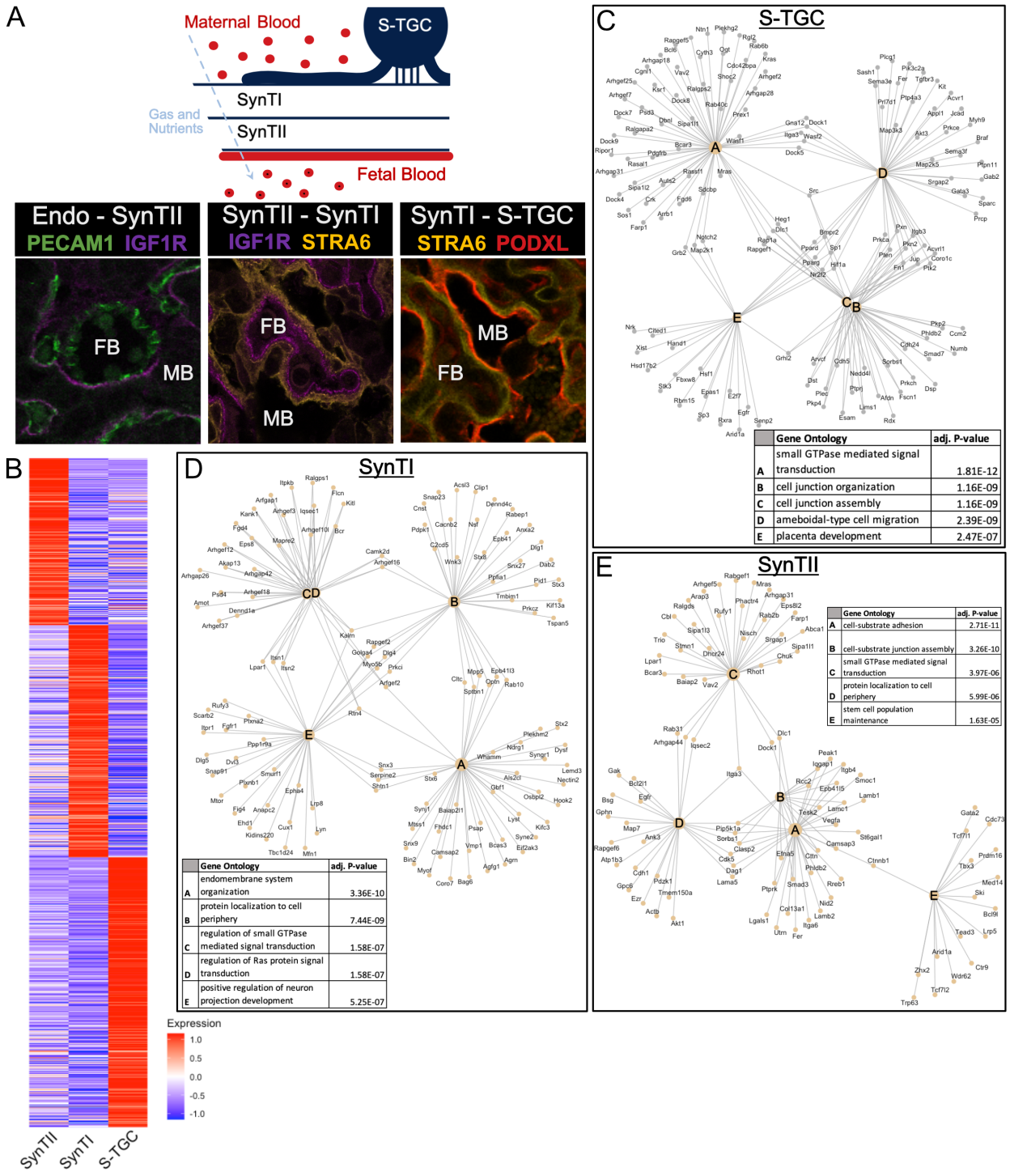

Figure 2.9 - Defining distinct roles of the trophoblast subtypes at the gas exchange interface.

(A) Schematic showing the relative location of the cell types at the gas and nutrient exchange interface of the labyrinth – S-TGC, SynTI, SynTII, (sometimes referred to as Trophoblast layer I, II, and III, respectively) and the fetal endothelium (top). Immunofluorescence staining resolving expression in each pair of neighboring cell types

– Endothelial/SynTII, SynTII/SynTI, and SynTI/S-TGC in E12.5 mouse placenta sections. (B) Heatmap of all differentially expressed genes by log fold change in SynTI, SynTII, and S-TGC clusters. (C-E) Network diagrams showing the top 5 Gene Ontology (Biological Process) enriched in marker genes (adj. P-value < 0.05, logFC > 0.5) in each cluster. Gene ontology categories are nodes and associated marker genes are annotated. Adjusted P-values for enrichment are listed in the table insets.

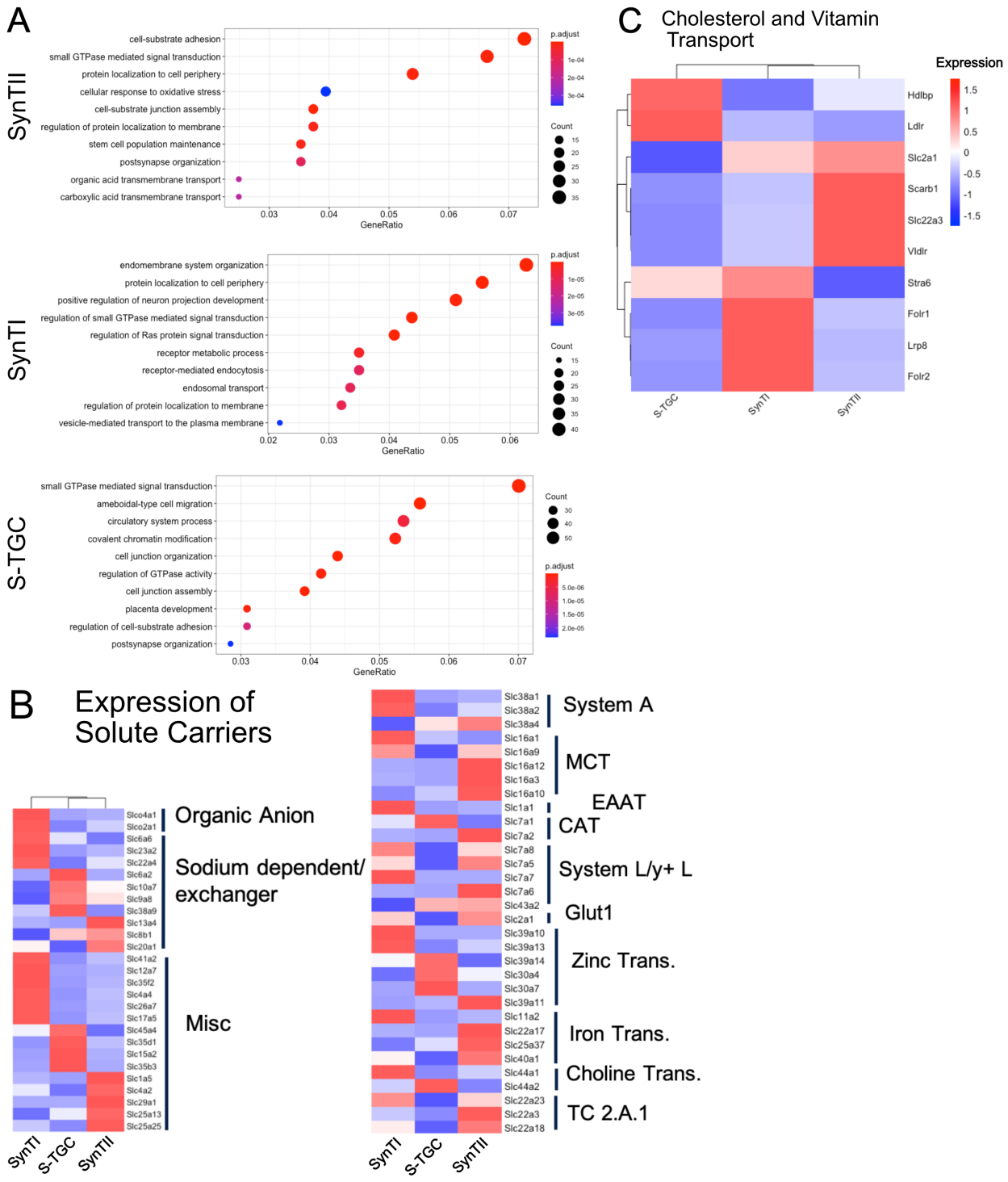

Figure 2.10 - Division of cellular function and nutrient transport in the labyrinth. (A) Gene Ontology (Biological Process) of differentially expressed genes SynTII (top), SynTI (middle), S-TGC (bottom). Significantly differentially expressed genes are defined by adj. P-value < 0.05 and logFC > 0.5. GeneRatio is the of the number of genes found the given ontology divided by the number of genes found in any ontology category. (B)

Heatmap of scaled expression all solute transporters showing differential expression (adj. P-value < 0.05) in SynTI, SynTII, S-TGC compared to all other trophoblast clusters. Genes are organized and annotated by class of transporter. (C) Heatmap of scaled expression of select genes involved in vitamin and cholesterol transport.

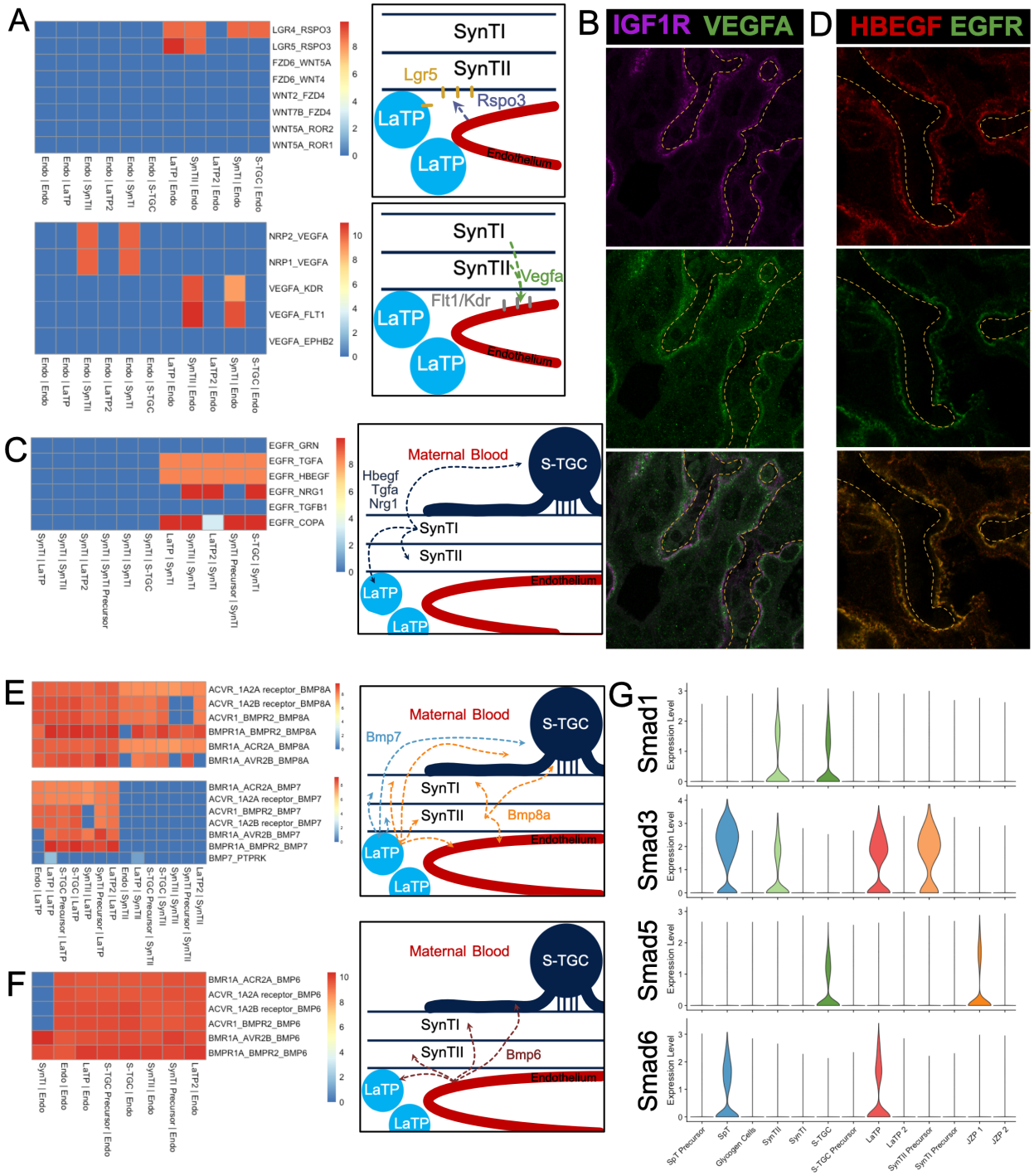

Figure 2.11 - Predicting Cell Signaling within the placental labyrinth.
(A) Heatmap showing all Wnt signaling interactions (top) and Vegf signaling (bottom) between the endothelium and labyrinth trophoblast populations. Left: schematics summarizing signaling interactions. (B) Immunofluorescence staining for VEGFA and IGF1R demonstrating colocalization in SynTII in E12.5 mouse placenta sections (63x). Fetal Vessels are outlined in yellow dashed line. (C) Heatmap showing all Egfr signaling

interactions between labyrinth populations. Schematic showing secretion of Egf ligands *Hbegf*, *Tgfa*, and *Nrg1* from SynTI to *Egfr* expressed on SynTII, LaTP, and S-TGC. (D) Immunofluorescence staining for HBEGF and EGFR demonstrating colocalization of the ligand and receptor SynTII, but only HBEGF expression in SynTI (E12.5 mouse placenta sections - 63x) (E) Heatmap showing signaling interactions of *Bmp8a* (top) and *Bmp7* (bottom), secreted by the LaTP and SynTII or LaTP only, respectively. (F) Heatmap showing predicted signaling interactions between *Bmp6* secreted by the endothelium to receptors on LaTP, SynTI, SynTII and S-TGC. (G) Transcript expression for the *Smad* TFs which are differentially regulated (*Smad1*/*3*/*5*/*6*).

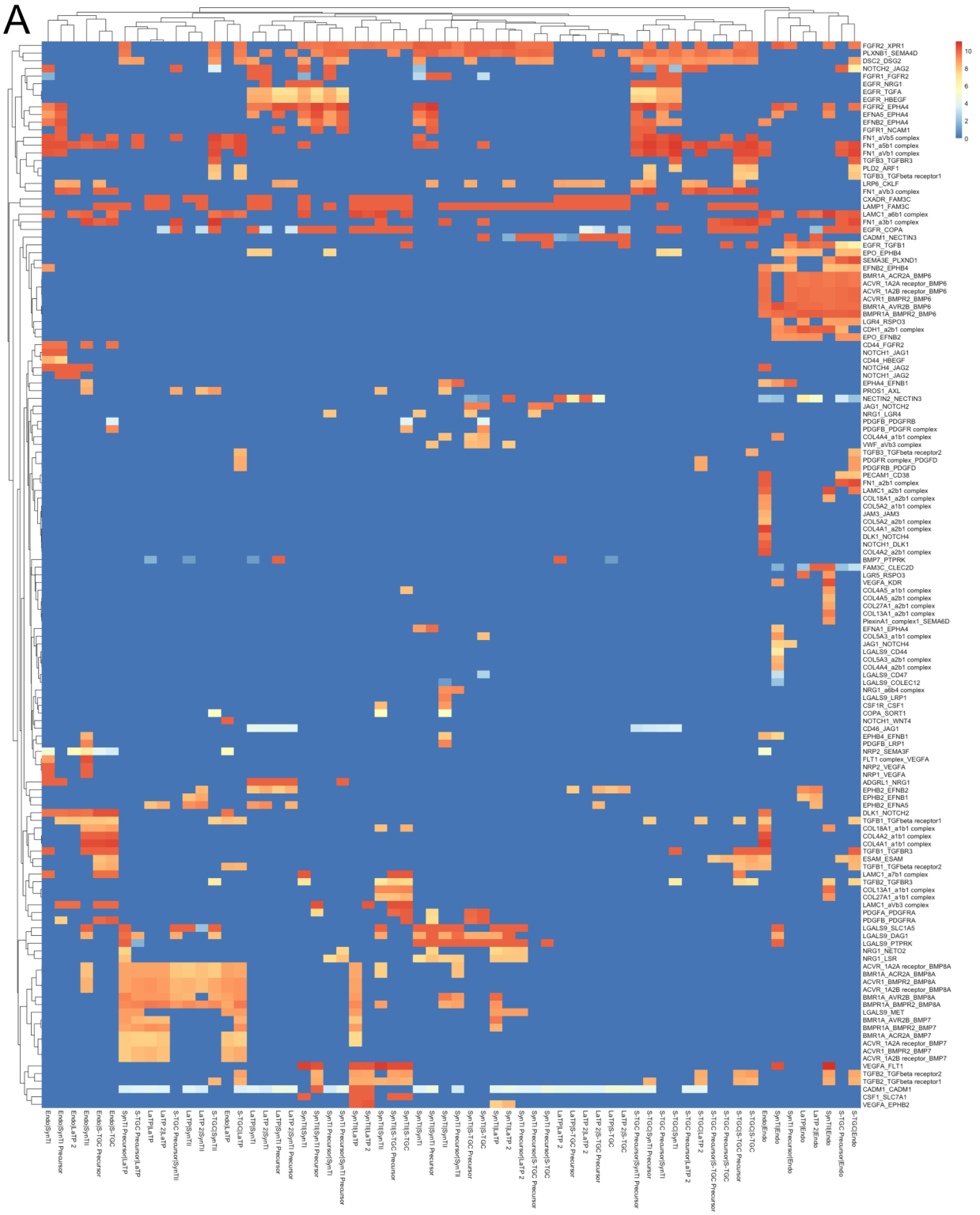

Figure 2.12 - Complete CellPhoneDB results
(A) Heatmap of 139 ligand-receptor interactions predicted by CellPhoneDB (p-value < 0.05 permutation test). The rows are Ligand-receptor pairs and columns are cell-cell pairings. Strength of interaction is shown by coloration. All interactions not reaching significance have a strength of zero (blue).

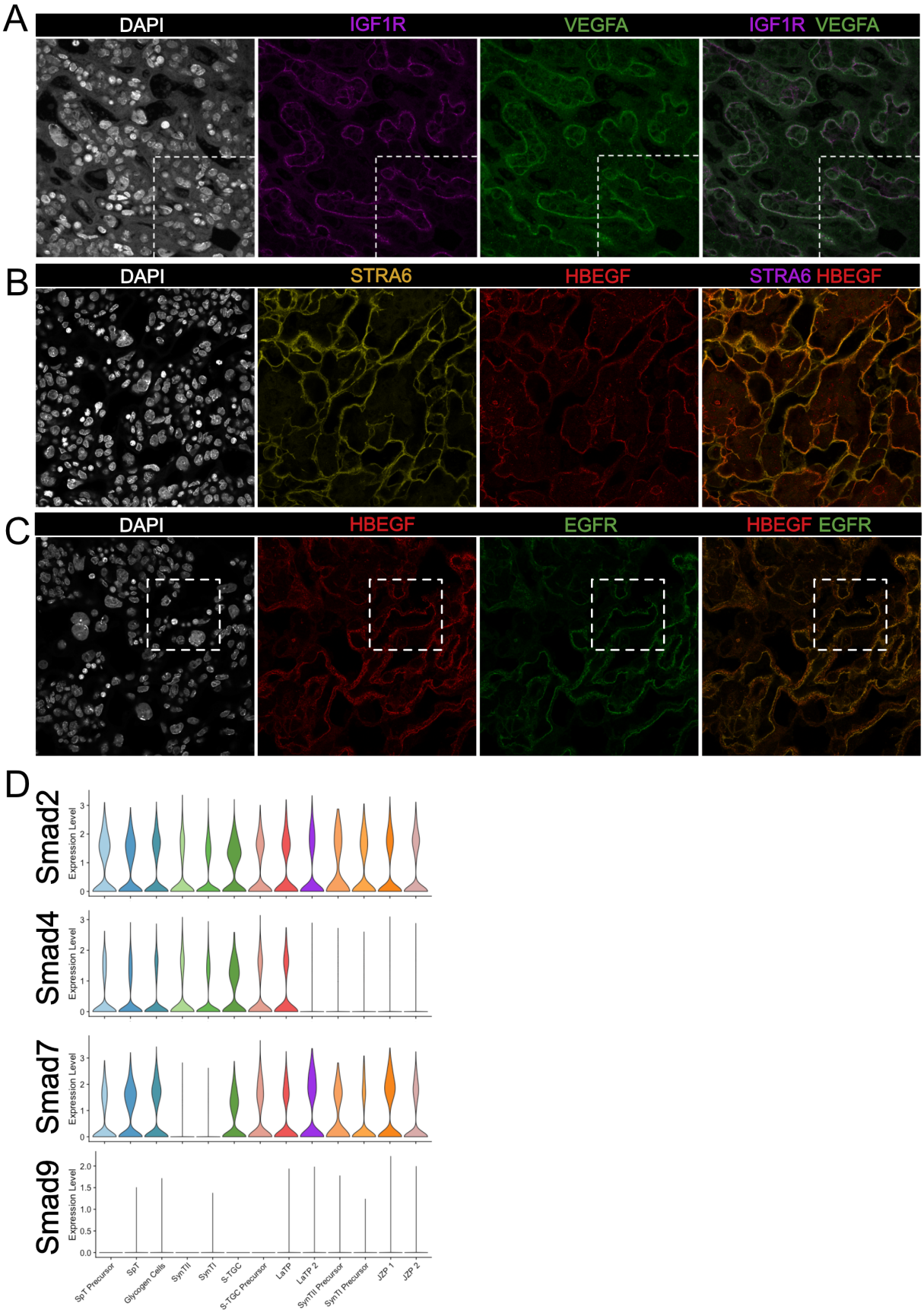
A
DAPI
IGF1R
VEGFA
IGF1R VEGFA
B
DAPI
STRA6
HBEGF
STRA6 HBEGF
C
DAPI
HBEGF
EGFR
HBEGF EGFR
D
Smad2
Smad4
Smad7
Smad9
Expression Level
SpT Precursor
SpT
Glycogen Cells
SynTII
SynTI
S-TGC
S-TGC Precursor
LaTP
LaTP 2
SynTII Precursor
SynTI Precursor
JZP 1
JZP 2

Figure 2.13 - Representative images supporting Figure 2.11.
(A-C) Immunofluorescence staining of sections from E12.5 placentas of (A) IGF1R (Purple) and VEGFA (Green); (B) STRA6 (Yellow) and HBEGF (Red); HBEGF (Red) and EGFR (Green) . The white dashed line in (A) and (B) outline the magnified areas shown in Fig 2.5B and Figure 2.11D, respectively. Fetal vessels are outlined by the yellow dashed lines. (D) Violin plots summarizing expression of *Smad2*/*4*/*7*/*9* in each trophoblast cluster.

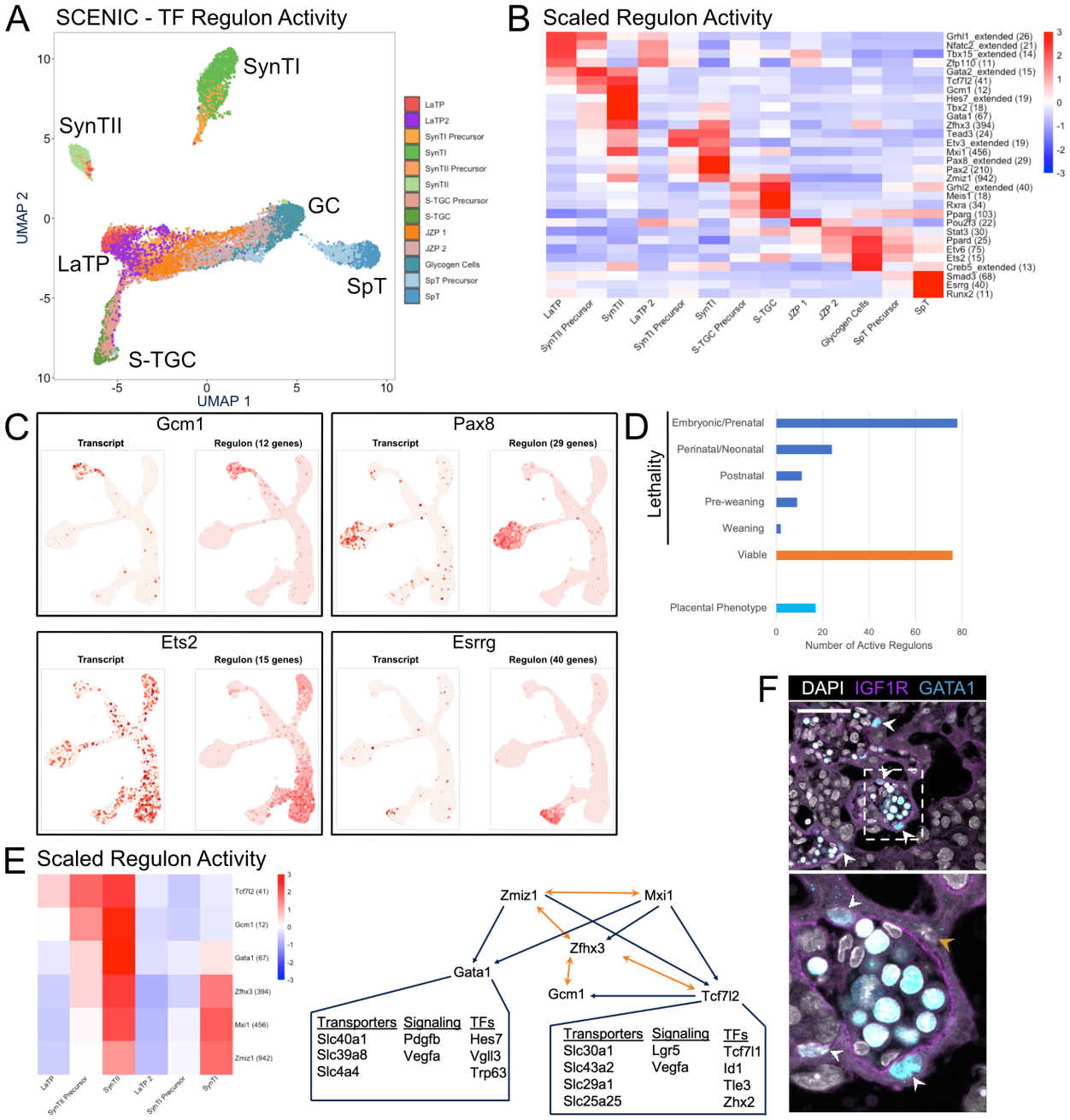

Figure 2.14 - Modeling transcription factor regulon activity identifies new candidate regulators of SynTII.

(A) UMAP projection derived from regulon activity predicted by SCENIC. The clusters are colored according to Seurat clustering of transcript data. The cluster identities of each of the five arms of the UMAP are annotated. (B) Heatmap of the scaled regulon activity for select regulons expressed in each trophoblast population. The number of genes predicted to be regulated by each transcription factor is included in parenthesis. (C) Comparison of transcript expression of the TF (left) and the regulon activity for that TF (right) at the single cell resolution projected in UMAP space for *Gcm1*, *Pax8*, *Ets2*, and *Esrrg*. The number of genes predicted to be regulated by each transcription factor

is denoted in parentheses. (D) Quantification of the number active regulons with a lethal phenotype in mouse according to the Jackson Laboratory MGI (Embryonic/Prenatal - 78, Perinatal/Neonatal - 24, Postnatal - 11, Pre-weaning - 9, lethality at weaning - 2, no developmental lethality - 76) and the number with known placental phenotypes *in vivo* (n=17). (E) Heatmap showing expression of a network of regulons enriched for expression in SynTII (left). Gene regulatory network of high confidence predicted interactions from GRNboost2 (right). Unidirectional regulation denoted by blue arrows and bidirectional regulation by yellow. Predicted targets of *Gata1* and *Tcf7l2* expressed in SynTII and important in SynTII differentiation or function are annotated. (F) Immunofluorescence staining for GATA1 and IGF1R showing GATA1 expressing nuclei in IGF1R SynTII cells (E12.5 mouse placenta sections - 63x). GATA1+ SynTII nuclei – white arrowheads, GATA1- putative SynTI nucleus – yellow arrowhead.

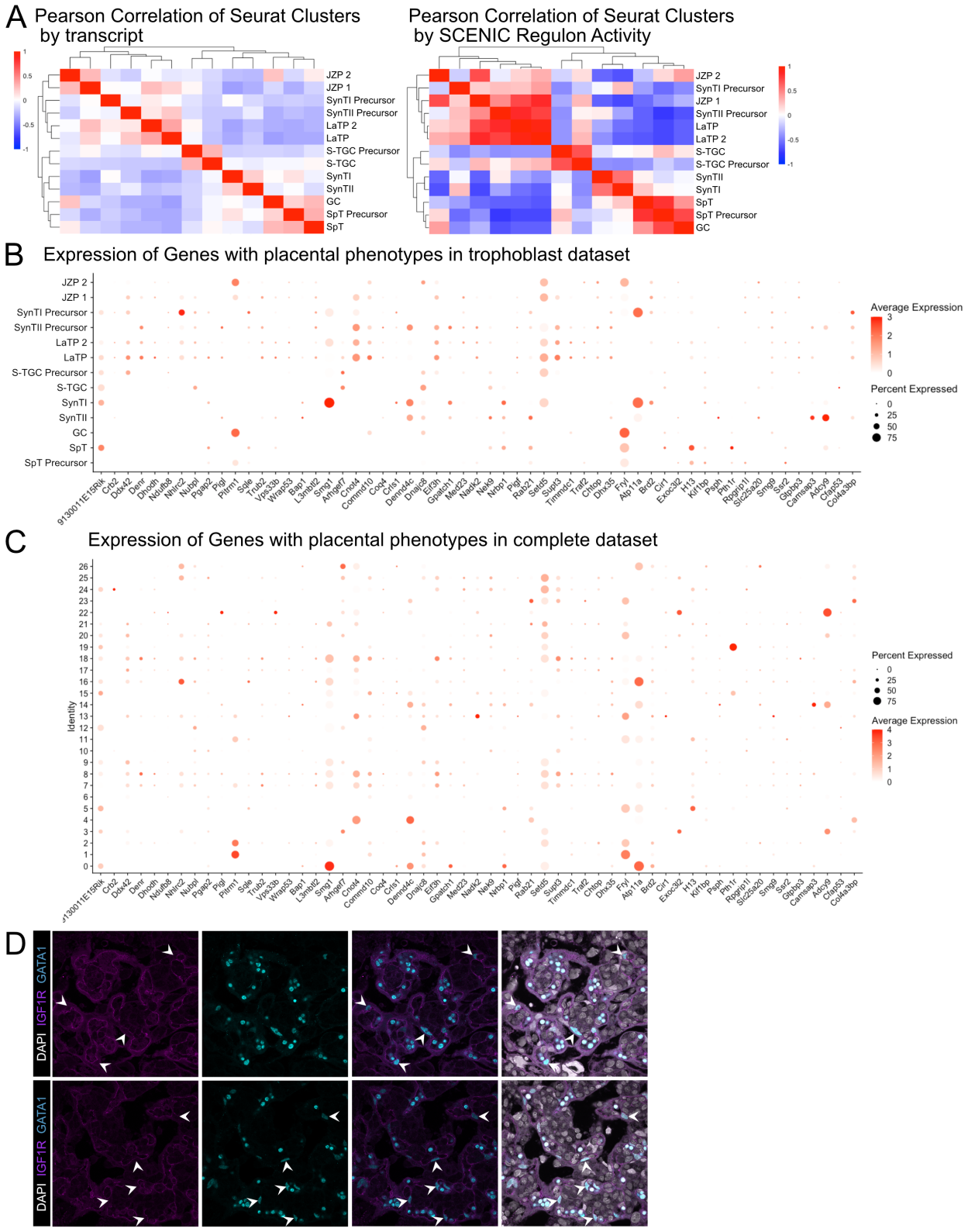

Figure 2.15 - Expression of Genes and TFs with placental phenotypes.
(A) Heatmaps showing the Pearson correlation values between cluster averages of transcript expression (left) and SCENIC regulon activity (right). Clusters are ordered by

hierarchical clustering with complete linkage. (B) Dot plot showing the average expression and percent of the nuclei in each cluster of all subviable genes with placental phenotypes from Perez-Garcia, V. et al. 2018 in the trophoblast clusters from Figure 2.2. (C) Dot plot showing the average expression and percent of the nuclei in each cluster of all subviable genes with placental phenotypes from Perez-Garcia, V. et al. 2018 in the conglomerate dataset clusters from Figure 2.1. (D) Additional immunofluorescence staining of GATA1 and Igfr1 at E12.5.

Methods

Animal Husbandry: All mice were maintained according to the UCSF guidelines and the Laboratory Animal Resource Center standards. All experiments were reviewed and approved by the UCSF Institutional Animal Care and Use Committee. To generate all placentas C57Bl/6J males between 3-6 months of age were bred to C57Bl/6J females between 6-12 weeks of age (Jackson Laboratory, Bar Harbor, ME). Developmental staging was assessed by days post coitum (dpc) and confirmed by embryo morphology.

Placental Dissection: Each placenta sample was dissected in 1x PBS at 4°C. The yolk sac and allantois were removed from the basal chorionic plate using forceps. The outermost layers of the decidua were also removed, taking care to not disrupt the cells of the labyrinth or junctional zone of the fetal placenta. Sample passing these criteria were used in nuclei isolation below

Nuclei Isolation: Whole dissected placental samples were placed in a 40mm plastic dish with 1mL of Nuclei EZ lysis buffer (Sigma-Aldrich, St.Louis, MO - NUC-101) and reduced to small pieces of tissues (<1mm) using a razor blade. The solution containing the tissue was then transferred to a dounce homogenizer and 1mL of Nuclei EZ lysis buffer added. The nuclei were lysed into solution by 10 strokes of the loose pestle (A) and 10 strokes of the tight pestle (B). Using a wide bore pipette the solution was transferred to a 15mL falcon tube, 2mL of Nuclei EZ lysis buffer added, and incubated on wet ice for 5 minutes with gentle mixing with a pipette. The solution was then passed through a 35uM filter and centrifuged at 500g for 5 minutes at 4°C. The resulting supernatant was removed, the

pellet gently resuspended in 1.5mL of Nuclei EZ lysis buffer and incubated on ice for 5 minutes, then centrifuged at 500g for 5 minutes at 4°C. The supernatant was removed and 1mL of Nuclei Wash and Resuspension Buffer (1x PBS, 1.0% BSA, 0.2 U/µl RNase Inhibitor) added without mixing or resuspension and incubated on ice for 5 minutes. After the incubation an additional 1mL of Nuclei Wash and Resuspension Buffer was added and the pellet gently resuspended. The solution was then centrifuged at 500g for 5 minutes at 4°C (in a swinging bucket rotor to prevent nuclei adhering to the sides of the tube), the supernatant discarded, and the nuclei resuspended in 1mL of Nuclei Wash and Resuspension Buffer. This final nuclei solution was passed through a 35uM filter and nuclei visually inspected on a hemocytometer to assess, morphology, damage, and aggregation. Finally, 1uL of DAPI stock solution (10ug/mL) was added to the nuclei solution in preparation for FACS.

FAC-sorting of Nuclei into 10x Genomic Reagents for transcriptome Capture: All cell sorting was performed on a FACS Aria II (BD Biosciences, San Jose, CA) using a 70uM nozzle. Nuclei sorting was performed according to steps outlined here - https://www.protocols.io/view/frankenstein-protocol-for-nuclei-isolation-from-f-3fkgjkw/abstract

Nuclei were sorted in the Nuclei Wash and Resuspension Buffer (described above) plus DAPI. 17,500 nuclei yielding a strong DAPI signal and DNA content profile were sorted into one well of a 96-well plate containing 10x Genomics V3 GEM mastermix without RT Enzyme C (20.0 uL RT Reagent Mix, 3.1 uL Template Switch Oligo, 2.0 uL Reducing Agent B, 27.1 uL nuclease free H2O). The volume of 17,500 sorted nuclei was previously

established to be 19.5uL. Immediately post sorting 8.3 uL of RT Enzyme C (10x Genomics, Pleasanton, CA) was added to the sample, and transcriptome collection on the 10x Chromium V3 platform performed

Single Cell RNA Sequencing and Analysis: To capture the transcriptome of individual nuclei we used the Chromium Single Cell 3' Reagent V3 Kit from 10X Genomics. For all samples 17,500 nuclei were loaded into one well of a Chip B kit for GEM generation. Library preparation including, reverse transcription, barcoding, cDNA amplification, and purification was performed according to Chromium 10x V3 protocols. Each sample was sequenced on a NovaSeq 6000 S4 to a depth of approximately 20,000-30,000 reads per nucleus. The gene expression matrices for each dataset was generated using the CellRanger software (v3.0.2 - 10x Genomics). A custom premRNA GTF was generated to create an intron-exon reference according to 10x Genomics recommendations and all reads aligned to mm10 using STAR. (https://support.10xgenomics.com/single-cell-gene-expression/software/pipelines/latest/advanced/references). The counts matrix was thresholded and analyzed in the package Seurat (v3.1.3). Nuclei with fewer than 500 or greater than 4000 unique genes, as well as all nuclei with greater than 0.25 percent mitochondrial counts, were excluded from all subsequent analyses. For each sample, counts were scaled and normalized using ScaleData and NormalizeData, respectively, with default settings and FindVariableFeatures used to identify the 2000 most variable genes as input for all future analyses. PCA was performed using RunPCA and significant PCs assessed using ElbowPlot and DimHeatmap. For individual analysis of each sample the number of PCs and the resolution parameter of FindClusters can be found in

Supplementary Table 1. Dimensionality reduction and visualization using UMAP was performed by RunUMAP. Differentially expressed genes were identified using FindAllMarkers. Integration of each timepoint into one dataset was performed using FindIntegrationAnchors and IntegrateData, both using 20 dimensions (after filtering each dataset for number of genes, mitochondrial counts, and normalizing as described above). Data scaling, PCA, selection of PCs, clustering and visualization proceeded as described above using 20 PCs and a resolution of 0.6. Each cluster was analyzed and clusters containing abnormal UMI and co-expression of multiple cell-type specific genes were determined to be enriched for doublets and removed from downstream analysis. The number of nuclei excluded represented an estimated doublet rate of ~3.9%. To generate the trophoblast only dataset, data from each timepoint was subset for only trophoblast clusters using the function SubsetData based upon annotations from marker genes identified by FindAllMarkers. Integration of the trophoblast only dataset was performed using the same integration methods above (using 20 dimensions for FindIntegrationAnchors and IntegrateData, and 20 PCs and a resolution of 0.6 for FindClusters and RunUMAP). Differentially expressed genes for each integrated dataset were identified using FindAllMarkers.

Slingshot: We used the Slingshot package to order cells for each SynTI, SynTII, and S-TGC lineage in pseudotime. Each lineage was subset and the 1000 most variable genes identified and used as input into the generalized linear model (GAM package). Expression is plotted for the top 200 most variable genes along each lineage and included in Supplementary data.

scVelo: RNA velocity analysis was applied to the entire conglomerate dataset using Velocyto to generate spliced and unspliced reads for all cells. This dataset was then subset for the trophoblast dataset introduced in Figure 2.3. The scVelo stochastic model was run with default settings and subset by each timepoint. The magnitudes were calculated from the UMAP cell embeddings.

Differential Expression between timepoints: To account for the different number of nuclei recovered within a cluster at each timepoint, we downsampled to the least number of cells collected and performed differential expression using FindMarkers function and repeated this for 100 random permutations of nuclei. Only genes found to be significant (adj. P-value <0.05) in all 100 permutations were retained in the final list of differentially expressed genes. To retain the power in the larger clusters we did not downsample all clusters to the same size. Therefore, the number of differentially expressed genes between timepoints cannot be compared between clusters.

Gene Ontology Analysis: Gene Onotology analysis was performed with clusterProfiler enrichGO function. The simplify function within this package was used to consolidate hierarchically related terms using a cutoff of 0.5. Terms were considered significantly enriched with an adjusted P-value of less than 0.05.

CellPhoneDB: Cluster annotations and counts data were used as input for CellPhoneDB with default settings (minimum of 10% of nuclei in a cluster expressing a gene, a p-value

cutoff of 0.05, and 10 permutations). The databases of receptor-ligand interactions were generated for human proteins, not for mouse. As such, we performed this analysis using orthogonal genes between species (a total of 724 genes in the CellPhoneDB receptor-ligand databases). However, this does not account for differences in receptor-ligand interactions that may be different between mouse and human. Raw data were analyzed and heatmaps generated in R using modified scripts from CellPhoneDB. For heatmaps, the mean values of each significant receptor-ligand pair are shown and we do not consider non-significant interactions, these have been given the mean value of zero.

Immunofluorescence: Placentas for cryosectioning were fixed in 4% PFA at 4°C for 8hrs, washed in 1x PBS, then submerged in 30% sucrose overnight at 4°C prior to embedding in OCT medium. Placentas were sectioned at 10uM for all conditions. In brief, slides were washed in 1x PBST (1x PBS, 0.05% Tween-20), blocked for 1hr (1x PBS 5% donkey serum + 0.3% TritonX), incubated in primary antibody diluted for 3 hours at room temperature (or overnight at 4°C), washed in 1x PBST, incubated in secondary antibody (Alexafluor 488, 594, and 680) for 1 hour at room temperature, incubated in DAPI for 10min at room temp, washed in 1x PBST, and mounted and sealed for imaging. Any antigen retrieval was performed prior to the blocking step by heating the slides in a 1x citrate buffer with 0.05% Tween-20 at 95C for 30 minutes. All antibodies and the dilutions are listed in the key resources table. All immunofluorescence staining was performed in n=3 biological replicates (3 distinct placentas) and representative image is shown.

Acknowledgements

We thank the members of the University of California – San Francisco National Center of Translational Research in Reproduction and Infertility for helpful comments during the design, execution, and publication of this project. A special thanks to Susan Fisher, Alex Pollen, and Peter Sudmant for insightful comments during data analysis and preparation on the manuscript. We would also like to thank all members of the Blelloch Lab for their comments and support, especially Brian DeVeale for help with data analysis and proofreading the manuscript. We would also like to acknowledge our finding source, the NIH Eunice Kennedy Shriver National Institute for Child Health and Human Development P50 HD055764.

Competing Interests

The authors declare no competing interests.

References

Adamson, S. L., Lu, Y., Whiteley, K. J., Holmyard, D., Hemberger, M., Pfarrer, C., & Cross, J. C. (2002). Interactions between trophoblast cells and the maternal and fetal circulation in the mouse placenta. Developmental Biology. https://doi.org/10.1016/S0012-1606(02)90773-6

Aiba, Y., Yamazaki, T., Okada, T., Gotoh, K., Sanjo, H., Ogata, M., & Kurosaki, T. (2006). BANK negatively regulates Akt activation and subsequent B cell responses. Immunity. https://doi.org/10.1016/j.immuni.2006.01.002

Aibar, S., González-Blas, C. B., Moerman, T., Huynh-Thu, V. A., Imrichova, H., Hulselmans, G., Rambow, F., Marine, J. C., Geurts, P., Aerts, J., Van Den Oord, J., Atak, Z. K., Wouters, J., & Aerts, S. (2017). SCENIC: Single-cell regulatory network inference and clustering. Nature Methods. https://doi.org/10.1038/nmeth.4463

Anson-Cartwright, L., Dawson, K., Holmyard, D., Fisher, S. J., Lazzarini, R. A., & Cross, J. C. (2000). The glial cells missing-1 protein is essential for branching morphogenesis in the chorioallantoic placenta. Nature Genetics. https://doi.org/10.1038/77076

Aoki, M., Mieda, M., Ikeda, T., Hamada, Y., Nakamura, H., & Okamoto, H. (2007). R-spondin3 is required for mouse placental development. Developmental Biology. https://doi.org/10.1016/j.ydbio.2006.08.018

Bakken, T. E., Hodge, R. D., Miller, J. A., Yao, Z., Nguyen, T. N., Aevermann, B., Barkan, E., Bertagnolli, D., Casper, T., Dee, N., Garren, E., Goldy, J., Graybuck, L. T., Kroll, M., Lasken, R. S., Lathia, K., Parry, S., Rimorin, C., Scheuermann, R. H., … Tasic, B. (2018). Single-nucleus and single-cell transcriptomes compared in matched cortical cell types. PLoS ONE. https://doi.org/10.1371/journal.pone.0209648

Beliakoff, J., Lee, J., Ueno, H., Aiyer, A., Weissman, I. L., Barsh, G. S., Cardiff, R. D., & Sun, Z. (2008). The PIAS-Like Protein Zimp10 Is Essential for Embryonic Viability and Proper Vascular Development. Molecular and Cellular Biology. https://doi.org/10.1128/mcb.00771-07

Bergen, V., Lange, M., Peidli, S., Wolf, F. A., & Theis, F. J. (2019). Generalizing RNA velocity to transient cell states through dynamical modeling. BioRxiv. https://doi.org/10.1101/820936

Björndahl, M., Cao, R., Nissen, L. J., Clasper, S., Johnson, L. A., Xue, Y., Zhou, Z., Jackson, D., Hansen, A. J., & Cao, Y. (2005). Insulin-like growth factors 1 and 2 induce lymphangiogenesis in vivo. Proceedings of the National Academy of Sciences of the United States of America. https://doi.org/10.1073/pnas.0507865102

Butler, A., Hoffman, P., Smibert, P., Papalexi, E., & Satija, R. (2018). Integrating single-cell transcriptomic data across different conditions, technologies, and species. Nature Biotechnology. https://doi.org/10.1038/nbt.4096

Cao, Y., Linden, P., Farnebo, J., Cao, R., Eriksson, A., Kumar, V., Qi, J. H., Claesson-Welsh, L., & Alitalo, K. (1998). Vascular endothelial growth factor C induces

angiogenesis in vivo. Proceedings of the National Academy of Sciences of the United States of America. https://doi.org/10.1073/pnas.95.24.14389

Coan, P. M., Ferguson-Smith, A. C., & Burton, G. J. (2005). Ultrastructural changes in the interhaemal membrane and junctional zone of the murine choriollantoic placenta across gestation. Journal of Anatomy. https://doi.org/10.1111/j.1469-7580.2005.00488.x

Cross, J. C., Baczyk, D., Dobric, N., Hemberger, M., Hughes, M., Simmons, D. G., Yamamoto, H., & Kingdom, J. C. P. (2003). Genes, development and evolution of the placenta. In Placenta. https://doi.org/10.1053/plac.2002.0887

Dackor, J., Caron, K. M., & Threadgill, D. W. (2009). Placental and embryonic growth restriction in mice with reduced function epidermal growth factor receptor alleles. Genetics. https://doi.org/10.1534/genetics.109.104372

Ding, J., Adiconis, X., Simmons, S. K., Kowalczyk, M. S., Hession, C. C., Marjanovic, N. D., Hughes, T. K., Wadsworth, M. H., Burks, T., Nguyen, L. T., Kwon, J. Y. H., Barak, B., Ge, W., Kedaigle, A. J., Carroll, S., Li, S., Hacohen, N., Rozenblatt-Rosen, O., Shalek, A. K., … Levin, J. Z. (2020). Systematic comparison of single-cell and single-nucleus RNA-sequencing methods. Nature Biotechnology. https://doi.org/10.1038/s41587-020-0465-8

Du, X., Tabeta, K., Hoebe, K., Liu, H., Mann, N., Mudd, S., Crozat, K., Sovath, S., Gong, X., & Beutler, B. (2004). Velvet, a Dominant Egfr Mutation that Causes Wavy Hair

and Defective Eyelid Development in Mice. Genetics. https://doi.org/10.1534/genetics.166.1.331

Eaton, M., Davies, A. H., Devine, J., Zhao, X., Simmons, D. G., Maríusdóttir, E., Natale, D. R. C., Matyas, J. R., Bering, E. A., Workentine, M. L., Hallgrimsson, B., & Cross, J. C. (2020). Complex patterns of cell growth in the placenta in normal pregnancy and as adaptations to maternal diet restriction. PLoS ONE. https://doi.org/10.1371/journal.pone.0226735

Efremova, M., Vento-Tormo, M., Teichmann, S. A., & Vento-Tormo, R. (2020). CellPhoneDB: inferring cell–cell communication from combined expression of multi-subunit ligand–receptor complexes. Nature Protocols. https://doi.org/10.1038/s41596-020-0292-x

Fondacci, C., Alsat, E., Gabriel, R., Blot, P., Nessmann, C., & Evain-Brion, D. (1994). Alterations of human placental epidermal growth factor receptor in intrauterine growth retardation. Journal of Clinical Investigation. https://doi.org/10.1172/JCI117067

Georgiades, P., Fergyson-Smith, A. C., & Burton, G. J. (2002). Comparative developmental anatomy of the murine and human definitive placentae. In Placenta. https://doi.org/10.1053/plac.2001.0738

Gerdes, J., Lemke, H., Baisch, H., Wacker, H. H., Schwab, U., & Stein, H. (1984). Cell cycle analysis of a cell proliferation-associated human nuclear antigen defined by the monoclonal antibody Ki-67. Journal of Immunology (Baltimore, Md. : 1950).

Griewank, K., Borowski, C., Rietdijk, S., Wang, N., Julien, A., Wei, D. G., Mamchak, A. A. A., Terhorst, C., & Bendelac, A. (2007). Homotypic Interactions Mediated by Slamf1 and Slamf6 Receptors Control NKT Cell Lineage Development. Immunity. https://doi.org/10.1016/j.immuni.2007.08.020

Guetg, A., Mariotta, L., Bock, L., Herzog, B., Fingerhut, R., Camargo, S. M. R., & Verrey, F. (2015). Essential amino acid transporter Lat4 (Slc43a2) is required for mouse development. Journal of Physiology. https://doi.org/10.1113/jphysiol.2014.283960

Habib, N., Avraham-Davidi, I., Basu, A., Burks, T., Shekhar, K., Hofree, M., Choudhury, S. R., Aguet, F., Gelfand, E., Ardlie, K., Weitz, D. A., Rozenblatt-Rosen, O., Zhang, F., & Regev, A. (2017). Massively parallel single-nucleus RNA-seq with DroNc-seq. Nature Methods. https://doi.org/10.1038/nmeth.4407

Home, P., Ghosh, A., Parikshan, R., Ganguly, A., Bhattacharya, Md., Islam, R., Ray, S., Gunewardena, S., & Paul, S. (2019). Trophoblast paracrine signaling regulates placental hematoendothelial niche. BioRxiv. https://doi.org/10.1101/840660

Johnson, J. L., Najor, N. A., & Green, K. J. (2014). Desmosomes: Regulators of cellular signaling and adhesion in epidermal health and disease. Cold Spring Harbor Perspectives in Medicine. https://doi.org/10.1101/cshperspect.a015297

Kazanskaya, O., Ohkawara, B., Heroult, M., Wu, W., Maltry, N., Augustin, H. G., & Niehrs, C. (2008). The Wnt signaling regulator R-spondin 3 promotes angioblast and vascular development. Development. https://doi.org/10.1242/dev.027284

Kubaczka, C., Senner, C. E., Cierlitza, M., Araúzo-Bravo, M. J., Kuckenberg, P., Peitz, M., Hemberger, M., & Schorle, H. (2015). Direct Induction of Trophoblast Stem Cells from Murine Fibroblasts. Cell Stem Cell. https://doi.org/10.1016/j.stem.2015.08.005

Lake, B. B., Chen, S., Sos, B. C., Fan, J., Kaeser, G. E., Yung, Y. C., Duong, T. E., Gao, D., Chun, J., Kharchenko, P. V., & Zhang, K. (2018). Integrative single-cell analysis of transcriptional and epigenetic states in the human adult brain. Nature Biotechnology. https://doi.org/10.1038/nbt.4038

Lee, K. M., McNerney, M. E., Stepp, S. E., Mathew, P. A., Schatzle, J. D., Bennett, M., & Kumar, V. (2004). 2B4 Acts As a Non-Major Histocompatibility Complex Binding Inhibitory Receptor on Mouse Natural Killer Cells. Journal of Experimental Medicine. https://doi.org/10.1084/jem.20031989

Lee, T. C., & Threadgill, D. W. (2009). Generation and validation of mice carrying a conditional allele of the epidermal growth factor receptor. Genesis. https://doi.org/10.1002/dvg.20464

Liu, Y., Fan, X., Wang, R., Lu, X., Dang, Y. L., Wang, H., Lin, H. Y., Zhu, C., Ge, H., Cross, J. C., & Wang, H. (2018). Single-cell RNA-seq reveals the diversity of trophoblast subtypes and patterns of differentiation in the human placenta. Cell Research. https://doi.org/10.1038/s41422-018-0066-y

Liu, Z., Skafar, D. F., Kilburn, B., Das, S. K., & Armant, D. R. (2019). Extraembryonic heparin-binding epidermal growth factor-like growth factor deficiency compromises placentation in mice. Biology of Reproduction. https://doi.org/10.1093/biolre/ioy174

Luetteke, N. C., Qiu, T. H., Peiffer, R. L., Oliver, P., Smithies, O., & Lee, D. C. (1993). TGFα deficiency results in hair follicle and eye abnormalities in targeted and waved-1 mice. Cell. https://doi.org/10.1016/0092-8674(93)90228-I

Luo, Y., Kumar, P., Chen, C. C., Latham, J., Wang, L., Tudela, C., Alexander, J. M., Shelton, J. M., McKown, L., & Mendelson, C. R. (2014). Estrogen-related receptor γ serves a role in blood pressure homeostasis during pregnancy. Molecular Endocrinology. https://doi.org/10.1210/me.2014-1003

Maltepe, E., & Fisher, S. J. (2015). Placenta: The Forgotten Organ. Annual Review of Cell and Developmental Biology. https://doi.org/10.1146/annurev-cellbio-100814-125620

Martinez, F. O., & Gordon, S. (2014). The M1 and M2 paradigm of macrophage activation: Time for reassessment. F1000Prime Reports. https://doi.org/10.12703/P6-13

Matsuura, K., Jigami, T., Taniue, K., Morishita, Y., Adachi, S., Senda, T., Nonaka, A., Aburatani, H., Nakamura, T., & Akiyama, T. (2011). Identification of a link between Wnt/I 2-catenin signalling and the cell fusion pathway. Nature Communications. https://doi.org/10.1038/ncomms1551

Miettinen, P. J., Berger, J. E., Meneses, J., Phung, Y., Pedersen, R. A., Werb, Z., & Derynck, R. (1995). Epithelial immaturity and multiorgan failure in mice lacking epidermal growth factor receptor. Nature. https://doi.org/10.1038/376337a0

Morrish, D. W., Bhardwaj, D., Dabbagh, L. K., Marusyk, H., & Siy, O. (1987). Epidermal growth factor induces differentiation and secretion of human chorionic gonadotropin and placental lactogen in normal human placenta. Journal of Clinical Endocrinology and Metabolism. https://doi.org/10.1210/jcem-65-6-1282

Nelson, A. C., Mould, A. W., Bikoff, E. K., & Robertson, E. J. (2016). Single-cell RNA-seq reveals cell type-specific transcriptional signatures at the maternal-foetal interface during pregnancy. Nature Communications. https://doi.org/10.1038/ncomms11414

Nguyen, H., Merrill, B. J., Polak, L., Nikolova, M., Rendl, M., Shaver, T. M., Pasolli, H. A., & Fuchs, E. (2009). Tcf3 and Tcf4 are essential for long-term homeostasis of skin epithelia. Nature Genetics. https://doi.org/10.1038/ng.431

Paikari, A., Belair, C. D., Saw, D., & Blelloch, R. (2017). The eutheria-specific miR-290 cluster modulates placental growth and maternal-fetal transport. Development (Cambridge). https://doi.org/10.1242/dev.151654

Parsons, M. J., Brancaccio, M., Sethi, S., Maywood, E. S., Satija, R., Edwards, J. K., Jagannath, A., Couch, Y., Finelli, M. J., Smyllie, N. J., Esapa, C., Butler, R., Barnard, A. R., Chesham, J. E., Saito, S., Joynson, G., Wells, S., Foster, R. G., Oliver, P. L., … Nolan, P. M. (2015). The Regulatory Factor ZFHX3 Modifies Circadian Function in SCN via an at Motif-Driven Axis. Cell. https://doi.org/10.1016/j.cell.2015.06.060

Perez-Garcia, V., Fineberg, E., Wilson, R., Murray, A., Mazzeo, C. I., Tudor, C., Sienerth, A., White, J. K., Tuck, E., Ryder, E. J., Gleeson, D., Siragher, E., Wardle-Jones, H., Staudt, N., Wali, N., Collins, J., Geyer, S., Busch-Nentwich, E. M., Galli, A., …

Hemberger, M. (2018). Placentation defects are highly prevalent in embryonic lethal mouse mutants. Nature. https://doi.org/10.1038/nature26002

Pique-Regi, R., Romero, R., Tarca, A. L., Sendler, E. D., Xu, Y., Garcia-Flores, V., Leng, Y., Luca, F., Hassan, S. S., & Gomez-Lopez, N. (2019). Single cell transcriptional signatures of the human placenta in term and preterm parturition. ELife. https://doi.org/10.7554/eLife.52004

Poidatz, D., Dos Santos, E., Brulé, A., De Mazancourt, P., & Dieudonné, M. N. (2012). Estrogen-related receptor gamma modulates energy metabolism target genes in human trophoblast. Placenta. https://doi.org/10.1016/j.placenta.2012.06.002

Rampon, C., Prandini, M. H., Bouillot, S., Pointu, H., Tillet, E., Frank, R., Vernet, M., & Huber, P. (2005). Protocadherin 12 (VE-cadherin 2) is expressed in endothelial, trophoblast, and mesangial cells. Experimental Cell Research. https://doi.org/10.1016/j.yexcr.2004.08.024

Roberts, J. M., & Escudero, C. (2012). The placenta in preeclampsia. In Pregnancy Hypertension. https://doi.org/10.1016/j.preghy.2012.01.001

Satija, R., Farrell, J. A., Gennert, D., Schier, A. F., & Regev, A. (2015). Spatial reconstruction of single-cell gene expression data. Nature Biotechnology. https://doi.org/10.1038/nbt.3192

Shahbazi, M. N., Scialdone, A., Skorupska, N., Weberling, A., Recher, G., Zhu, M., Jedrusik, A., Devito, L. G., Noli, L., MacAulay, I. C., Buecker, C., Khalaf, Y., Ilic, D.,

Voet, T., Marioni, J. C., & Zernicka-Goetz, M. (2017). Pluripotent state transitions coordinate morphogenesis in mouse and human embryos. *Nature*. https://doi.org/10.1038/nature24675

Simmons, D. G., Fortier, A. L., & Cross, J. C. (2007). Diverse subtypes and developmental origins of trophoblast giant cells in the mouse placenta. Developmental Biology. https://doi.org/10.1016/j.ydbio.2007.01.009

Simmons, D. G., Natale, D. R. C., Begay, V., Hughes, M., Leutz, A., & Cross, J. C. (2008). Early patterning of the chorion leads to the trilaminar trophoblast cell structure in the placental labyrinth. Development. https://doi.org/10.1242/dev.020099

Simmons, D. G., Rawn, S., Davies, A., Hughes, M., & Cross, J. C. (2008). Spatial and temporal expression of the 23 murine Prolactin/Placental Lactogen-related genes is not associated with their position in the locus. *BMC Genomics*. https://doi.org/10.1186/1471-2164-9-352

Solloway, M. J., & Robertson, E. J. (1999). Early embryonic lethality in Bmp5;Bmp7 double mutant mice suggests functional redundancy within the 60A subgroup. Development.

Soncin, F., Natale, D., & Parast, M. M. (2015). Signaling pathways in mouse and human trophoblast differentiation: A comparative review. In Cellular and Molecular Life Sciences. https://doi.org/10.1007/s00018-014-1794-x

Street, K., Risso, D., Fletcher, R. B., Das, D., Ngai, J., Yosef, N., Purdom, E., & Dudoit, S. (2018). Slingshot: Cell lineage and pseudotime inference for single-cell transcriptomics. BMC Genomics. https://doi.org/10.1186/s12864-018-4772-0

Strunk, K. E., Amann, V., & Threadgill, D. W. (2004). Phenotypic variation resulting from a deficiency of epidermal growth factor receptor in mice is caused by extensive genetic heterogeneity that can be genetically and molecularly partitioned. Genetics. https://doi.org/10.1534/genetics.103.020495

Sun, X., Fu, X., Li, J., Xing, C., Martin, D. W., Zhang, H. H., Chen, Z., & Dong, J. T. (2012). Heterozygous deletion of Atbf1 by the Cre-loxP system in mice causes preweaning mortality. In Genesis. https://doi.org/10.1002/dvg.22041

Suryawanshi, H., Morozov, P., Straus, A., Sahasrabudhe, N., Max, K. E. A., Garzia, A., Kustagi, M., Tuschl, T., & Williams, Z. (2018). A single-cell survey of the human first-trimester placenta and decidua. Science Advances. https://doi.org/10.1126/sciadv.aau4788

Tremblay, K. D., Dunn, N. R., & Robertson, E. J. (2001). Mouse embryos lacking Smad1 signals display defects in extra-embryonic tissues and germ cell formation. Development.

Tseng, Y. Y., Moriarity, B. S., Gong, W., Akiyama, R., Tiwari, A., Kawakami, H., Ronning, P., Reuland, B., Guenther, K., Beadnell, T. C., Essig, J., Otto, G. M., O'Sullivan, M. G., Largaespada, D. A., Schwertfeger, K. L., Marahrens, Y.,

Kawakami, Y., & Bagchi, A. (2014). PVT1 dependence in cancer with MYC copy-number increase. Nature. https://doi.org/10.1038/nature13311

Ueno, M., Lee, L. K., Chhabra, A., Kim, Y. J., Sasidharan, R., VanHandel, B., Wang, Y., Kamata, M., Kamran, P., Sereti, K. I., Ardehali, R., Jiang, M., & Mikkola, H. K. A. (2013). C-Met-Dependent Multipotent Labyrinth Trophoblast Progenitors Establish Placental Exchange Interface. Developmental Cell. https://doi.org/10.1016/j.devcel.2013.10.019

Veillette, A. (2006). Immune regulation by SLAM family receptors and SAP-related adaptors. In Nature Reviews Immunology. https://doi.org/10.1038/nri1761

Vento-Tormo, R., Efremova, M., Botting, R. A., Turco, M. Y., Vento-Tormo, M., Meyer, K. B., Park, J. E., Stephenson, E., Polański, K., Goncalves, A., Gardner, L., Holmqvist, S., Henriksson, J., Zou, A., Sharkey, A. M., Millar, B., Innes, B., Wood, L., Wilbrey-Clark, A., … Teichmann, S. A. (2018). Single-cell reconstruction of the early maternal–fetal interface in humans. Nature. https://doi.org/10.1038/s41586-018-0698-6

Walentin, K., Hinze, C., & Schmidt-Ott, K. M. (2016). The basal chorionic trophoblast cell layer: An emerging coordinator of placenta development. In BioEssays. https://doi.org/10.1002/bies.201500087

Walentin, K., Hinze, C., Werth, M., Haase, N., Varma, S., Morell, R., Aue, A., Pötschke, E., Warburton, D., Qiu, A., Barasch, J., Purfürst, B., Dieterich, C., Popova, E., Bader, M., Dechend, R., Staff, A. C., Yurtdas, Z. Y., Kilic, E., & Schmidt-Ott, K. M.

(2015). A Grhl2-dependent gene network controls trophoblast branching morphogenesis. Development (Cambridge). https://doi.org/10.1242/dev.113829

Ware, C. B., Horowitz, M. C., Renshaw, B. R., Hunt, J. S., Liggitt, D., Koblar, S. A., Gliniak, B. C., McKenna, H. J., Papayannopoulou, T., Thoma, B., Cheng, L., Donovan, P. J., Peschon, J. J., Bartlett, P. F., Willis, C. R., Wright, B. D., Carpenter, M. K., Davidson, B. L., & Gearing, D. P. (1995). Targeted disruption of the low-affinity leukemia inhibitory factor receptor gene causes placental, skeletal, neural and metabolic defects and results in perinatal death. Development.

Woods, L., Perez-Garcia, V., & Hemberger, M. (2018). Regulation of Placental Development and Its Impact on Fetal Growth—New Insights From Mouse Models. Frontiers in Endocrinology. https://doi.org/10.3389/fendo.2018.00570

Yamamoto, H., Flannery, M. L., Kupriyanov, S., Pearce, J., McKercher, S. R., Henkel, G. W., Maki, R. A., Werb, Z., & Oshima, R. G. (1998). Defective trophoblast function in mice with a targeted mutation of Ets2. Genes and Development. https://doi.org/10.1101/gad.12.9.1315

Yu, G. (2018). clusterProfiler: universal enrichment tool for functional and comparative study. BioRxiv. https://doi.org/10.1101/256784

Zhao, G. Q., & Hogan, B. L. M. (1996). Evidence that mouse Bmp8α (Op2) and Bmp8b are duplicated genes that play a role in spermatogenesis and placental development. Mechanisms of Development. https://doi.org/10.1016/0925-4773(96)00543-6

Zhu, D., Gong, X., Miao, L., Fang, J., & Zhang, J. (2017). Efficient Induction of Syncytiotrophoblast Layer II Cells from Trophoblast Stem Cells by Canonical Wnt Signaling Activation. Stem Cell Reports. https://doi.org/10.1016/j.stemcr.2017.10.014

Chapter 3: Regionally distinct trophoblast regulate barrier function and invasion in the human placenta

Bryan Marsh[1, 2, 3, 4], **Yan Zhou**[1, 3, 5], **Mirhan Kapidzic**[1, 3, 5], **Susan Fisher**[1, 3, 5*], and **Robert Blelloch**[1,2, 3*]

[1]The Eli and Edythe Broad Center of Regeneration Medicine and Stem Cell Research, University of California, San Francisco, San Francisco, CA 94143, USA

[2]Department of Urology, University of California, San Francisco, San Francisco, CA 94143, USA

[3]Center for Reproductive Sciences, University of California, San Francisco, San Francisco, CA 94143, USA

[4]Developmental and Stem Cell Biology Graduate Program, University of California, San Francisco, San Francisco, CA 94143, USA

[5]Department of Obstetrics, Gynecology, and Reproductive Sciences, University of California, San Francisco, San Francisco, CA 94143, USA

*Correspondence: robert.blelloch@ucsf.edu; susan.fisher@ucsf.edu

Abstract

The human placenta contains two specialized regions: the villous chorion where gases and nutrients are exchanged between maternal and fetal blood, and the smooth chorion which surrounds more than 70% of the developing fetus but whose cellular composition and function is poorly understood. Here, we use single cell RNA sequencing to compare the cell types and molecular programs between these two regions in the second trimester human placenta. Each region consists of progenitor cytotrophoblasts (CTBs) and extra-villous trophoblasts (EVTs) with similar gene expression programs. While CTBs in the villous chorion differentiate into syncytiotrophoblasts, they take an alternative trajectory in the smooth chorion producing a previously unknown CTB population which we term

smooth-chorion-specific CTBs (SC-CTBs). Marked by expression of region-specific cytokeratins, the SC-CTBs form a stratified epithelium above a basal layer of progenitor CTBs. They express epidermal and metabolic transcriptional programs consistent with a primary role in defense against physical stress and pathogens. Additionally, we show that SC-CTBs closely associate with EVTs and secrete factors that inhibit the migration of the EVTs. This restriction of EVT migration is in striking contrast to the villous region where EVTs migrate away from the chorion and invade deeply into the decidua. Together, these findings add an important new dimension to our understanding of CTB differentiation in these distinct regions of the human placenta. This knowledge has broad implications for studies of the development, functions, and diseases of the human placenta.

This study was published on BioRxiv in 2022 (Marsh et al., 2022) and is under review at eLife.

Impact Statement

Single cell RNA-sequencing of distinct regions of the human placenta identifies a smooth chorion-specific cytotrophoblast population responsible for unique functions of the smooth chorion, including acting as a barrier and restricting invasion.

Introduction

The human placenta is the first organ to develop and forms the essential bridge between maternal and fetal tissues beginning at implantation (Knöfler et al., 2019; Turco and Moffett, 2019). The placenta must develop rapidly upon conception as it performs myriad

functions that remain rudimentary in the developing embryo/fetus such as nutrient and oxygen transport and protection from mechanical and pathogenic insults. The placenta also performs unique functions such as modulation of maternal tolerance and hormone production (Maltepe and Fisher, 2015; Knöfler et al., 2019; Turco and Moffett, 2019). Beginning at implantation, placental development proceeds asymmetrically to produce two distinct regions. At the human implantation site, the embryonic pole, trophectoderm and associated mesoderm cells give rise to the villous chorion including the placental villi and basal plate, which are essential for the exchange of gases and nutrients. The chorionic villi that arise from the opposite side, the abembyronic pole, undergo a cycle of generation and degeneration eventually forming the smooth chorion, which fuses with the amnion and constitutes the fetal membranes. (Hamilton and Boyd, 1960; Boyd and Hamilton, 1967; Benirshcke et al., 2006). Compared to the villous chorion, little effort has been made to analyze types and functions of the CTBs that comprise the smooth chorion (Benirshcke et al., 2006, Garrido-Gomez et al., 2017).

The anatomical processes associated with the formation of the fetal membranes have been well described (Benirschke et al., 2006; Hamilton and Boyd, 1960; Boyd and Hamilton, 1967). The first month of placental development proceeds in a uniform fashion, with the expansion and establishment of villi surrounding the entire developing embryo. These villi have the same complement of trophoblasts as more mature villi including diploid cytotrophoblast (CTB) and multinucleate syncytiotrophoblast (STB) [Knöfler et al., 2019]. The villi surrounding the embryo expand, branch, and are colonized by the fetal vasculature until 6-7 weeks of gestation, when degeneration begins in the future smooth

chorion. In this region, villi continue to recede towards the basal plate. By the time the process is complete in the second trimester, villi are restricted to the discoid placenta that gives rise to the CTBs that invade the decidua (Hamilton and Boyd, 1960; Knöfler et al., 2019). As the developing fetus expands into the uterine cavity, the fetal membranes become juxtaposed to the decidual wall away from the discoid placenta, eventually fusing with these maternal cells at approximately 18 weeks of gestation. (Boyd and Hamilton, 1967).

The fetal membranes have a complex cellular makeup, which includes amniocytes, mesenchymal stromal cells, immune cells, and CTBs (Benirschke et al., 2006). The CTBs of the smooth chorion persist until term as an epithelial like structure. Non-functional "ghost villi" can occasionally be found in the smooth chorion, but lack STBs and fetal vasculature, and thus cannot function in a manner comparable to the chorionic villi (Benirschke et al., 2006). Furthermore, in contrast to the villous chorion where CTBs invade and remodel the maternal arteries, the CTBs of the smooth chorion do not invade the adjacent decidua and the maternal blood vessels it contains (Genbacev et al., 2015). Thus, the function of these CTBs remains unclear.

Several pieces of evidence suggest that the smooth chorion is not simply a vestigial structure. First, an intact CTB layer, which contains proliferating cells persists through the final 20 weeks of gestation (Yeh et al., 1989; Benirschke et al., 2006, 1979; Garrido-Gomez et al., 2017). Second, the histological heterogeneity among smooth chorion CTBs suggests functional distinctions. Yeh et al. (1989) characterize two distinct populations of

vacuolated and eosinophilic CTBs. Vacuolated CTBs were positive for placental lactogen and placental alkaline phosphatase, while the eosinophilic subpopulations was not. Both populations were rich in keratin and neither had the known characteristics of villous CTBs. Bou-Resli et al. (1981) also note high levels of variation among CTBs in the smooth chorion and the existence of a vacuolated population. A more molecular characterization was carried out by Garrido-Gomez et al. (2017), which demonstrated heterogeneity of ITGA4 and HLA-G expression, markers previously associated with stemness and invasion, respectively (Genbacev et al., 2016, McMaster et al., 1995). This study also uncovered an expansion of the smooth chorion in cases of severe pre-eclampsia, along with a disease-specific gene expression pattern. In sum, these results suggest the smooth chorion CTBs are a heterogeneous and dynamic collection of cells with important functions in development and disease.

Single cell RNA-sequencing (scRNA-seq) has emerged as the standard for transcriptional characterization of complex organs. This methodology was previously applied to the placenta, but with a focus on the maternal-fetal interface, specifically the chorionic villi and basal plate (Liu et al., 2018; Suryawanshi et al. 2018; Vento-Tormo et al., 2018). Recently, scRNA-seq was used to profile the fetal membranes at term. However, in this study CTBs were not identified in the smooth chorion, possibly due to apoptosis and/or changes in the membrane at term (Pique-Regi et al., 2019; Yuan et al., 2006; Yuan et al., 2008; Yuan et al., 2009). To fill this information gap, we applied scRNA-seq to matching samples of cells isolated from the villous and smooth chorion regions of human samples from late in the second trimester. We used scRNA-seq to compare the composition and

developmental trajectories of CTBs in the villous and smooth chorion. The data were validated and extended with functional studies. These results identified a novel smooth chorion-specific CTB population important for establishment of a protective barrier and the suppression of trophoblast invasion. In addition, these data represent a resource of CTB types, proportions, and gene expression at mid-gestation against which age related and pathogenic alterations can be measured.

Results

The transcriptional landscape of the villous and smooth chorion at mid-gestation.

To understand the cellular composition of the smooth chorion, we isolated and profiled cells from both the villous (VC) and the smooth chorion (SC) regions of four second trimester human placentas spanning gestational weeks 18 to 24 (GW18-24) using single cell RNA-sequencing (Figure 3.1a). We chose to analyze second trimester samples because the maturation of the smooth chorion is complete but the inflammation and apoptosis associated with membrane rupture and parturition is absent (Benirshcke et al., 2006; Yuan et al., 2006; Yuan et al., 2008; Yuan et al., 2009; Figure 3.1a). For the purpose of establishing internal and patient controls purposes we isolated SC and VC cells from each human placental sample. CTBs were enriched over stromal and immune cells by using our previously published method (Garrido-Gomez et al. 2017). The transcriptomes of the resulting cells were captured using the 10x Genomics scRNA-seq platform.

Each of the eight datasets (GW17.6, 18.2, 23.0, 24.0; VC and SC) were captured independently, then integrated computationally (Figure 3.1b; Stuart et al., 2019). We

classified the cells of the integrated dataset into broad cell type clusters according to functional identities and annotated each by expression of canonical markers. CTBs were annotated as *KRT7*+, *HLA-G*-; extravillous trophoblasts (EVTs) as *KRT7*+, *HLA-G*+; immune cells as *CD45*+, *VIM*-; stromal cells as *VIM*+, *CD45*-; and the uterine epithelium by expression of *EPCAM*+, *MUC1*+ and *MUC16*+ (Figure 3.1c; Lee et al., 2016; McMaster et al., 1995; Vento-Tormo et al., 2018). Cells expressing exclusive markers of disparate cell types (co-expression of *KRT7, HLA-G, HLA-A, VIM, ACTA2*) were labelled as doublets and excluded from further analysis. The complete dataset used for further analysis contained 50,496 cells that passed quality control (between 500 and 6500 unique genes, fewer than 15% mitochondrial reads, doublets removed) [Figure 3.2a; McGinnis et al., 2019]. Cells originating from each placental region (VC - 25,367 and SC – 25,129) and each placental sample (7,181-17,705 cells per sample) were well represented (Figure 3.1b; Figure 3.2b and c). The number of cells in each broad cell type cluster demonstrated enrichment for CTB, which represent more than 60% of the cells in the integrated dataset (Figure 3.2d).

While the enrichment protocol was designed to enrich for CTBs cells, several immune and stromal subtypes were recovered, providing insight into the composition of these cells from each region. The immune and stromal cells were subset and re-clustered, allowing the annotation of subtypes within each group (Figure 3.3a and b; Figure 3.4a and b). The majority, if not all, immune cells were of maternal origin (Figure 3.3c). Almost two-fold more immune cells were recovered from the VC than the SC, although it cannot be ruled out that this change in proportion is not an artifact of dissection or enrichment protocol

(Figure 3.3d). Comparing the immune cell types identified in each region revealed a higher proportion of macrophages in the VC as compared to the SC, which contained a greater proportion of NK/T cells (Figure 3.3e). These differences may reflect the fact that SC samples contain a higher proportion of decidua and its resident immune cells than their VC counterparts. Additionally, this result may suggest differences in the maternal immune cells that interact with the two compartments.

While few stromal cells were isolated in the preparations, sub-clustering still revealed a differential composition of fetal stromal cells between the VC and SC (Figure 3.4a and b). The majority of stromal cells recovered originated from the SC (2,941 compared to 942 from VC). These cells included lymphatic endothelium (Pique-Regi et al., 2019) and two largely SC-specific mesenchymal cell populations of fetal origin, Mesenchyme 1 and Mesenchyme 3 (Figure 3.4c-e). These two clusters are marked by elevated expression of *EGFL6*, *DLK1*, and uniquely by expression of *COL11A1*, which is observed only in the SC (Figure 3.4 b and f). Interestingly, several canonical CTB support factors including HGF, WNT2, and RSPO3, were expressed in fetal stromal populations in both placental regions, suggesting shared requirements for WNT and MET signaling (Figure 3.4g). Taken together these data demonstrate the identification of broad classes of CTBs, immune, and support cells from both the VC and SC regions of the human placenta.

Identification of a smooth chorion-specific cytotrophoblast population.

CTBs are the fetal cells that perform the specialized functions of the VC, and are required for normal fetal growth and development (Maltepe and Fisher, 2015; Turco and Moffett,

2019; Knöfler et al., 2019). To better understand the composition of CTBs in the SC versus the VC, we sub-clustered this population (*KRT7*+, *VIM*-, *CD45*-, *MUC1*-). The CTB subset is comprised of 29,668 cells with similar representation and cell quality control metrics across all eight samples (Figure 3.6a, b, and c). This analysis identified 13 clusters including several CTB, EVT, and STB subtypes (Figure 3.5a).

Broad classes of trophoblast were annotated by established markers (STBs - *CGA*, *CYP19A1*, *CSH1*, *CSH2*; EVTs - *HLA-G, DIO2*; CTBs - *PAGE4*, *PEG10,* and no expression of EVT and STB markers) [Figure 3.5b and Figure 3.7a; McMaster et al., 1995; Lee et al. 2016, Suryawanshi et al. 2018, Liu et al. 2018]. Two cell clusters showed high expression of canonical phasic transcripts, including *MKI67*, with the S-phase cluster denoted by expression of *PCNA* and the G2/M-phase cluster by expression of *TOP2A* (Figure 3.7b; Tirosh et al. 2015). Both populations share gene expression with all clusters of CTBs, and therefore, were identified as actively cycling (Figure 3.7a). No STB or EVT markers were identified in the cycling clusters as was expected due to the requirement for cell cycle exit upon terminal differentiation to these lineages (Lu et al. 2017, Genbacev et al., 1997).

CTBs separated into four clusters, CTB 1-4. CTB 1 cells highly expressed *PAGE4*, *PEG10*, and *CDH1* (Figure 3.5b, Figure 3.7a, Figure 3.8a), which have been shown to be canonical markers of villous CTB (Lee et al. 2016, Suryawanshi et al. 2018). Overall, CTB 2-4 were more transcriptionally similar to each other than to CTB 1, indicating a transcriptional program that was distinct from canonical villous CTBs (Figure 3.7a and c).

CTB 2-4 existed along a gradient of gene expression changes suggestive of various stages of a common differentiation pathway. However, each population expressed distinct transcripts corresponding to important proposed functions of the smooth chorion. CTB 2 cells highly expressed *CLU*, *CFD*, and *IFIT3*, suggesting roles in responding to bacterial or viral infection through the innate arm of the immune system (Thurman and Hollers., 2006; Liu et al., 2011). CTB 3 cells upregulated *EGLN3* and *SLC2A3*, indicating a HIF-mediated response to hypoxia and a switch toward glucose metabolism, likely as an adaptation to the decreased oxygen levels in the largely avascular smooth chorion region (del Peso et al. 2003, Maxwell et al., 1997). Finally, CTB 4 specifically expressed several cytokeratins — *KRT6A*, *KRT17*, and *KRT14*, found in many epithelial barrier tissues and important for maintenance of integrity in response to mechanical stressors (Karantza, 2011; Figure 3.5b, Figure 3.7a). These results establish a previously underappreciated transcriptional diversity of CTB subpopulations.

Quantification of cells showed a strong regional bias in the number and proportion contributing to each CTB cluster (Figure 3.5c and d). In the VC samples, 53.8% of CTBs clustered in CTB 1 compared to 11.1% in the SC (Supplementary Table 1). In contrast, the SC had a much larger proportion of the CTB 2-4 clusters. In this region, 71.3% of CTBs were nearly equally distributed among CTB 2 (25.6%), CTB 3 (24.9%), and CTB 4 (20.8%). In the VC, only 24.1% of CTBs were found in the same clusters, with the majority in CTB 2 (16.1%). The contribution to cycling clusters was consistent across regions: 22.1% and 17.5% of CTBs in the VC and SC, respectively. The relative proportions of CTB 1-4 in the VC and SC were consistent across individual samples indicating that this

difference was biological rather than driven by sample variability or an artifact of sample integration (Figure 3.6b-c).

Next, we immunolocalized the protein products of genes that distinguished the subpopulations. At the mRNA level, *PAGE4* expression was highest in CTB 1 and decreased across CTB 2-4 (Figure 3.5b and e). In the VC, the CTB monolayer between the fetal mesenchymal villous core and the overlying STB layer showed strong PAGE4 immunoreactivity, which diminished upon differentiation to EVT (Figure 3.5f - left). PAGE4 mRNA and protein expression matched that of known villous CTB marker CDH1 (Figure 3.8a and b; Zhou et al., 1997). In the SC, the PAGE4 signal was strong in the epithelial layer directly adjacent to the fetal mesenchyme and then decreased in cells distant from the basal layer, again matching CDH1 (Figure 3.5f - right, Figure 3.8b - right). Both RNA expression and protein localization were consistent with CTB 1 cells existing on both sides of the placenta and occupying a similar niche.

Staining for KRT6, a marker highly enriched in CTB 4 cells (Figure 3.5g) showed a strikingly different result. Cells occupying the upper layers of SC epithelium showed a strong KRT6 signal, a pattern opposite to CDH1 (Figure 3.5h and i - right). KRT6 was absent from either the floating or anchoring villi of the VC (Figure 3.5h and i - left). Rare decidual resident KRT6 positive CTBs were also identified in the VC region. (Figure 3.8c, Figure 3.20 - top). KRT6 isoforms, KRT6B and KRT6C, were not expressed, confirming KRT6A transcript and protein as highly specific markers of a CTB population found only in the smooth chorion (Figure 3.8d). These data describe a novel subpopulation of CTBs

unique to the SC, which going forward we term CTB 4 or SC-CTBs for smooth chorion-specific CTBs.

A common CTB progenitor gives rise to STBs in the VC and SC-CTBs in the SC.

Next, we investigated the developmental origin of the SC-CTBs. We performed RNA velocity analysis to predict the relationships between cells based on the proportion of exonic and intronic reads. These predictions are shown as vectors representing both the magnitude (predicted rate) and the direction of differentiation (Bergen et al. 2020). We first asked whether RNA velocity could recapitulate the well-established differentiation trajectories of trophoblasts in the VC (Knöfler et al., 2019; Turco and Moffett, 2019; Vento-Tormo et al. 2018). In accordance with previous results, RNA velocity projections identified CTB 1 as the root for three differentiation trajectories: self-renewal, differentiation to STBs, and differentiation to EVTs (Figure 3.9a). Cells at the boundary of the CTB 1 cluster showed differentiation vectors of high magnitude toward STB Precursors and upregulated canonical drivers of STB differentiation and fusion (*ERVW-1* and *ERVFRD-1*). These cells also expressed transcription factors (*GCM1* and *HOPX*) and hormones (*CSH1*) necessary for STB function (Figure 3.10a; Baczyk et al., 2009; Mi et al., 2000; Blaise et al., 2003; Yabe et al., 2016).

In the SC, CTB 1 cells once again were identified as the root for differentiation. However, CTB 1 cells showed strong directionality and magnitude toward CTB 2-4 (Figure 3.9b). All cells in CTB 1-4 clusters displayed uniform directionality indicating a robust

differentiation trajectory ending at CTB 4. High levels of transcriptional similarity between CTB 2-4 compared to CTB 1 suggested CTB 2 and 3 are intermediate states between CTB 1 and CTB 4 (Figure 3.7c). Mitotic KRT6+ cells were identified, suggesting that differentiation to SC-CTB does not require cell cycle exit (Figure 3.10b). In contrast to the VC, we observed no velocity vectors with directionality toward the STB lineage from the CTB clusters in the SC samples. Further, the smaller number of STB precursors (460 cells) and STBs (14 cells) exhibited reduced expression of STB canonical markers such as ERVFRD-1 and GCM1, and notably, a near absence of ERVW-1 (Figure 3.10a). These cells may be associated with ghost villi (Benirschke et al., 2006). In sum, these data show differential developmental trajectories for the CTB 1 cells in the SC and VC, with the former largely giving rise to SC-CTBs and the latter to STBs.

To identify the genes that were correlated with progression from CTB 1-4 in the SC, we used the velocity vector predictions to construct a pseudotemporal model of differentiation. All the cells in these clusters were plotted in one dimension from the least to the most differentiated according the pseudotime model (Figure 3.9c). Genes that were highly expressed at the start of the pseudotemporal differentiation included pan-trophoblast factors such as *EGFR*, which was expressed throughout all four CTB populations in both the VC and SC. Progression along the pseudotime trajectory identified regulators of cell fate and function, including the transcription factor *KLF4* and extracellular matrix (ECM) components *COL5A1* and *LAMA3* (Figure 3.9c-d); all demonstrated SC-specific expression. Elevated expression of ECM transcripts (*COL4A2*, *FN1*) and transcription factors responsive to cell contact and mechanical stress *(HES1*,

YAP1) were coordinately upregulated, potentially highlighting the effects of the extracellular environment on fate specification (Figure 3.10c). These data demonstrated that SC-CTBs originate from CTB 1 progenitors common to both the VC and SC. In the SC, instead of upregulating syncytialization factors such as *GCM1* and *ERVFRD-1*, CTB 1 progenitors upregulate transcription factors such as *KLF4*, *YAP1*, and *HES1*, which drive an epithelial cell fate in other contexts (Segre et al., 1999, Harvey et al., 2013; Rock et al., 2011).

SC-CTBs express a distinct epidermal transcriptional program.

Next, we sought a better understanding of the physiological functions of the SC trophoblast clusters. We performed gene ontology analysis as a summary of functional processes (Figure 3.11a, Figure 3.12; Yu et al., 2012). We focused on the progenitor CTB 1 and terminally differentiated SC-CTBs as they showed enrichment for strikingly different functional categories. In CTB 1, we identified enrichment for WNT signaling, epithelial morphogenesis, and membrane transport, categories commonly associated with progenitors (Figure 3.11a, Figure 3.12). We validated the activity of WNT signaling and the location of these cells by immunolocalization of non-phosphorylated CTNNB1 (intact form of the protein). β-Catenin was localized to the most basal epithelial layer nearest to the stroma in both the VC and SC regions (Figure 3.11b), matching expression of the CTB 1 marker CDH1 (Figure 3.13a). WNT signaling has an important role in the maintenance of villous CTBs *in vivo* and in the derivation and culture of self-renewing human trophoblast stem cells (Knöfler et al., 2019; Haider et al., 2018; Okae et al., 2018). We investigated proliferation of CTNNB1 expressing cells in both regions using KI67 as

a mitotic marker. This revealed a similar percentage of KI67+ CTB 1 cells, suggesting similar proliferative capacity across regions (Figure 3.11b and c). We next analyzed regional differences within CTB 1. Gene ontology identified an enrichment for oxidative phosphorylation and epithelial signaling cues in VC CTB 1 cells (Figure 3.13b). This is in direct contrast to SC CTB 1 cells that displayed elevated levels of hypoxia response genes (Figure 3.13b-c). KLF4 was identified in the RNA velocity analysis as gaining expression from CTB1-4, but also showed greater expression in CTB1 in the SC compared to the VC (Figure 3.9d). In accordance with the mRNA expression data, KLF4 protein often co-localized to CTB1 in the SC, but was only observed in rare cells in the VC (Figure 3.11d). These data further support a similar location and function for CTB 1 in the SC and VC, with transcriptional and metabolic differences that presage distinct developmental trajectories.

CTB 4 ontological analysis strongly supported important roles for these cells in the formation of a protective barrier. The greatest enrichment was for cell junction and cell substrate adhesion genes that included numerous integrin and laminin subunits as well as junctional proteins *PATJ*, *DSP*, and *JUP*. An enrichment for both skin and epidermal development correlated with upregulation of the ECM and junctional transcripts. These categories included many cytokeratins (*KRT6A, 7, 8, 14, 17, 18,* and *19*) and transcription factors (*KLF4*, *YAP1)* required for epidermal identity and maintenance (Segre et al., 1999; Schlegelmilch et al., 2011). The organization of the SC is reminiscent of stratified epidermal cells of the skin, with progenitors adherent to the basal lamina and more differentiated cells progeny forming the upper layers. In many tissues, the specific

domains of cytokeratin expression correspond to stratified cell layers with different functions. We asked if this was also the case in the SC epithelium. Cytokeratins 7, 8, and 18 were expressed in all trophoblast regardless of region (Figure 3.14a), but cytokeratin 6A, 14, and 17 displayed smooth chorion-specific expression that increased with differentiation towards CTB 4 (Figure 3.14b). Immunofluorescence localization confirmed expression of KRT14 as specific to the CTBs in the SC and inclusive of all KRT6 expressing cells (Figure 3.11e). These data support a model of accumulated cytokeratin expression that begins with CTB 1 (*KRT7, KRT8, KRT18*), increases in CTB 2-3 (*KRT14, KRT17*), and culminates in CTB 4 (*KRT6A*). Together these data are consistent with a central role for the CTBs of the SC in establishing a protective epithelial barrier for the rapidly growing fetus.

Beyond forming a physical barrier, important placental functions include protection from bacterial and viral infections. We identified an enrichment for genes involved in antiviral response in SC-CTBs, and in SC cells more broadly. For example, IFITM3, a restriction factor preventing entry of viruses into cells, is highly expressed in CTBs from the SC compared to the VC (Figure 3.15; Bailey et al., 2014; Spence et al., 2019). IFITM proteins have also been reported to inhibit syncytialization (Buchrieser et al. 2019), suggesting IFITM3 may also function to block differentiation of CTBs into STBs in the SC. Taken together, these data establish SC-CTBs as the building blocks and critical regulators of the SC barrier, responsible for both protection against physical forces and pathogen infection.

EVTs of the VC and SC regions are behaviorally distinct but transcriptionally similar.

EVTs are the invasive trophoblasts of the placenta (Knöfler et al., 2019; Turco and Moffett, 2019; Red-Horse et al., 2004). While the EVTs of the VC migrate away from the villi, invade the decidua, and replace the endothelial lining of the uterine arteries, the EVTs of the SC adhere to the decidua and do not home to the maternal vasculature (Genbacev et al., 2015). To understand the basis for these differences, we compared EVT subpopulations isolated from the VC and SC. Expression of the canonical marker of EVTs, *HLA-G*, was similarly abundant among the cells isolated from both placental regions (Figure 3.16a and b). A greater number (VC - 6572; SC - 5021) and larger proportion (VC – 46.83%; SC – 32.12%) of CTBs from the VC expressed HLA-G as compared to the analogous population from the SC (Figure 3.16c). Consistent with the transcript expression data, immunolocalization of HLA-G showed strong staining of cells in both the VC and SC. However, VC derived HLA-G positive cells were found deep in the maternal decidua. In contrast, HLA-G positive cells in the SC remained in the epithelial layer (Figure 3.16b).

EVTs were further divided into clusters 1-4. No clusters were specific to the VC or SC, except for the small number of putative EVT Precursors (VC – 99 cells; SC – 8 cells) [Figure 3.16d, Figure 3.9a]. Previous work has classified EVTs on the villous side of the placenta as columnar, interstitial, or endovascular based on behavior and location in the decidua (Tilburgs et al., 2015; Knöfler et al., 2019). The columnar subpopulation is believed to represent newly differentiated EVTs, which lie at the base of the columns that

connect the anchoring villi to the uterine wall. Interstitial EVTs migrate through the decidua homing to maternal arteries, which they invade. Within the arterial wall, this subpopulation further differentiates to endovascular EVTs and replaces the maternal arterial endothelium (Harris et al. 2009, Red-Horse et al. 2004). We expected to capture both columnar and interstitial EVT populations, but few endovascular EVTs as the cellular preparations were largely devoid of arteries. We investigated the four clusters of EVT identified in our analysis in the context of the VC and the SC. Both placental regions contained cells from all clusters, although distinct regional biases were evident (Supplementary Table 1). The SC region contained almost twice as many EVT 1 cells as the VC (VC – 684; SC – 1256), whereas the VC contained almost twice as many EVT 2-4 as the SC (VC – 5789; SC – 3757). We next asked which of the EVT clusters corresponded to known EVT classifications, indicating maturation state or invasive capacity. Gene ontology analysis showed an enrichment for placental development and antigen presentation categories in EVT 1 (Figure 3.17a). Representative marker genes for these categories in EVT 1 included several lineage-specific transcription factors including *GCM1*, *PPARG*, and *CEBPB* (Figure 3.17b; Knöfler et al., 2019, Ferreira et al., 2016). In contrast, EVT 2-4 showed enrichment for extracellular structure and matrix organization, glycosylation, and peptidase activity. EVT clusters 3-4 specifically showed increased expression for transcripts of proteases such as *HTRA1*, *MMP2*, and *MMP11* (Figure 3.17c). Based on the GO and specific gene enrichments, EVT 1 appeared most similar to columnar EVTs, while EVT 2-4 were consistent with interstitial EVTs that gain invasive capacity. The relative enrichment for EVT 1 in the SC (VC – 10.57% of EVT; SC – 25.05% of EVT) suggested an expansion in columnar-like EVTs at the expense of

interstitial EVT. Conversely, the relative enrichment for EVT 2-4 in the VC region suggested an expansion of the invasive subpopulation (Figure 3.16d).

As almost 75% of EVTs from the SC region were in EVT clusters 2-4, we next asked if there were differences in gene expression between interstitial EVTs isolated from each region. This analysis identified relatively few differentially expressed genes, with the vast majority identified having a log fold change less than 1 (Figure 3.18a). The small number of differentially expressed genes with a fold change greater than 1 was typically identified across multiple EVT clusters, suggesting an overriding transcriptional program that might supersede subcluster designations. To identify genes associated with this program, we combined all EVT subclusters into one cluster for analysis (Figure 3.16e). Differential expression analysis revealed the hormone CSH1 and several proteases including HTRA1, HTRA4, and PAPPA to be expressed at significantly higher levels in the more invasive VC EVTs. However, of the most differentially expressed transcripts only CSH1, ITM2C, and DNASE1L3 were exclusive to the VC (Figure 3.18b). Immunolocalization of CSH1 confirmed this result (Figure 3.16f). CSH1, also known as human prolactin, is a secreted hormone that signals through the receptor PRLR found on maternal cells. As such, the primary effect of CSH1 is likely non-cell autonomous, raising the possibility that the largest differences in EVTs between regions may not be in inherent invasive capacity, but rather their ability to communicate with the neighboring cells.

We next asked whether the gene expression differences between the VC and SC were smaller for EVT clusters than for all other trophoblast clusters. Calculating the Spearman

Correlation coefficient across each cluster, EVT 3, EVT 4, and CTB 1 (which we have established as common to both regions) were most similar and the only clusters with a coefficient greater than 0.75 (Figure 3.18c). Since this analysis does not account for cluster heterogeneity or size, we quantified the number of differentially expressed genes between 100 randomly selected cells from each placental region within each cluster. Across 100 permutations, the number of differentially expressed genes between regions was the lowest for all four EVT clusters (Figure 3.16g). Together, these results showed that the EVTs of the VC and SC are surprisingly similar even though they have distinct behaviors *in vivo*, suggesting a cell non-autonomous, rather than cell autonomous, regulation of invasion.

CTBs of the SC inhibit EVT invasion.

Given the transcriptional similarity between EVT clusters originating from the VC and SC, we wondered if a non-cell autonomous program could explain their distinct migratory properties. Immunofluorescence co-localization of CTB 1, SC-CTBs, and EVTs showed striking differences in the relative positioning of the EVTs and CTBs in the two placental regions (Figure 3.19a and b). On the VC side, which lacks SC-CTBs cells, HLA-G+ EVTs were distant from the np-CTNNB1+ CTB 1 cell population as expected (Genbacev et al., 2015). By the second trimester they had migrated away from the cell column of the anchoring villi into the uterine stroma (Figure 3.19a). In contrast, HLA-G+ EVTs in the SC were adjacent to and in physical contact with KRT6+ SC-CTBs (Figure 3.19b). The interactions between SC-CTBs and EVTs were numerous and widespread throughout the SC epithelium. Contacts between CTB 1 and EVTs in the SC were not observed and the

VC contain only rare and irregular KRT6+ cells (Figure 3.20). This close association suggested possible paracrine signaling events between SC-CTBs and EVTs, which might impact each cell type.

To test this theory, we attempted to recapitulate the differential invasive properties of VC and SC EVTs in a transwell migration assay. Briefly, these cells were enriched using the same protocol as described for the scRNA-seq experiments. The cells were plated on Matrigel coated transwell filters and cultured for 39 hours. Trophoblast projections that reached the underside of the filter, a proxy for invasion, were visualized by immunostaining with a pan-cytokeratin antibody. (Figure 3.19c, Figure 3.21). Consistent with the differences observed *in vivo*, there was greater invasion of VC as compared to SC trophoblast (Figure 3.19c). Next, we asked whether EVTs from the SC region secreted soluble factors that inhibited invasion. The invasion assays were repeated with VC cells cultured with conditioned medium from SC cells and vice versa. While VC conditioned medium had no impact on either VC or SC cells, SC conditioned medium significantly reduced migration of VC cells (Figure 3.19d). Neither conditioned medium impacted the density of VC or SC cells (Figure 3.22). Therefore, a secreted factor from SC cells inhibited the migration of VC EVTs. Given that SC-CTBs were unique to the SC side, it is highly likely that they produced secreted factors that inhibit the invasion of EVTs to which they are juxtaposed.

Discussion

This study profiled the developing 2nd trimester placenta, providing a high-resolution molecular description of the trophoblast in the smooth chorion and placing them in context of the trophoblast from the VC of the same placenta. In doing so, we addressed long standing observations concerning apparent similarities and differences between VC and SC trophoblast, deconstruct the trophoblast populations in the SC, and ascribe functions to the cells of this understudied region. Our study characterized a novel trophoblast population distinct from both extant CTB in the VC and from EVT found in either placental region. These trophoblasts reside only in stratified epithelium of the smooth chorion, express a specific cytokeratin (KRT6), and comprise at least 25% of all trophoblast in the region. Lineage reconstruction by RNA velocity suggested the progenitors for these smooth chorion-specific CTBs are a resident proliferative progenitor trophoblast with a transcriptional profile that matches villous CTB. We identified several potential regulators of the transition from a common villous CTB-like cell to SC-CTB, including epidermal transcription factors such as KLF4 and YAP1. These molecules along with region-specific signaling events drive an epidermal transcriptional program creating the building blocks for a barrier against both physical and pathogen stressors. Finally, we identified CTB-EVT interactions occurring only in the smooth chorion and provide evidence that paracrine signaling between these populations restricts trophoblast invasion.

Since the smooth chorion is created by a degenerative process, consensus has been that these cells are remnants of this process, making the smooth chorion a vestigial structure (Benirschke et al., 2006). However, several previous observations suggested this might

be an oversimplification. First, these cells were noted to be proliferative, suggesting either cellular expansion or turnover (Benirschke et al., 2006). We confirmed the presence of proliferative trophoblasts in the smooth chorion. Each cycling CTB cluster expressed markers of CTB 1-4 in both regions (Figure 3.7a) and both CTB 1 (Figure 3.11b-c) and SC-CTBs (Figure 3.10b) also expressed KI67 protein. Proliferation of both the progenitor and differentiated cells suggested a need for expansion coordinated with the growth of the developing fetus. Second, the importance of the smooth chorion was suggested by the noted heterogeneity of the trophoblasts within this region (Yeh et al., 1989; Bou-Resli et al., 1981; Garrido-Gomez et al., 2017; Benirschke et al., 2006). In agreement, our scRNA-seq results showed the smooth chorion to be a complex tissue with several trophoblast types. We identified, by differential transcription and function, at least two distinct CTB cell types, columnar and interstitial EVT, and a small number of STB Precursors. As discussed, all CTB and EVT populations either matched those found in the VC or had new region-specific functions. The only evidence of degeneration was the STB Precursor population within the smooth chorion, which lacked expression of both *ERVW-1* and *ERVFRD-1*, the fusogens necessary to form STB (Mi et al., 2000; Blaise et al., 2003; Liu et al., 2018). In sum, these studies suggested that the SC is a complex and functional tissue, not simply the remnant of villous degeneration.

We focused on CTB 4, a novel population found exclusively in the SC, in the context of the unique functions of this placental region. CTB 4 were enriched for epidermal, skin development, and antiviral gene categories suggesting concerted roles in the creation of a barrier against external forces and pathogens. Previous studies have noted that CTBs

residing in the SC have high levels of keratin expression and are associated with extensive ECM deposits rich in laminin, collagen, and fibronectin (Yeh et al., 1989; Bou-Resli et al., 1981; Benirschke et al., 2006). Among all smooth chorion CTB populations, but most notably in CTB 4, we identified the upregulation of ECM components, including *LAMA3*, *COL5A1* and *FN1*. Expression of ECM molecules in the SC is essential to protect against premature rupture of the fetal membranes, but its deposition has previously been ascribed to stromal cells in the chorion (Parry and Strauss, 1998). This result also suggested that these trophoblasts create a specific ECM environment distinct from other placental regions. This altered composition likely has wide-ranging effects on trophoblast fate, gene expression, and behavior. It will be interesting to explore the impact of advancing gestational age on the SC epithelium, especially with respect to the ECM. Presumably, cellular and structural changes precede the normal process of membrane rupture prior to delivery at term. Whether premature rupture of the membranes phenocopies these events or is a unique process is an important open question.

Pathogen defense is another important function of the placenta. Infections of the chorion and amnion (chorioamnionitis) often result in adverse outcomes for mother and fetus, primarily preterm birth (Romero et al., 2014). We identified specific expression of the antiviral gene IFITM3 in CTB 4. IFITM3 expression is particularly interesting due to the recent finding that it blocks STB fusion mediated by the endogenous retroviral elements, ERVW-1 and ERVFRD-1. Therefore, IFITM3 expression in SC-CTBs may have a dual role – restricting viral entry into the cell and blocking the formation of STBs in the SC. Its

expression also provides a mechanism by which the lack of STBs in the smooth chorion is maintained after degradation of the villi is complete.

A distinct feature of the CTBs of the SC was remodeling of the cytokeratin network coordinated with differentiation from CTB 1 to SC-CTBs. The progressive expression of KRT14, KRT17, and KRT6A is reminiscent of the cytokeratin code found in the epithelial cell layers of many tissues (Karantza et al., 2011). KRT14 is recognized as a marker of all stratified epithelium including subsets of basal progenitor and stem cells in several tissues, usually alongside KRT5 (Moll et al., 1982; Nelson et al., 1983; Rock et al., 2009). While we did not identify expression of KRT5 in any trophoblast, the KRT14 expressing proliferative cells of the SC fit the profile of stratified epithelia in other locations. The roles of KRT17 and KRT6 are less clear. Most knowledge about the function of these molecules comes from the epidermis in the context of injury and disease. KRT6 and KRT17 are upregulated rapidly upon epidermal injury and are expressed through the repair phase, each contributing specific functions. (Takahashi et al., 1998; McGowan and Coulombe, 1998). KRT17 promotes proliferation and increases in cell size through Akt/mTOR and STAT3, respectively (Kim et al., 2006; Yang et al., 2018). KRT6 is a negative regulator of cell migration through the inhibition of Src kinase and associations with myosinIIA (Wong and Coulombe, 2003; Rotty and Coulombe, 2012; Wang et al., 2018). Finally, this molecule promotes expression of Desmoplakin and the maintenance of desmosomes, the latter, a long-established feature of SC trophoblasts (Bou-Resli et al., 1981; Bartels and Wang, 1983; Benirschke et al., 2006). Taken together, these observations are consistent with data on SC-CTBs. We found no evidence of their invasion, but did identify

frequent interactions with the ECM, CTBs, and EVTs. The coordinated expression of these cytokeratins and the transcriptional profile writ large, suggested the SC has the properties of a highly specialized epidermis with a robust proliferative capacity and strong cohesive properties, but lacking migratory or invasive behavior.

As previous work has demonstrated or assumed, the majority of trophoblast identified are represented in both the VC and SC (Benirschke et al., 2006; Garrido-Gomez et al., 2017; Pique-Regi et al., 2019). We identified two cell types with striking transcriptional similarity between regions, CTB 1 and EVT. CTB 1 cells in the VC matched canonical villous CTB in transcriptional profile, behavior, and niche. Surprisingly, we identified a similar population in the SC. They are localized to an epithelial sheet juxtaposed to the fetal mesenchyme, separated by a thin basal lamina. These cells are supported by similar signaling pathways in both regions, including HGF and WNT (Figure 3.4g; Dokras et al., 2001; Okae et al., 2018; Zhou et al., 2002). The similarities in location and growth factor requirements demonstrate that a niche similar to the villous trophoblast membrane, exists in the SC. Additionally, we identified CTB 1 as the progenitor population for SC-CTB, and possibly for EVT in the SC. Thus, CTB 1 in both regions function as multipotent progenitors. Despite the many similarities, the developmental trajectories emerging from CTB 1 differ in a region-specific manner. At present, it is unclear whether CTB 1 cells in both regions originally have the same potential or if fate restriction occurs as the fetal membranes form. Future experiments will need to functionally address whether CTB 1 from the VC can be coerced to generate SC-CTBs and if CTB 1 from the SC can efficiently generate STBs and invasive EVTs. Multipotent trophoblasts have been generated from

first trimester smooth chorion cells, however, these cells have a distinct transcriptional profile from the second trimester cells we characterized (Genbacev et al., 2016).

Similarities between the EVT of each region, as defined by contact with the decidua, has been documented in observational, molecular, and most recently, transcriptomic studies (Benirschke et al., 2006, Pique-Regi et al., 2019). Our data confirmed a strong correlation between gene expression for all EVT populations, regardless of regional identity. Based on previously established EVT subtypes, we identified a reduction in the proportion of interstitial EVTs and a concomitant increase in columnar-like EVTs of the SC. However, we did not find evidence of specific EVT subpopulations or intrinsic gene expression programs that would explain the differences in the depth of invasion of EVT in each placental region. However, we did uncover CTB-EVT interactions specific to the SC epithelium. Rather than physically separating as they do in the VC, CTBs and EVTs co-occupy the stratified epithelium of the SC, providing a contained environment for paracrine signaling, cell contact mediated signaling, and cell-ECM interactions that may impact trophoblast invasion. In this study we verified that soluble signaling factors from SC cells restrict the invasion of their counterparts from the VC. We can speculate on potential candidates that may function across multiple biological systems to restrict invasion. CTB 4 cells express high levels of TIMP1, TIMP3, and SERPINE1 (PAI-1), which inhibit the function and/or activation of MMPs necessary for trophoblast invasion (Fisher et al., 1989; Zhu et al., 2012). Addition of recombinant TIMPs or a function blocking antibody against plasminogen (whose processing is inhibited by SERPINE1) reduced trophoblast invasion *in vitro* (Lala and Graham, 1990). While these molecules

are expressed by decidual cells, we identified their expression within the SC epithelium directly adjacent to EVTs. Another candidate regulator of invasion expressed by CTB 4 is TNFα. Treatment of trophoblasts with TNFα increases EVT apoptosis, decreases protease expression, increases SERPINE1 expression, and decreases invasion *in vitro* (Otun et al., 2011; Xu et al., 2011). These data suggest that SC-CTBs secrete multiple molecules that could decrease the survival and invasion of EVTs in the SC. In this study we explored the role of secreted factors, but SC-CTBs may also influence EVTs through cell contact mediated signaling and the deposition of an ECM distinct from the basal plate. Future experiments will be necessary to explore the contributions of these distinct signaling pathways and matrices.

In summary, this study provides a high-resolution molecular accounting of the trophoblast that occupy smooth chorion. By comparison with trophoblasts isolated from the VC of the same placentas, we identified key similarities and differences to better understand the molecular determinants of trophoblast function and behavior in the SC. We characterized a novel CTB population, marked by KRT6A expression, that is central to three key functions of the SC: formation of an epidermal-like barrier, blockage of aberrant STB differentiation, and restriction of EVT invasion. These data provide a better understanding of molecular and cellular pathways that control human placental development and against which disease related changes can be identified and therapeutic targets discovered.

Figures

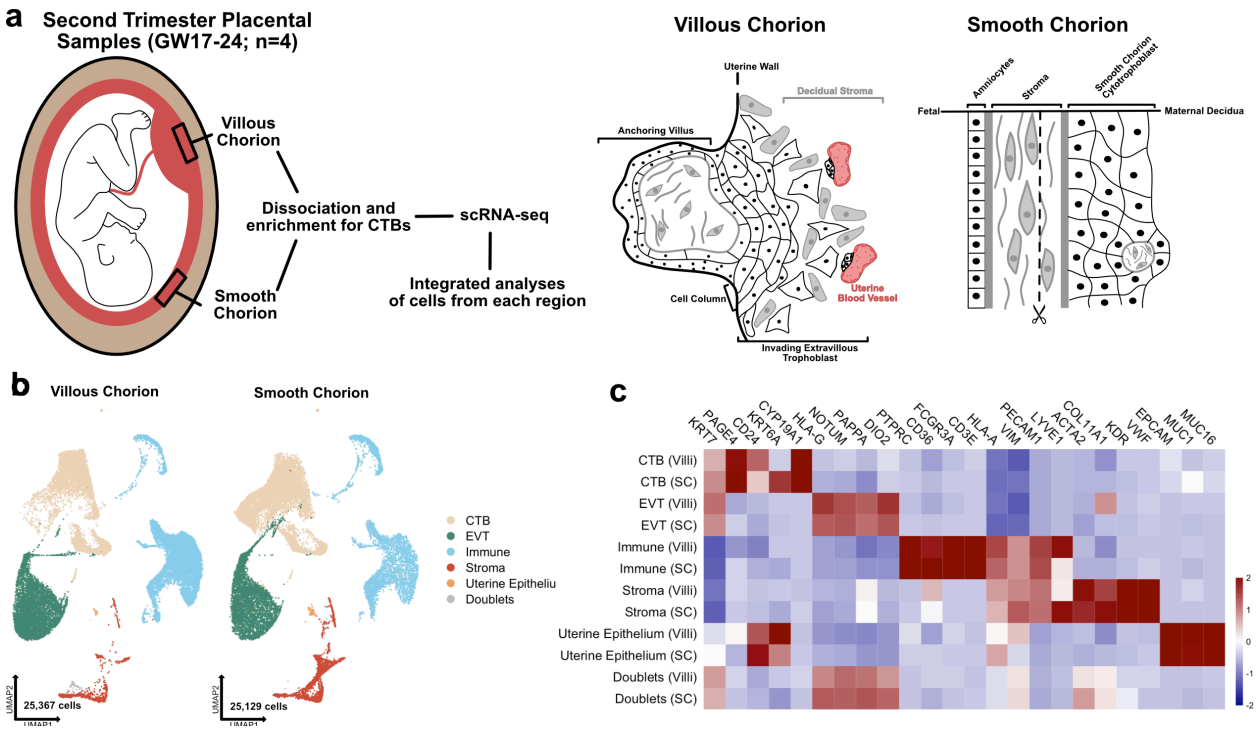

Figure 3.1 - The transcriptional landscape of the villous and smooth chorion at mid-gestation.
(a) Left - Schematic of the placenta at mid-gestation, highlighting the regions sampled, together with the methods used for cell isolation and characterization. Right – schematic of the cell types and their organization in each region. **(b)** UMAP projections of integrated samples, shown by region of origin (Left – VC, Right – SC), and colored according to broad cell type clusters. **(c)** Heatmap of the transcript expression of select cell identity markers across broad cell type clusters and regions. Values are scaled expression across the clusters of each region independently.

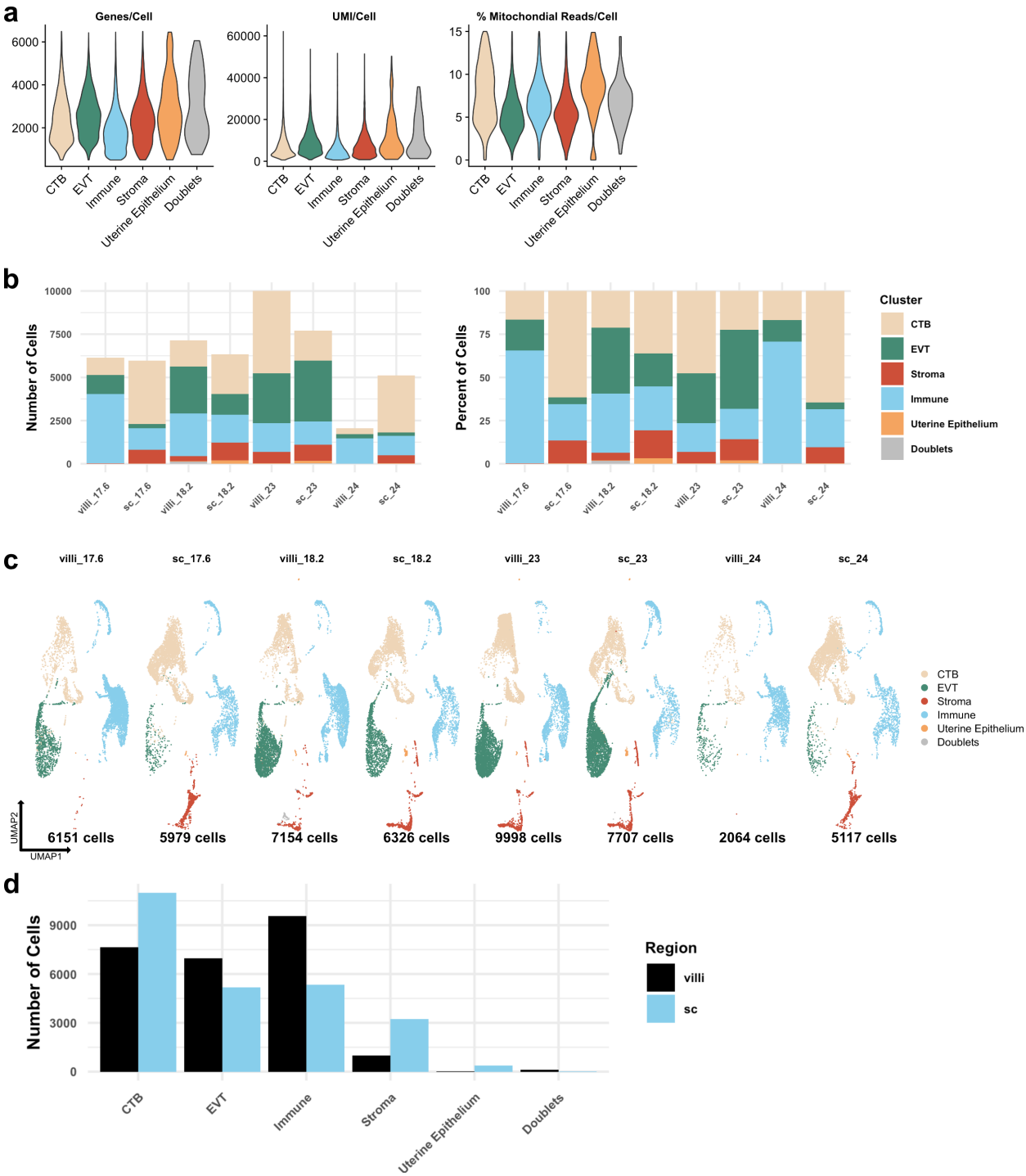

Figure 3.2 - Metrics of the integrated dataset.
(a) Violin plots of the number of unique genes (Left), number of UMI (Middle), and the percent of mitochondrial reads (Right) per cell for each broad cell type cluster. **(b)** The total number of cells (Left) and the percent of the total library (Right) in each broad cell type cluster from each placental sample are shown. **(c)** UMAP projections of the integrated dataset shown by each placental sample. Colors correspond to each broad cell type cluster in the legend at the right. The number of cells analyzed from each

placental sample is listed beneath. **(d)** The number of cells in each broad cell type cluster from each placental region (VC – black; SC – blue).

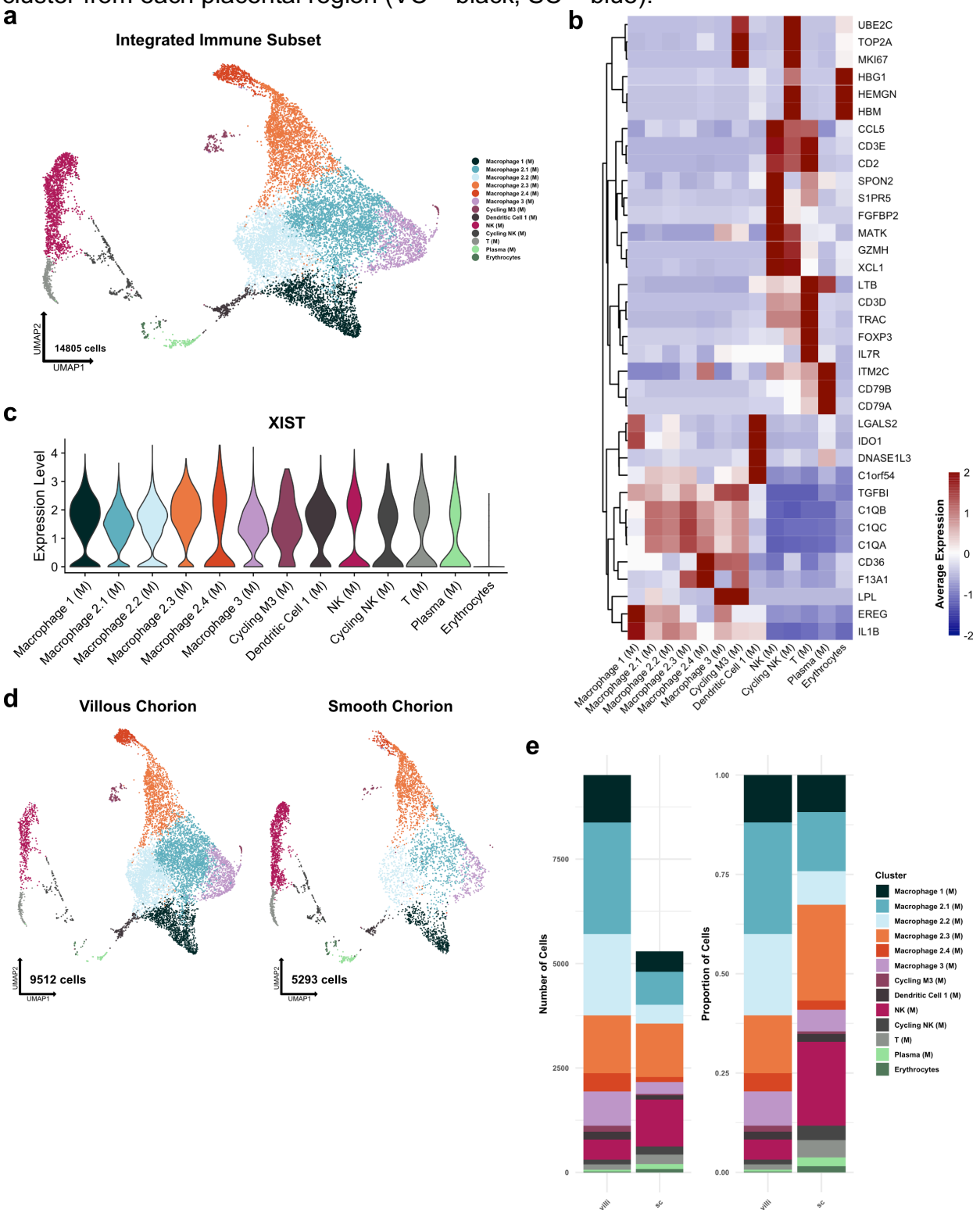

Figure 3.3 - Metrics and markers of the immune cell subset.

(a) UMAP projection of all subclustered immune cells (n=14,805). Colors correspond to the clusters in the legend at the right. **(b)** Heatmap of selected marker genes of each immune cell cluster. Expression was displayed as the scaled mean expression in the cluster. **(c)** Violin plot of XIST expression in each immune cell cluster. **(d)** UMAP projection of immune cells shown by region of origin. **(e)** Stacked bar chart of the number of cells (left) or proportion of cells (right) in each cluster by region of origin.

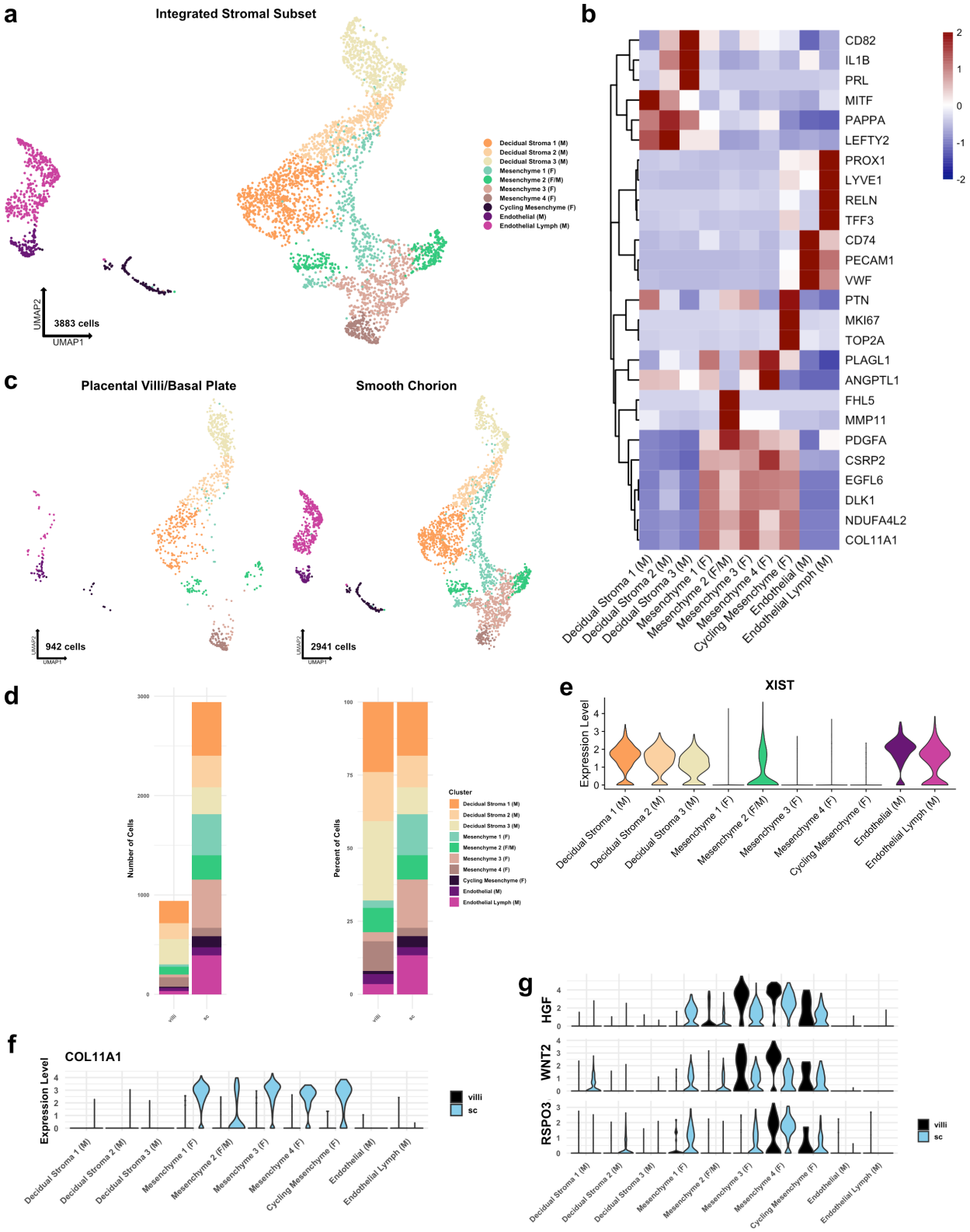

Figure 3.4 - Metrics and markers of the stromal cell subset.
(a) UMAP projection of subclustered stromal cells (n=3,883). Colors correspond to the clusters in the legend at the right. **(b)** Heatmap of selected marker genes for each

stromal cell cluster. Expression was displayed as the scaled mean expression in the cluster. **(c)** UMAP projection of stromal cells shown by region of origin. **(d)** Stacked bar chart of the number of cells (left) or percent of cells (right) in each cluster by region of origin. **(e)** Violin plot of XIST expression in each stromal cell cluster. **(f)** Violin plot of COL11A1 expression in each cluster shown by each region, showing expression in only SC cells **(g)** Violin plots of HGF, WNT2, and RSPO3 expression in each cluster and shown by each region, showing expression in both VC and SC cells.

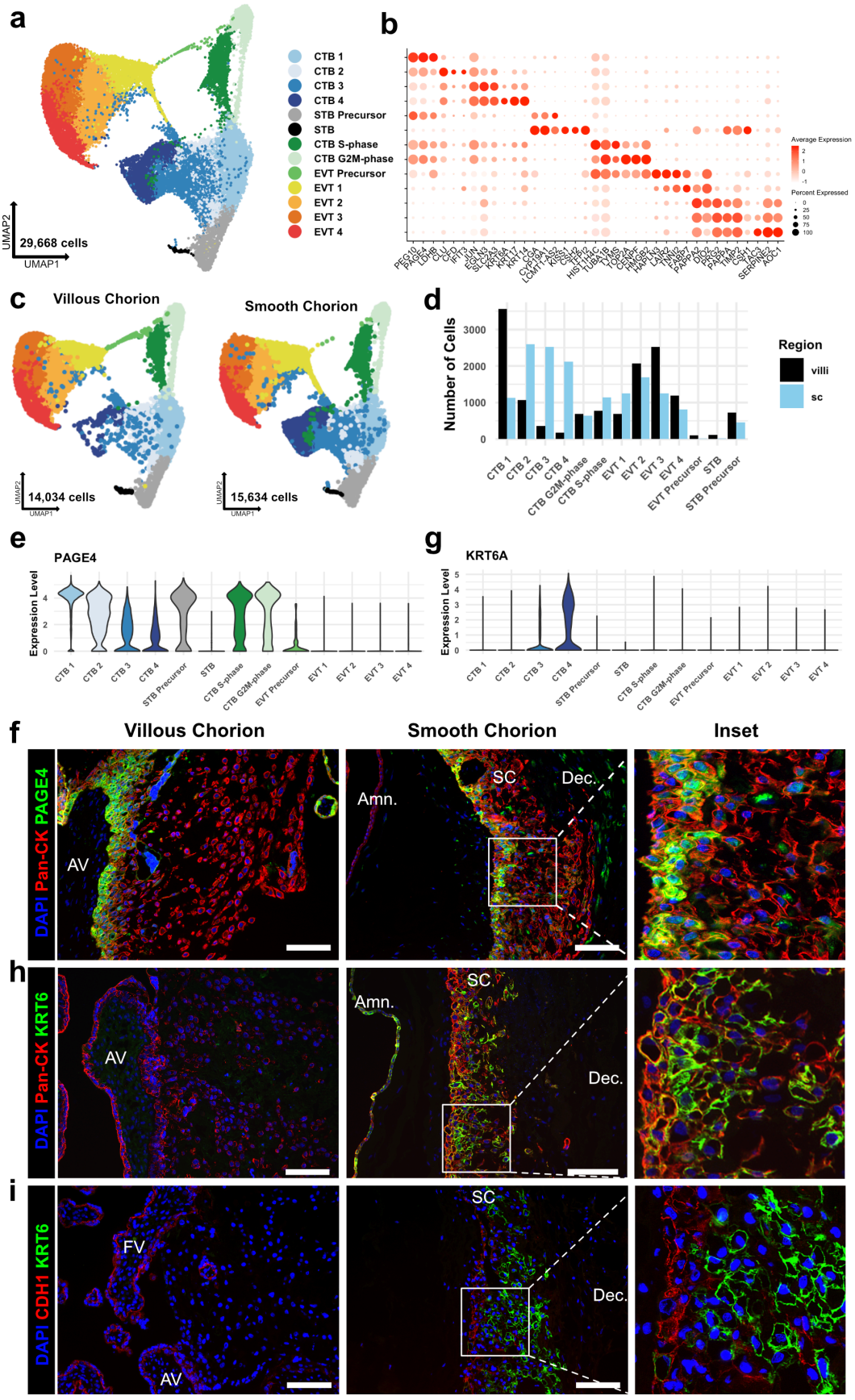
a
UMAP2
UMAP1
29,668 cells
CTB 1
CTB 2
CTB 3
CTB 4
STB Precursor
STB
CTB S-phase
CTB G2M-phase
EVT Precursor
EVT 1
EVT 2
EVT 3
EVT 4
b
Average Expression
Percent Expressed
c
Villous Chorion
Smooth Chorion
14,034 cells
15,634 cells
d
Number of Cells
Region
villi
sc
e
PAGE4
Expression Level
g
KRT6A
Expression Level
f
Villous Chorion
Smooth Chorion
Inset
DAPI Pan-CK PAGE4
AV
Amn.
SC
Dec.
h
DAPI Pan-CK KRT6
i
DAPI CDH1 KRT6
FV

Figure 3.5 - Identification of a smooth chorion-specific cytotrophoblast.
(a) UMAP projection of subclustered trophoblasts (n=29,668). Colors correspond to the clusters at the right. **(b)** Dot plot showing average expression and percent of cells in each cluster as identified by the marker genes listed on the x-axis. The clusters are listed on the y-axis. **(c)** UMAP projection of subclustered trophoblasts from the VC (Left) or the SC (Right). Clusters and colors are the same as in panel a. **(d)** Quantification of the number of cells in each trophoblast cluster from each region. Cells from the VC are shown in black. Cells from the SC are shown in blue. **(e)** Violin plot of *PAGE4* transcript expression across all trophoblast clusters. (**f)** Immunofluorescence co-localization of PAGE4 with pan-cytokeratin (marker of all trophoblast) in the VC (Left) or SC (Right). **(g)** Violin plot of *KRT6A* transcript expression across all trophoblast clusters. **(h)** Immunofluorescence co-localization of KRT6 with pan-cytokeratin (marker of all trophoblast) in the VC (Left) or SC (Right). **(i)** Immunofluorescence co-localization of CDH1 and KRT6 in the VC (Left) or SC (Middle). High magnification inset is denoted by the white box (Right). For all images nuclei were visualized by DAPI stain; Scale bar = 100μm. Abbreviations: AV = Anchoring Villi; FV = Floating Villi; SC = Smooth Chorion epithelium; Amn. = Amnion; Dec. = Decidua.

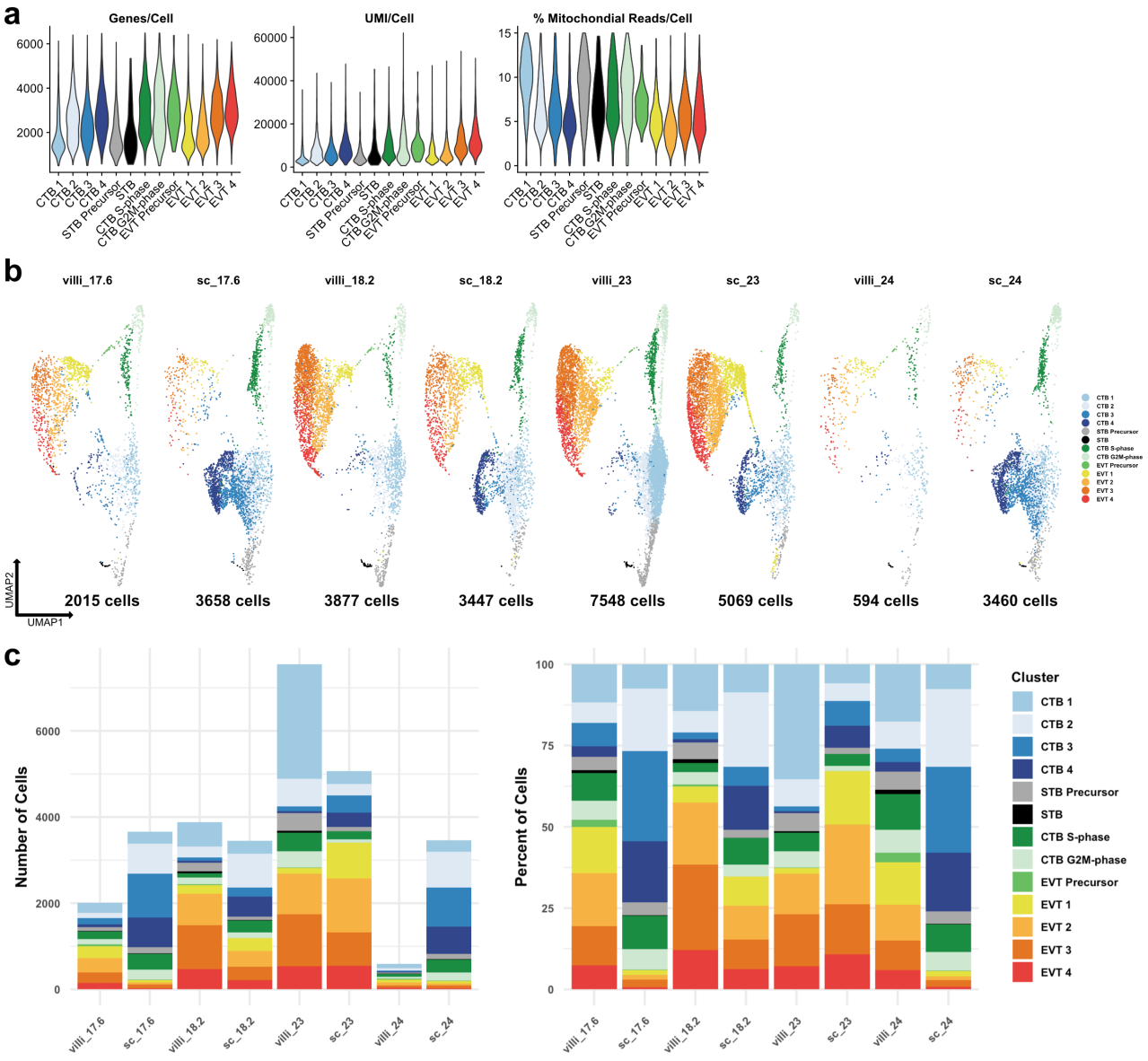

Figure 3.6 - Metrics of the trophoblast subset.
(a) Violin plots of the number of unique genes (left), number of UMI (middle), and the percent of mitochondrial reads (right) per cell for each trophoblast cluster. **(b)** UMAP projections of the trophoblast dataset shown by each placental sample. Colors correspond to each trophoblast cluster shown in the legend at the right. The number of cells analyzed from each placental sample is listed beneath. **(c)** The number of cells (left) and the percentage (right) in each trophoblast cluster from each placental sample.

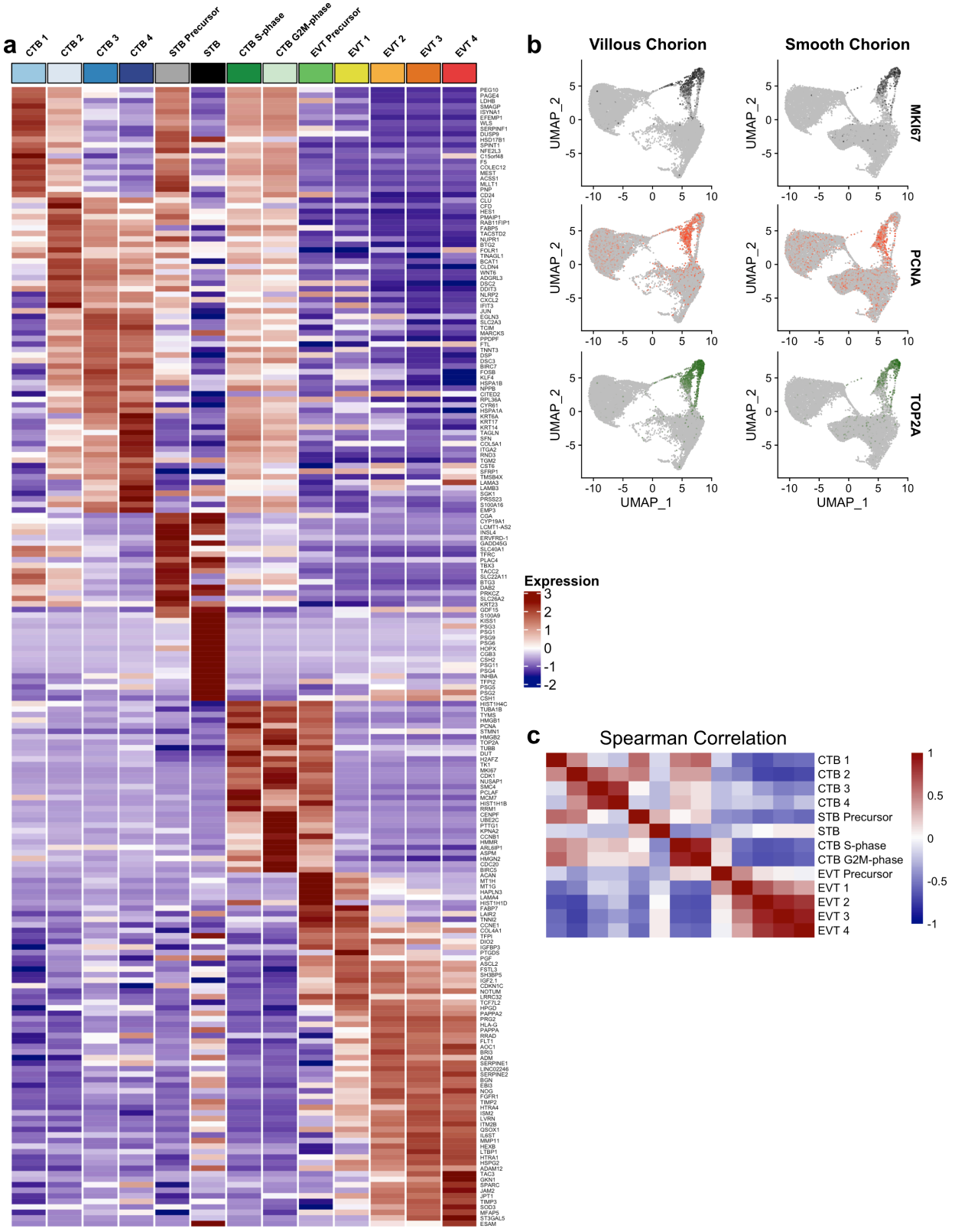

Figure 3.7 - Metrics of the trophoblast subset.
(a) Heatmap of the expression of the top 20 marker genes for each trophoblast population. **(b)** Expression of phasic transcripts MKI67 (top), PCNA (middle), and

TOP2A (bottom) were projected in UMAP space. **(c)** Heatmap of the Spearman Correlation coefficients between each trophoblast population.

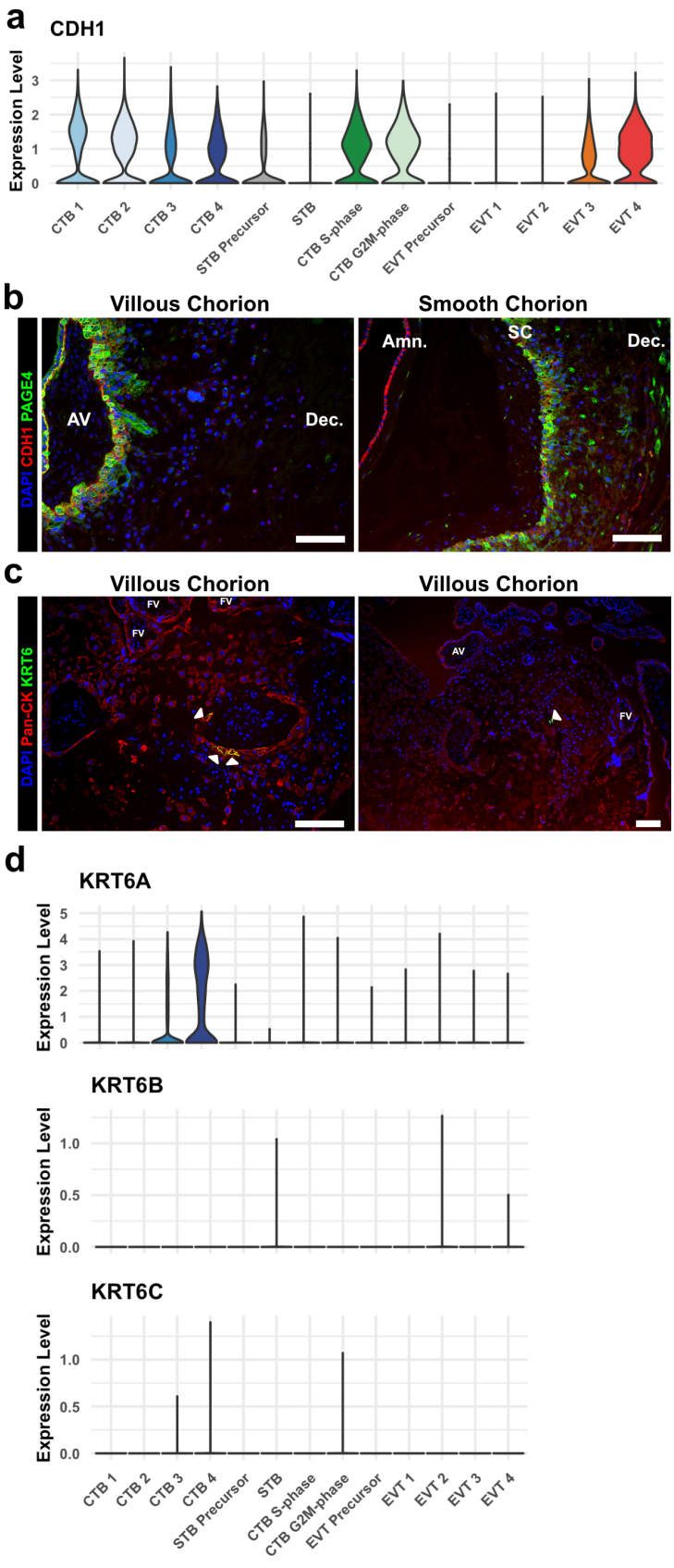
a
CDH1
Expression Level
0
1
2
3
CTB 1
CTB 2
CTB 3
CTB 4
STB Precursor
STB
CTB S-phase
CTB G2M-phase
EVT Precursor
EVT 1
EVT 2
EVT 3
EVT 4
b
Villous Chorion
Smooth Chorion
DAPI CDH1 PAGE4
AV
Dec.
Amn.
SC
Dec.
c
Villous Chorion
Villous Chorion
DAPI Pan-CK KRT6
FV
FV
FV
AV
FV
d
KRT6A
KRT6B
KRT6C
Expression Level
0
1
2
3
4
5
0.0
0.5
1.0
CTB 1
CTB 2
CTB 3
CTB 4
STB Precursor
STB
CTB S-phase
CTB G2M-phase
EVT Precursor
EVT 1
EVT 2
EVT 3
EVT 4

Figure 3.8 - KRT6 expression in the VC region.
(a) Violin plot of *CDH1* transcript expression across all trophoblast clusters. **(b)** Immunofluorescence co-localization of CDH1 and PAGE4 in the VC (Left) and SC (Right). **(c)** Immunofluorescence co-localization of Pan-CK (marker of all trophoblast) and KRT6 in the VC. Arrowheads denote KRT6+ cells. **(d)** Violin plots of expression of each KRT6 isoform, showing expression of only KRT6A in trophoblasts. For all images nuclei were visualized by DAPI stain; Scale bar = 100μm. Abbreviations: AV = Anchoring Villi; Amn. = Amnion; SC = Smooth Chorion epithelium; Dec. = Decidua; FV = Floating Villi.

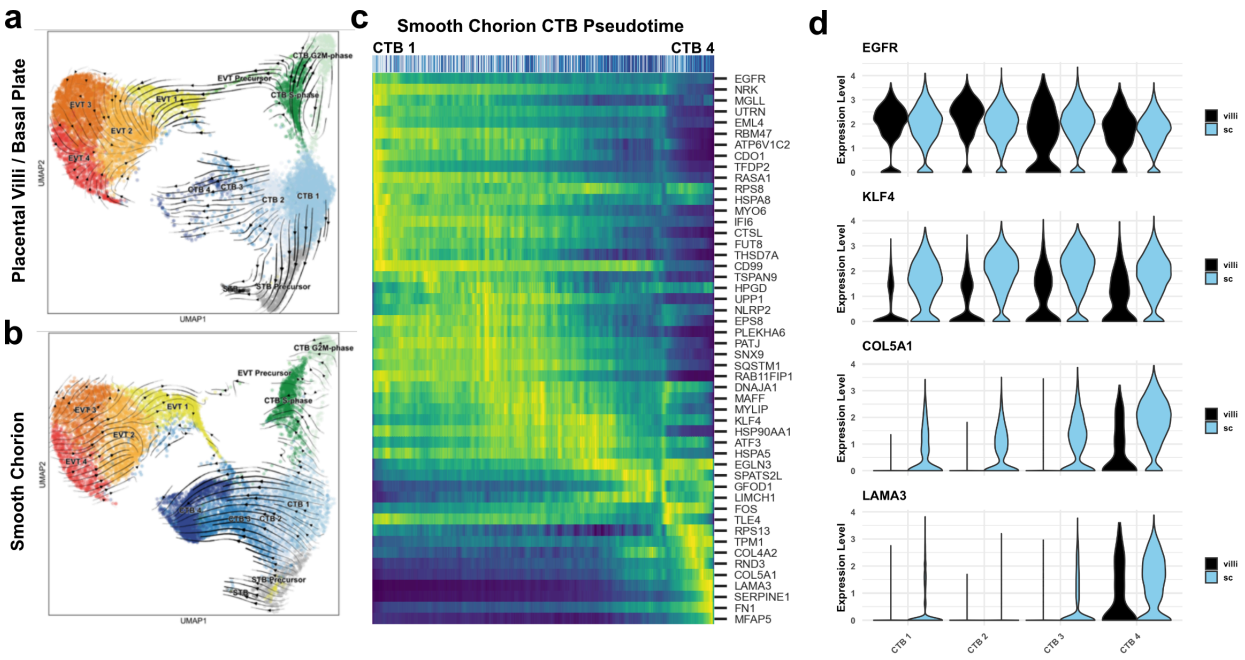

Figure 3.9 - A common CTB progenitor gives rise to STBs in the VC and SC-CTBs in the SC.

RNA velocity vector projections overlaid on to UMAP projections for trophoblast cells isolated from the **(a)** VC and **(b)** SC. Arrows denote direction and magnitude is represented by line thickness. **(c)** Pseudotime reconstruction of SC derived CTB 1-4 clusters from the scVelo dynamical model of latent time. Each column represents one cell. Cells at the left are clustered in CTB 1 and progress through CTB 2, 3, and 4 along the x-axis. Select genes that were the major drivers of the pseudotime alignment are shown on the y-axis. Expression ranged from dark blue (lowest) to yellow (highest). **(d)** Violin plots of select factors from (c) demonstrated shared or region-specific expression for genes associated with the CTB 4 differentiation trajectory.

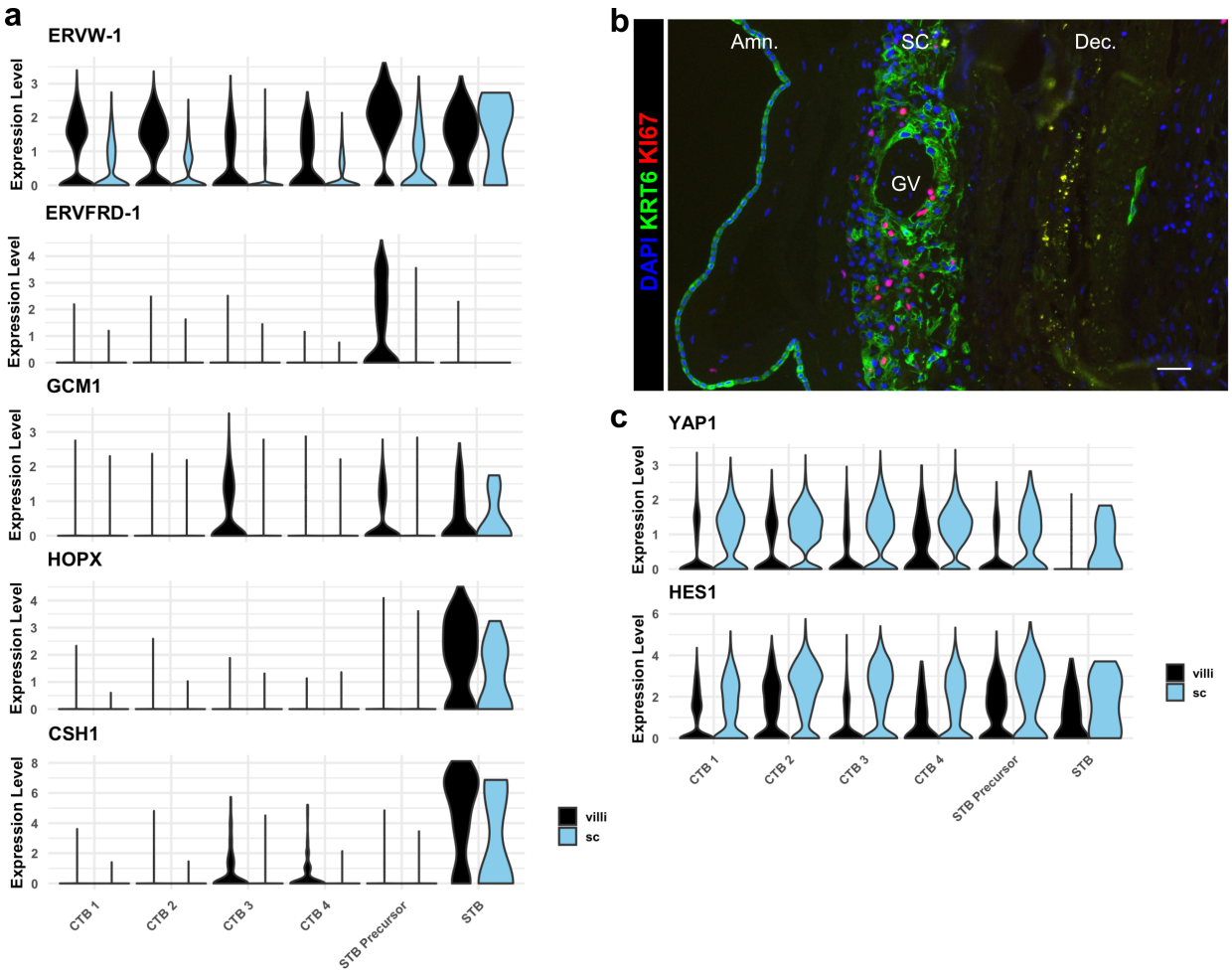

Figure 3.10 - SC trophoblast display reduced expression of STB and increased expression of epithelial TFs.
(a) Violin plots of expression of markers of STB differentiation in each trophoblast cluster shown by region, demonstrating reduced expression all markers in STB Precursor and STB clusters. **(c)** Violin plots of expression of YAP1 and HES1, demonstrating increasing expression in CTB1-4 and greater expression in the SC compared to the VC.

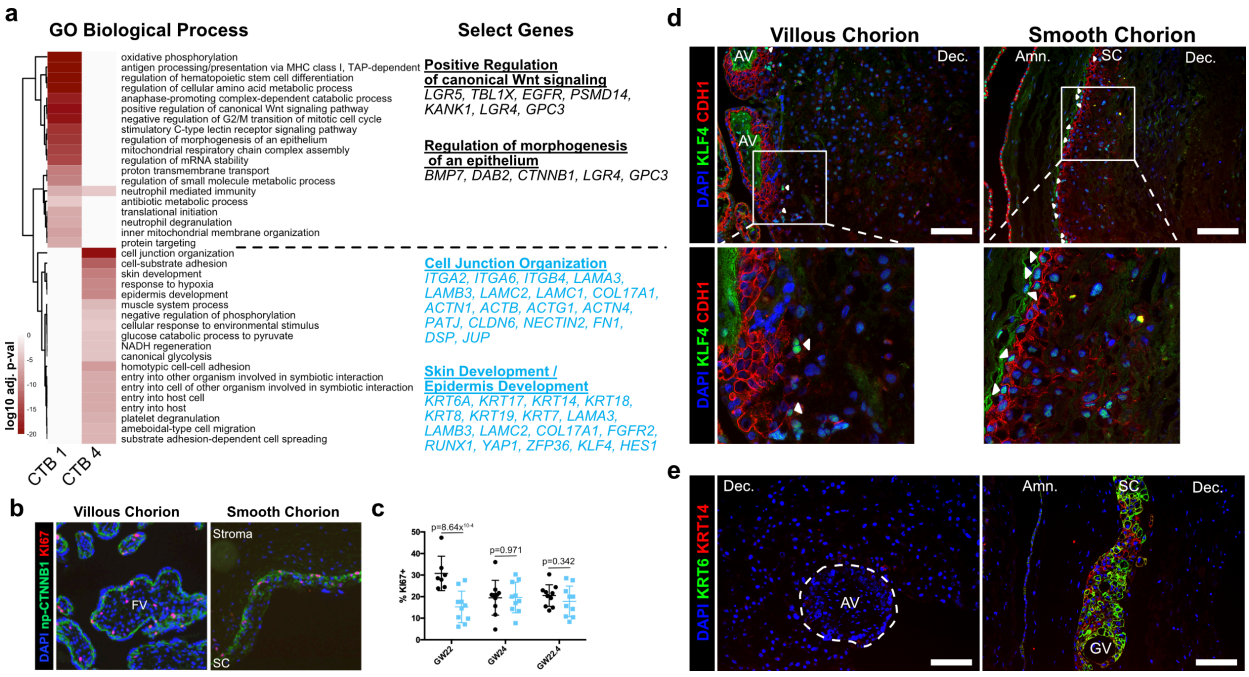

Figure 3.11 - SC-CTBs express a distinct epidermal transcriptional program. **(a)** Heatmap of gene ontology analysis adjusted p-values. Dark red corresponds to the lowest p-values and white represents p-values greater than 0.0005. Ontology categories are organized by hierarchical clustering along the y-axis. Marker genes for each cluster were used as inputs for the analysis. A subset of genes in selected categories are listed at the right. Categories and genes enriched in CTB 1 or CTB 4 are in black or blue, respectively. **(b)** Representative immunofluorescence co-localization of non-phosphorylated CTNNB1 and KI67 in the VC (Left) and SC (Right). **(c)** Quantification of the percent of np-CTNNB1 cells with KI67 expression in each region in three placental samples. Each dot represents the percentage in one field of view (at least 7 per region per sample) as an estimate of mitotic cells per population. Percentages for the VC region are shown in black and the SC region in blue. **(d)** Immunofluorescence co-localization of CDH1 and KLF4 protein in the VC (Left) or SC (Right). Arrowheads denote CDH1+/KLF4+ cells. **(e)** Immunofluorescence co-localization of KRT14 and KRT6 protein in the VC (Left) or SC (Right). The outline of the Anchoring Villi (AV) is denoted by the white dashed line. For all images nuclei were visualized by DAPI stain; Scale bar = 100μm. Abbreviations: AV = Anchoring Villi; FV = Floating Villi; SC = Smooth Chorion epithelium; Amn. = Amnion; Dec. = Decidua; GV = Ghost Villi.

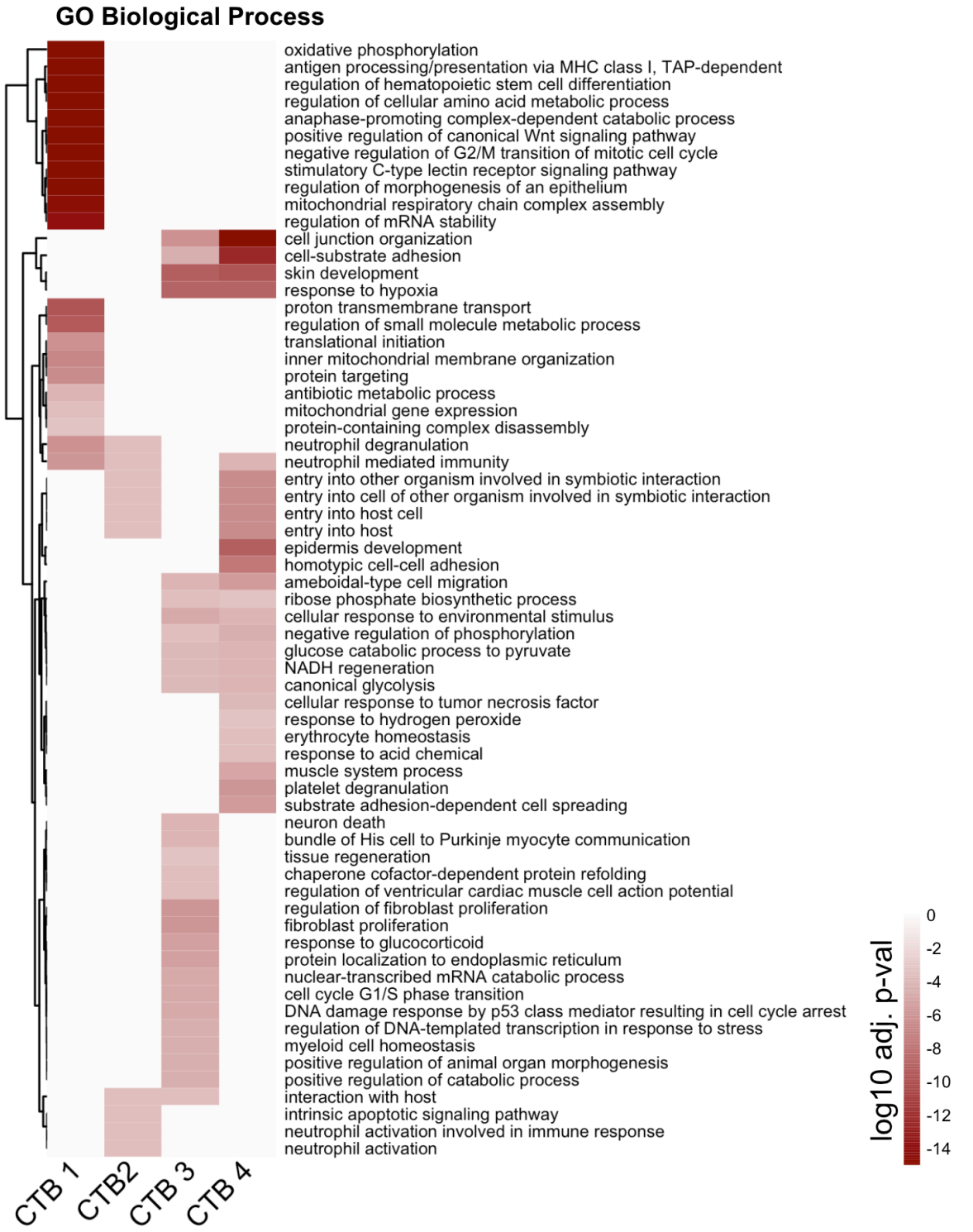

Figure 3.12 - Complete CTB Gene Ontology Analysis.
The unabridged Gene Ontology results from each CTB cluster, displayed as adjusted p-values. Dark red corresponds to the lowest p-values and white represents p-values greater than 0.0005. Ontology categories are organized by hierarchical clustering along the y-axis. Marker genes for each cluster were used as inputs for the analysis.

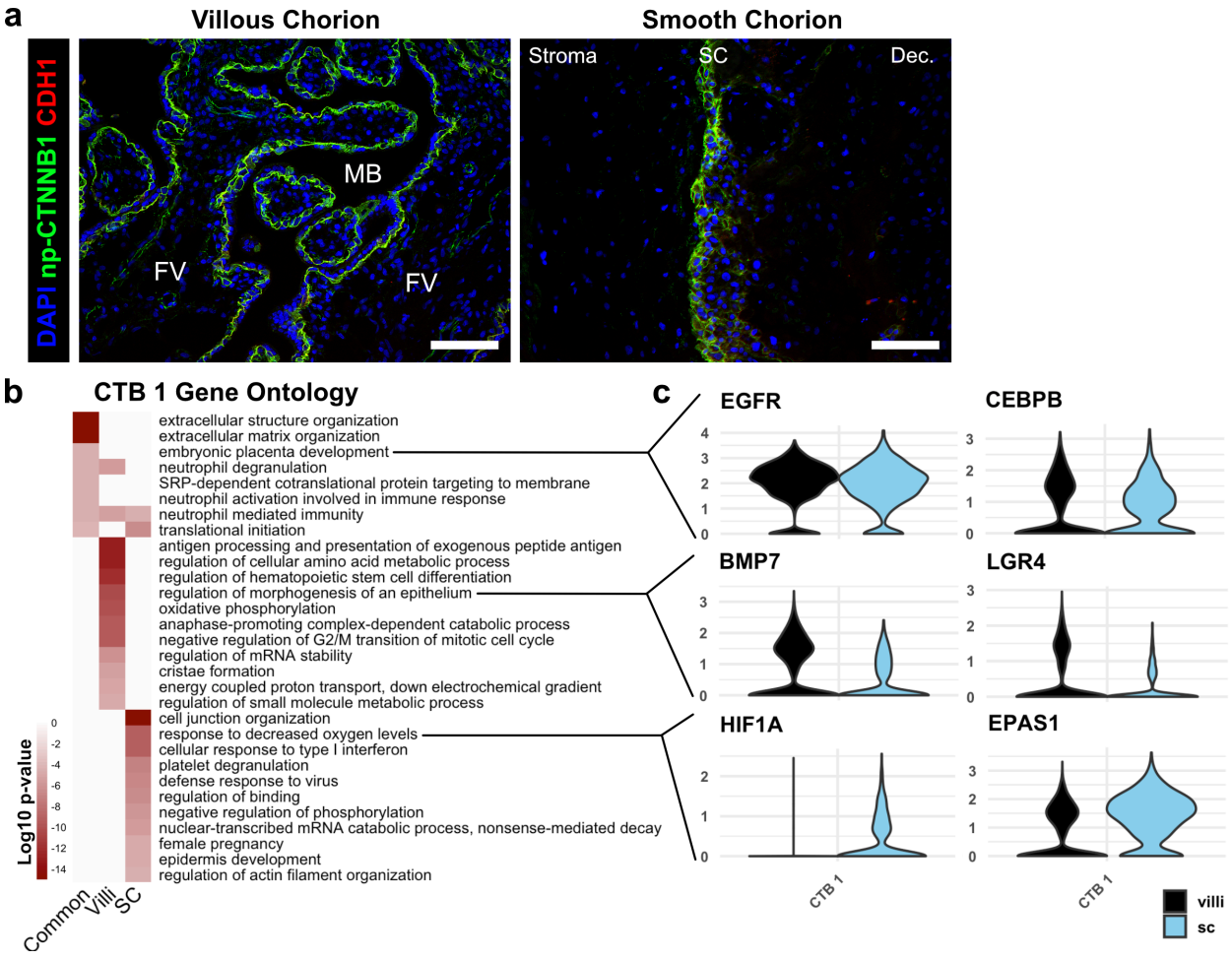

Figure 3.13 - Similarities and differences between CTB 1 in VC and SC.
(a) Immunofluorescence co-localization of CDH1 and non-phosphorylated CTNNB1 in the VC (left) and SC (right), showing identical domains of expression in both regions. For all images nuclei were visualized by DAPI stain; Scale bar = 100μm. Abbreviations: FV = Floating Villi; MB = Maternal Blood space; SC = Smooth Chorion epithelium; Dec. = Decidua. **(b)** Gene ontology analysis for CTB 1 genes common to VC and SC, genes enriched in VC, and genes enriched in SC. **(c)** Violin plots of genes within the gene ontology categories indicated in (b) for common categories (top), VC enriched categories (middle), and SC enriched categories (bottom).

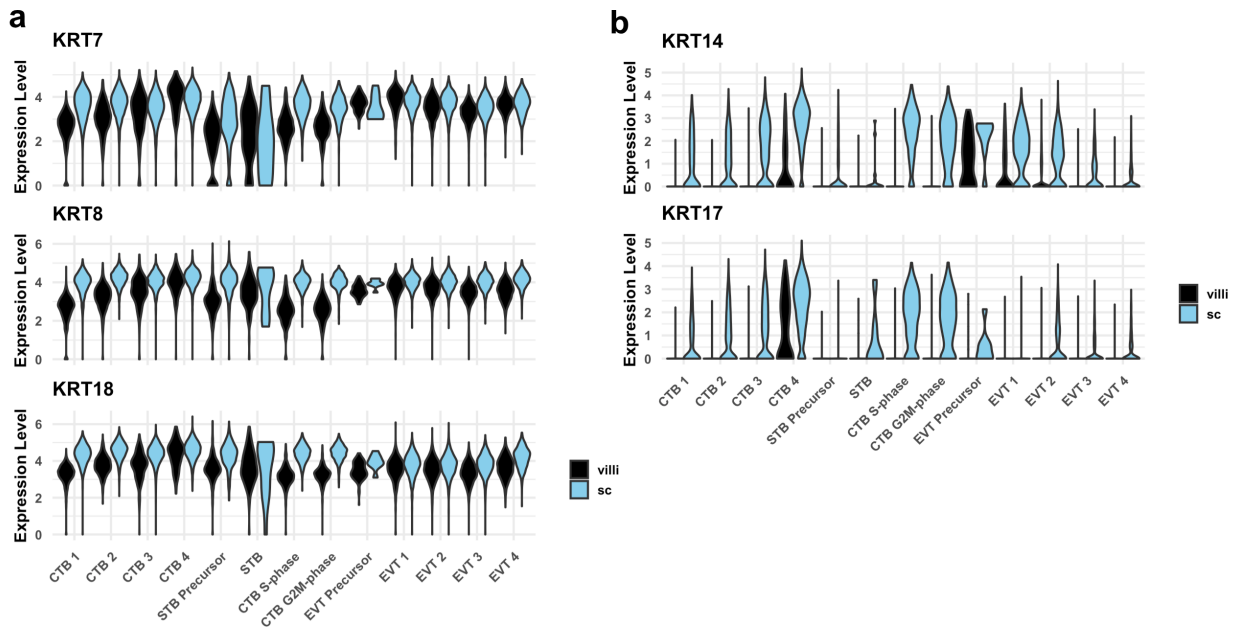

Figure 3.14 - Cytokeratin expression in VC and SC trophoblast.
(a) Violin plots of cytokeratins expressed in trophoblast in both VC and SC regions by cluster and region of origin. **(b)** Violin plots of cytokeratins expressed in SC trophoblast by cluster and region of origin.

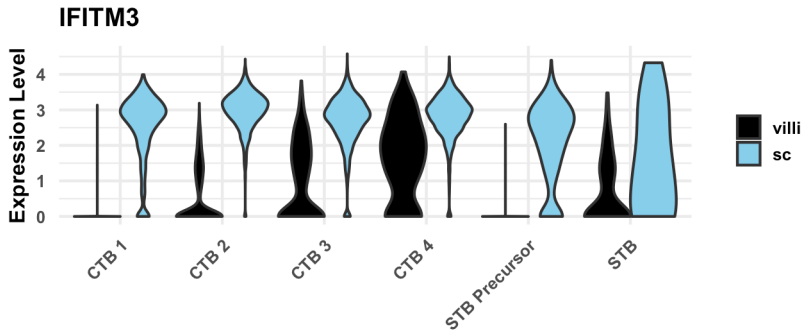

Figure 3.15 - IFITM3 expression in CTB populations.
Violin plot of IFITM3 expression in trophoblast clusters by region, showing increased expression in SC compared to VC.

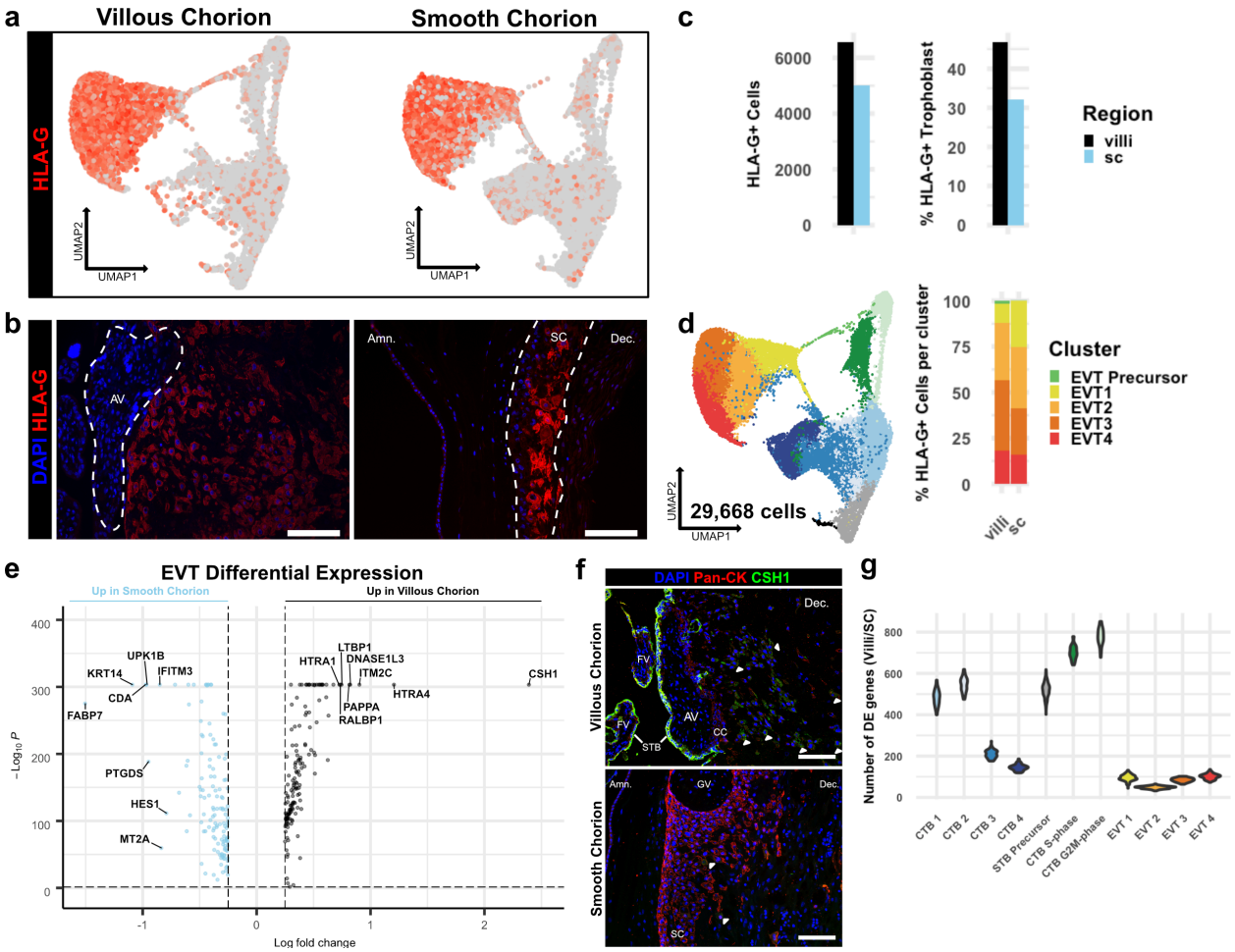

Figure 3.16 - EVTs of the VC and SC regions are behaviorally distinct but transcriptionally similar.

(a) Expression of *HLA-G* transcript per cell projected in UMAP space for the VC (Left) and SC (Right). Expression ranged from low in light gray to high in dark red. **(b)** Immunofluorescence localization of HLA-G in the VC (Left) and SC (Right). The Anchoring Villi (AV) are outlined in white (Left). The boundaries of the smooth chorion epithelium are denoted by the white lines (Right) **(c)** Quantification of the number of *HLA-G* expressing EVT (Left) and the percent of total trophoblast that express *HLA-G* (Right) for each placental region. **(d)** UMAP projection of all trophoblast cells including the EVT clusters (Left). The percent of EVT cells in each cluster from each region (Right). **(e)** Volcano plot of the differentially expressed genes between regions for all EVTs. All genes with a log fold change greater than an absolute value of 0.25 and a p-value of less than 0.05 were plotted. Those with greater expression in VC EVT are shown in black. Those with greater expression in SC EVT are shown in blue. **(f)** Immunofluorescence localization of CSH1 in the VC Top) and SC (Bottom). Arrowheads denote CSH1 expressing cells **(g)** Violin plots of the number of differentially expressed genes between 100 cells from each placental region within each cluster (100 permutations). Clusters with less than 100 cells per region were omitted due to the small sample size. For all images nuclei were visualized by DAPI stain; Scale bar =

100μm. Abbreviations: AV = Anchoring Villi; FV = Floating Villi; SC = Smooth Chorion epithelium; Amn. = Amnion; Dec. = Decidua; STB = Syncytiotrophoblast; CC = Cell Column.

a **Gene Ontology**

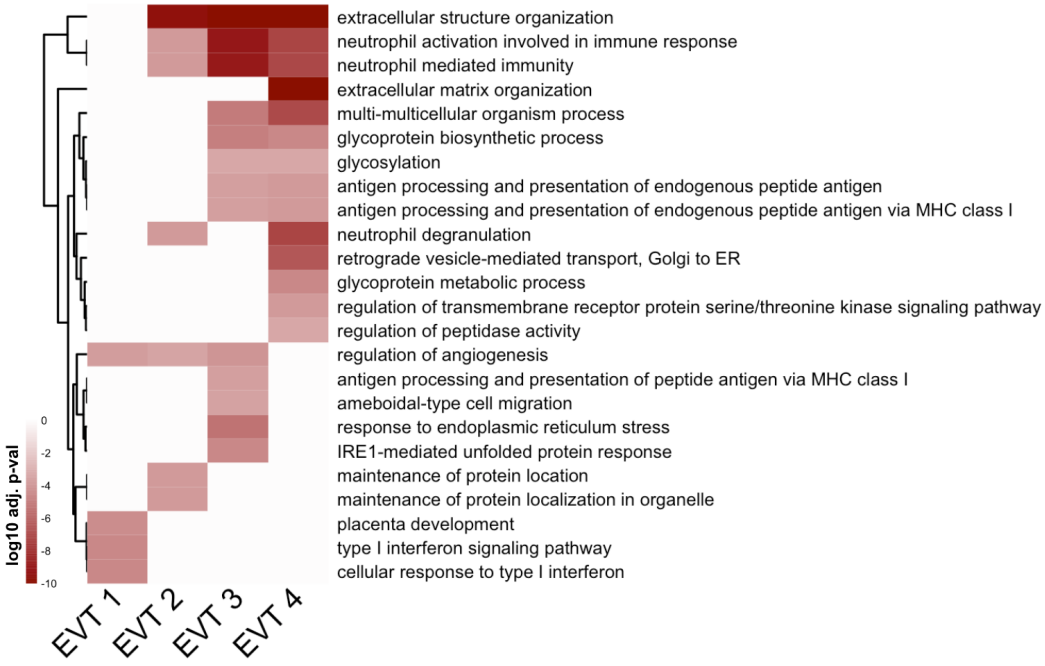

b

Placenta Development
ASCL2, GCM1, CEBPB, EPAS1, PPARG, ADAM19, DLX3

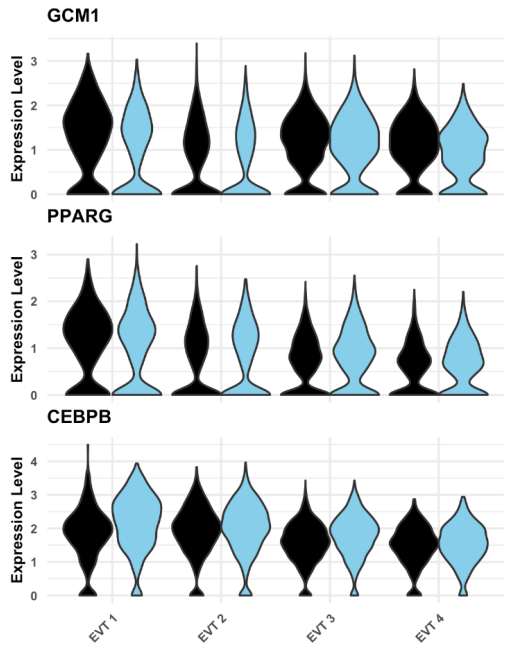

c

Extracellular Structure Organization
TIMP1, TIMP2, MMP2, MMP11, HTRA1, ADAM12, ADAM19, ADAM10, ADAM15, ITGA1, ITGA5, ITGB1, FN1, COL4A2, COL27A1, SMAD3

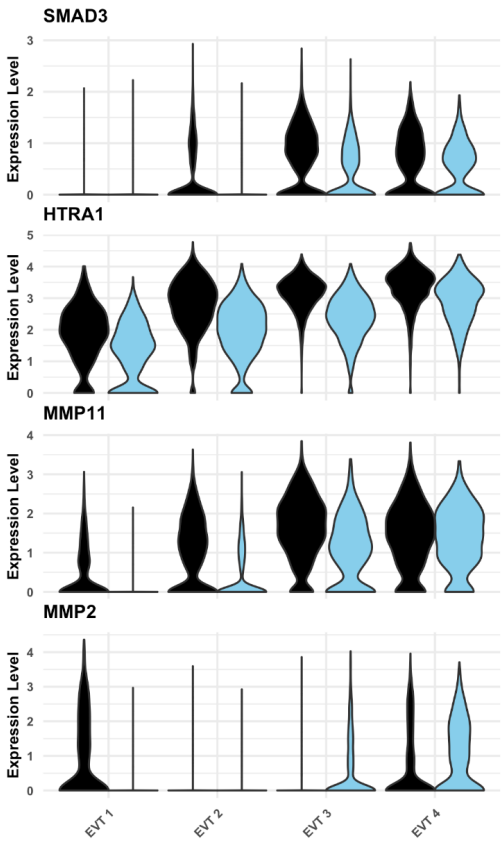

Figure 3.17 - Functional annotation of EVT clusters.
(a) Gene Ontology results from each EVT cluster displayed as adjusted p-values. Dark red corresponds to the lowest p-values and white represents p-values greater than 0.0005. Ontology categories are organized by hierarchical clustering along the y-axis. Marker genes for each cluster were used as inputs for the analysis. **(b)** Selected genes in the 'placenta development' gene ontology category (top). Violin plots of expression for selected genes in each EVT cluster by region. **(c)** Selected genes in the 'Extracellular Structure Organization' gene ontology category (top). Violin plots of expression for selected genes in each EVT cluster by region.

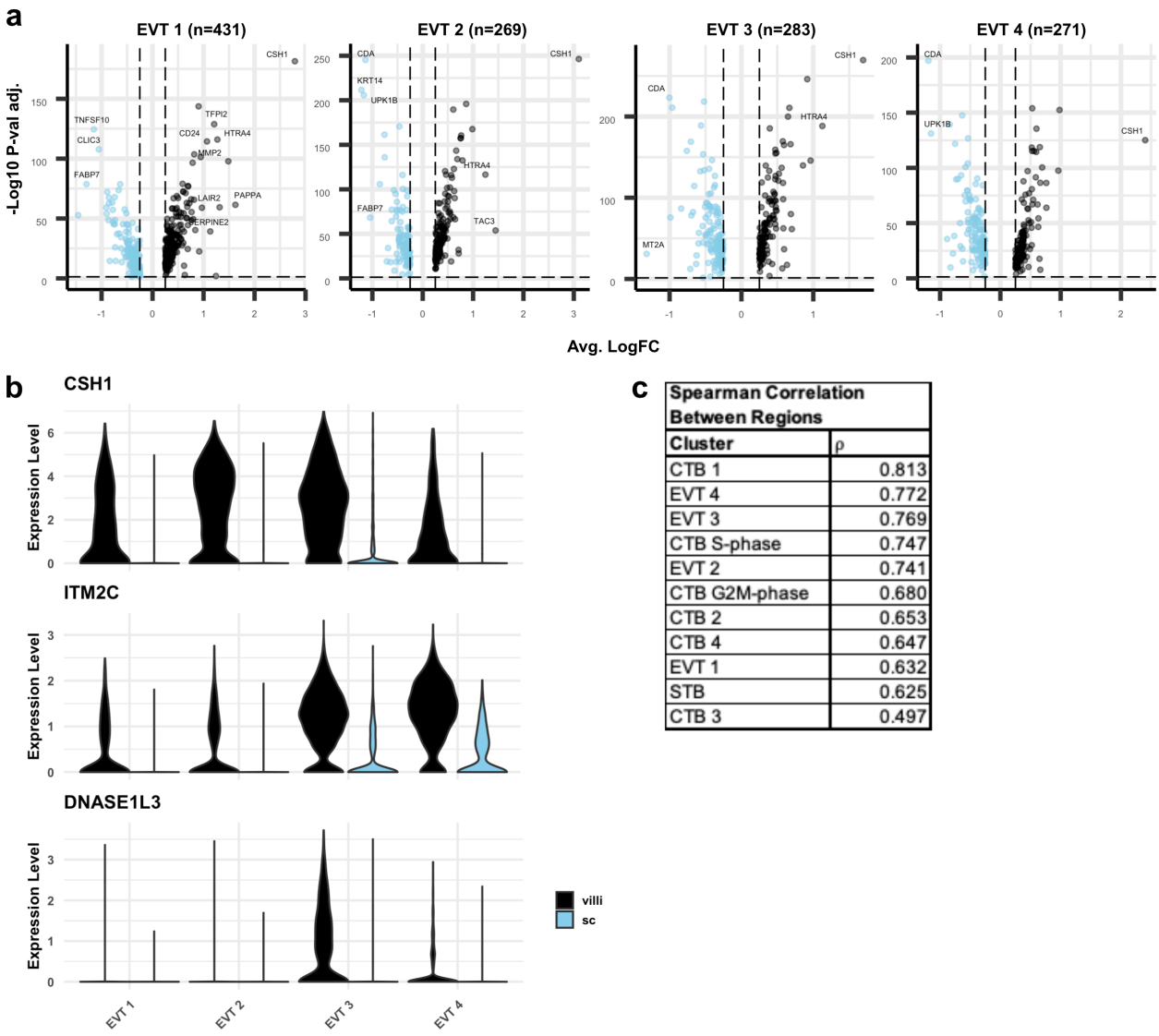

c

Spearman Correlation Between Regions	
Cluster	**ρ**
CTB 1	0.813
EVT 4	0.772
EVT 3	0.769
CTB S-phase	0.747
EVT 2	0.741
CTB G2M-phase	0.680
CTB 2	0.653
CTB 4	0.647
EVT 1	0.632
STB	0.625
CTB 3	0.497

Figure 3.18 - Differential expression between EVT from VC and SC.
(a) Volcano plots showing the differentially expressed genes the VC or SC for each EVT cluster. Only significantly differentially expressed genes are plotted (p-value <0.05). Genes with higher expression in VC compared to SC are shown in black. Genes with higher expression in SC compared to VC are shown in blue. Selected differentially expressed genes are labelled. **(b)** Violin plots of VC-specific genes in EVTs. **(c)** Spearman correlation coefficients between VC and SC for each cluster ranked from greatest to least similarity across regions. STB and EVT Precursor populations are excluded due to the low number of cells recovered in the SC.

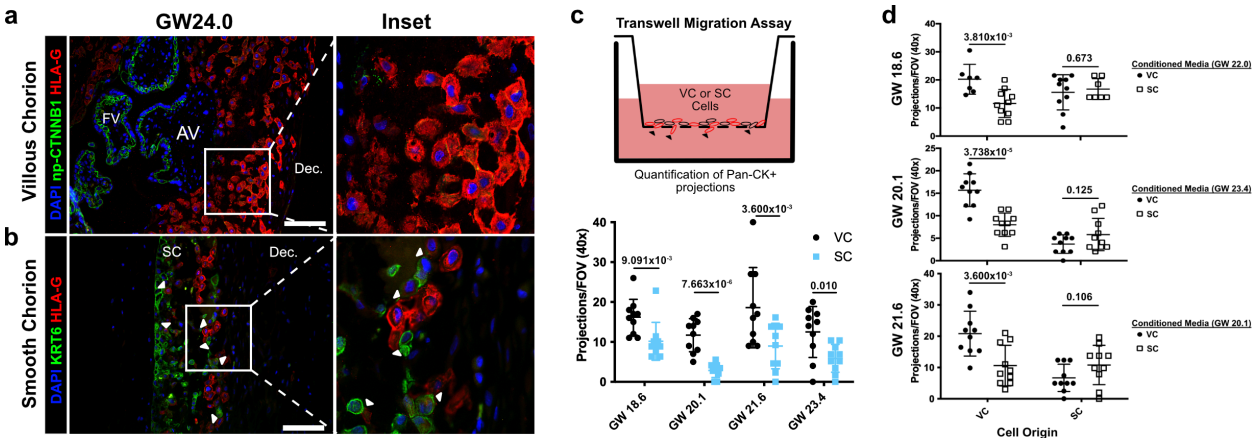

Figure 3.19 - CTBs of the SC inhibit EVT invasion.
(a) Immunofluorescence co-localization of np-CTNNB1 and HLA-G in the VC. **(b)** Immunofluorescence co-localization of KRT6 and HLA-G in the SC. Arrowheads denote CTB and EVT interactions. **(c)** Schematic of the transwell invasion assay (top). Cells from either placental region were plated in the upper chamber of the transwell. After 39 hours of culture, the transwell membrane was fixed and stained with a Pan-cytokeratin antibody. The projections through the membrane are denoted by black arrowheads and quantified below. Results from the VC derived cells are shown in black, and the results from the SC derived cells are shown in blue. **(d)** Results from three biological replicates from each placental region cultured with conditioned medium from either VC or SC cells. The gestational ages of the plated cells is shown adjacent to the y-axis. The gestational ages of the cells from which conditioned medium was collected are noted in the legends at the right. The results for cells cultured with VC cell conditioned medium are denoted by black dots, and the results for those cultured in SC cell conditioned medium are denoted by open squares. P-values were determined by t-test and are listed above each comparison. For all images nuclei were visualized by DAPI staining ; Scale bar = 100μm. Abbreviations: AV = Anchoring Villi; FV = Floating Villi; SC = Smooth Chorion epithelium; Dec. = Decidua.

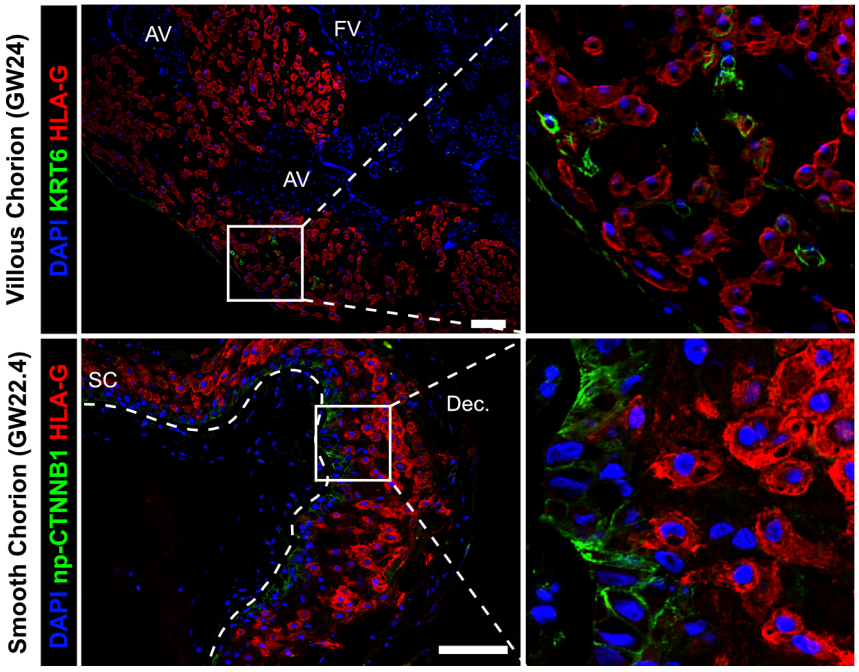

Figure 3.20 - CTB-EVT interactions in the VC or SC region.
Colocalization of KRT6 (SC-CTB marker) and HLA-G (EVT marker) showing rare KRT6+ cells in the VC (top). These cells are few and do not interact with EVT in the same manner as was observed in the SC. Co-localization of non-phosphorylated CTNNB1 (CTB 1 marker) and HLA-G (EVT marker) in the SC (Bottom). Limited interactions between these populations was observed. The basal lamina separating the fetal stroma from the SC epithelium is marked by the white dashed line. For all images nuclei were visualized by DAPI stain; Scale bar = 100μm. Abbreviations: AV = Anchoring Villi; FV = Floating Villi; SC = Smooth Chorion epithelium; Dec. = Decidua.

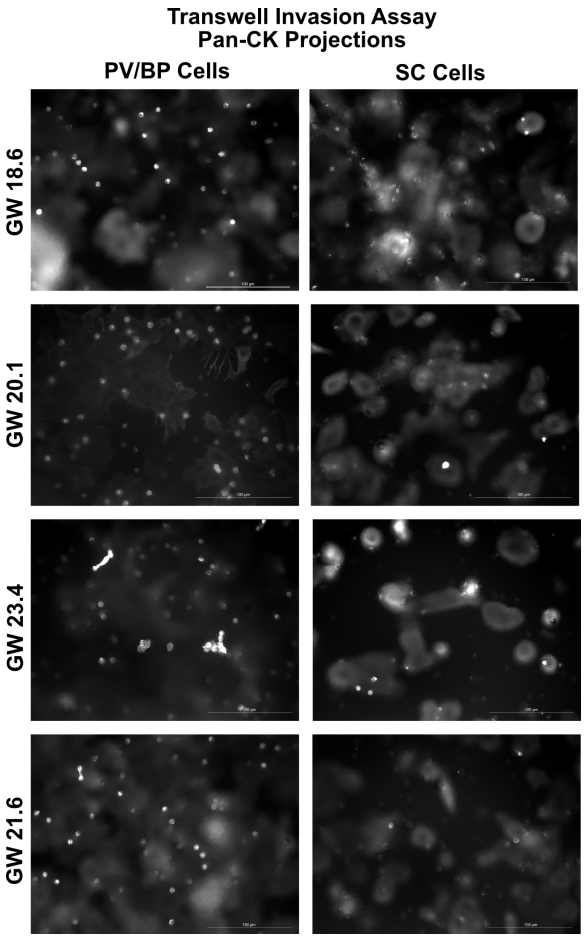

Figure 3.21 - Representative images of the transwell invasion assay.
Representative images of trophoblast projections through the transwell filter are seen as white dots. For quantification, the number of projections (white bright dots) were counted. For each sample, the median DAPI area was quantified across the transwell membrane, and then the projections multiplied by a factor to normalize for cell density. Scale bar = 100μm.

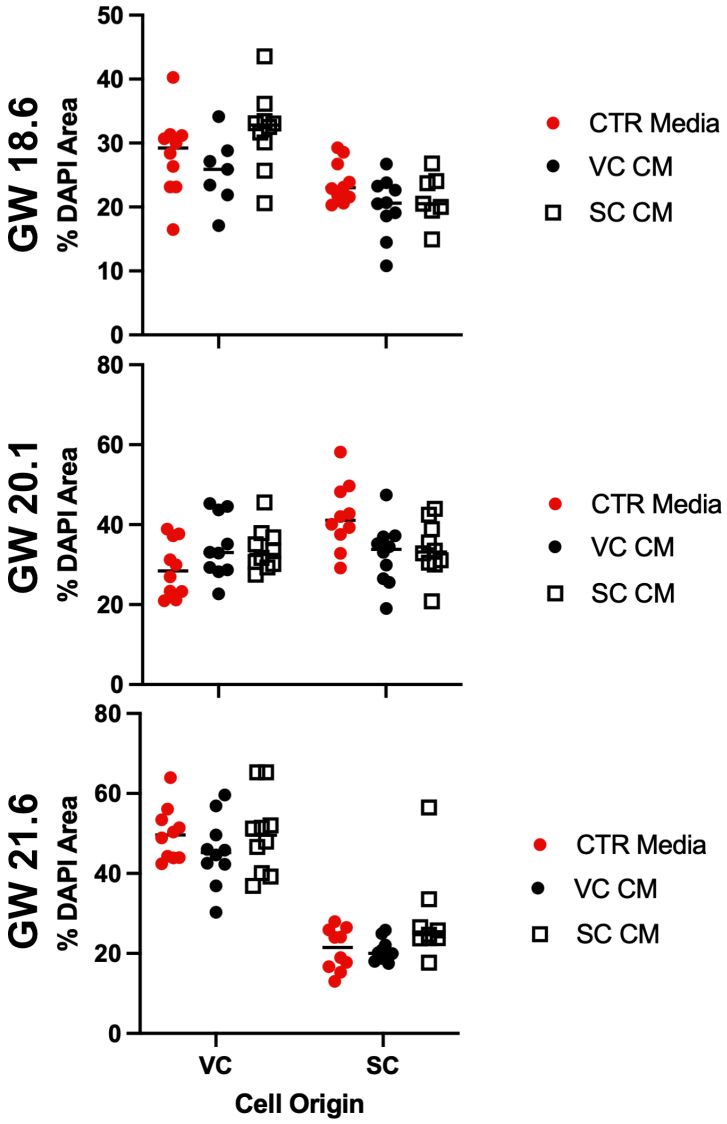

Figure 3.22 - Cell density is not correlated with culture in conditioned media.
The DAPI+ area in each field of view was quantified and plotted as a measure of cell density. Each dot represents the percent area of the field of view which stained with DAPI. Measurements from each experiment are shown and the gestational ages of the cultured cells is on the y-axis at the left. Measurements of cells treated with control media (Serum Free Media) are shown in red, VC cell conditioned media are shown in black, and SC cell conditioned media are shown in open squares.

Methods

Tissue Collection: The University of California, San Francisco (UCSF) Institutional Review Board approved this study. All donors gave informed consent.

Cellular Isolation of VC trophoblast: Trophoblast were isolated from both floating and anchoring villi dissected from 2nd trimester human placentas. Trophoblast were isolated according to previously published protocols (Fisher et al., 1989; Kliman and Feinberg, 1990).

Cellular Isolation of SC trophoblast: Trophoblast were isolated according to previously published protocols (Garrido-Gomez et al., 2017).

Single Cell RNA-Sequencing and Analysis: To capture the transcriptome of individual cells we used the Chromium Single Cell 3' Reagent V3 Kit from 10X Genomics. For all samples 17,500 cells were loaded into one well of a Chip B kit for GEM generation. Library preparation including, reverse transcription, barcoding, cDNA amplification, and purification was performed according to Chromium 10x V3 protocols. Each sample was sequenced on a NovaSeq 6000 S4 to a depth of approximately 20,000-30,000 reads per cell. The gene expression matrices for each dataset was generated using the CellRanger software (v3.0.2 - 10x Genomics). All reads were aligned to GRCh38 using STAR. (https://support.10xgenomics.com/single-cell-gene-expression/software/pipelines/latest/advanced/references). The counts matrix was thresholded and analyzed in the package Seurat (v3.1.3). Cells with fewer than 500 or

greater than 6000 unique genes, as well as all cells with greater than 15 percent mitochondrial counts, were excluded from all subsequent analyses. Doublet detection was performed for each sample using DoubletFinder and all doublets were excluded from analysis. For each sample, counts were scaled and normalized using ScaleData and NormalizeData, respectively, with default settings FindVariableFeatures used to identify the 2000 most variable genes as input for all future analyses. PCA was performed using RunPCA and significant PCs assessed using ElbowPlot and DimHeatmap. Dimensionality reduction and visualization using UMAP was performed by RunUMAP.

Integration of each timepoint into one dataset was performed using FindIntegrationAnchors and IntegrateData, both using 20 dimensions (after filtering each dataset for number of genes, mitochondrial counts, and normalizing as described above). Data scaling, PCA, selection of PCs, clustering and visualization proceeded as described above using 30 PCs and a resolution of 0.6.

To generate the trophoblast, stroma, and immune cell subsets, the respective clusters were subset from the integrated dataset using the function SubsetData based upon annotations from marker genes identified by FindAllMarkers. After subsetting, counts were scaled and normalized using ScaleData and NormalizeData, respectively, with default settings FindVariableFeatures used to identify the 2000 most variable genes. Differentially expressed genes for each integrated dataset were identified using FindAllMarkers.

scVelo: RNA velocity analysis was applied to the entire conglomerate dataset using Velocyto to generate spliced and unspliced reads for all cells. This dataset was then subset for the trophoblast dataset introduced in Figure 2.2. The scVelo dynamical model was run with default settings and subset by each timepoint.

Differential expression between regions: The number of trophoblast cells in each cluster were downsampled to 100 cells from each region of origin and performed differential expression using FindMarkers function and repeated this for 100 permutations. The number of genes found to be significantly differentially expressed (adj. P-value <0.05) from each permutation are plotted. Clusters having less that 100 cells from each region were excluded from this analysis.

Gene Ontology Analysis: Gene Ontology analysis was performed with ClusterProfiler enrichGO function. The simplify function within this package was used to consolidate hierarchically related terms using a cutoff of 0.5. Terms were considered significantly enriched with an adjusted P-value of less than 0.05.

Immunofluorescence Staining: Placental tissue for cryosectioning was fixed in 3% PFA at 4°C for 8hrs, washed in 1x PBS, then submerged in 30% sucrose overnight at 4°C prior to embedding in OCT medium. Placental tissue in OCT was sectioned at 5μm for all conditions. In brief, slides were washed in 1x PBST (1x PBS, 0.05% Tween-20), blocked for 1hr (1x PBS + 5% donkey or goat serum + 0.3% TritonX), incubated in primary antibody diluted for 3 hours at room temperature (or overnight at 4°C), washed in 1x

PBST, incubated in secondary antibody (Alexafluor 488 or 594) for 1 hour at room temperature, incubated in DAPI for 10min at room temp, washed in 1x PBST, and mounted and sealed for imaging. Any antigen retrieval was performed prior to the blocking step by heating the slides in a 1x citrate buffer with 0.05% Tween-20 at 95C for 30 minutes. All antibodies and the dilutions are listed in the key resources table. All immunofluorescence staining was performed in n=3 biological replicates (3 distinct placentas) and representative image is shown.

Transwell Invasion Assay: 24-well plate transwell inserts with an 8 μM polycarbonate membrane (Corning Costar 3422) were coated with 10μL of Matrigel (growth factor-containing, Corning Corp, USA) diluted 1:1 in Serum Free Media (95% DME H-21 + Glutamine, 2% Nutridoma (mostly β-D xylopyranose), 1% Pen Strep, 1% Hepes, 0.1% Gentamycin). Cells from each region of the placenta were isolated as described above and then plated in the upper well of the transwell insert at a density of 250,000 cells in 250μL of Serum Free Media, with 1mL of Serum Free Media (or conditioned media) in the well below the insert. The cells were then cultured for 39 hours. The cells in the transwell were then fixed in 3% PFA for 10min at 4C, permeabilized in ice cold methanol for 10min at 4C, then washed in 1x PBS, incubated in Pan-CK primary antibody for 3 hours at 37C, washed in 1x PBS, incubated with secondary antibody (Alexafluor 594) and DAPI for 1 hour at 37C, washed in 1x PBS, then mounted and sealed for imaging. All experiments were performed in n=3 biological replicates (3 distinct placentas). For conditioned media experiments n=3 biological replicates were analyzed (cells and conditioned medium derived from 3 distinct placentas) .

Transwell Invasion Assay Quantification: Transwell membranes mounted on slides were imaged at 40x magnification and the number of Pan-CK positive projections through the membrane counted. Normalization for changes in cell density across fields of view and culture conditions was performed by quantifying the DAPI positive area of each image and the number of projections normalized to the median across comparisons. Between 7-10 fields of view were quantified for each transwell membrane. P-values were determined by t-test.

Culture of placental cells and generation of conditioned media: Each well of a 24-well plate was coated with 20μL of Matrigel undiluted (growth factor-containing, Corning Corp, USA) prior to cell seeding. Cells from each region of the placenta were isolated as described above and then plated into wells of a 24-well plate at a density of $1x10^6$ cells in 1mL of Serum Free Media (95% DME H-21 + Glutamine, 2% Nutridoma (mostly β-D xylopyranose), 1% Pen Strep, 1% Hepes, 0.1% Gentamycin). The cells were cultured for 39 hours. After 39 hours in culture the media was removed and centrifuged at 2000g for 10mins to remove cellular debris. The supernatant was then removed, snap frozen in LN2, and stored at -80C. This media was then thawed and used as conditioned media.

Data Availability

All sequencing data is available at the NCBI Gene Expression Omnibus GSE198373. Processed data are available as R objects at https://figshare.com/projects/Regionally_distinct_trophoblast_regulate_barrier_function_

and_invasion_in_the_human_placenta/135191. Code to process all raw data and generate the datasets analyzed are available at https://github.com/marshbp/Regionally-distinct-trophoblast-regulate-barrier-function-and-invasion-in-the-human-placenta.

Acknowledgements

We thank the members of the University of California – San Francisco National Center of Translational Research in Reproduction and Infertility for helpful comments during the design, execution, and publication of this project. We would also like to thank all members of the Blelloch and Fisher Labs for their comments and support. We specifically thank Ali San and Nasim Zeighami for their research contributions. We would also like to acknowledge our funding sources, the NIH Eunice Kennedy Shriver National Institute for Child Health and Human Development P50 HD055764 and NIH R37 HD076253.

Competing Interests

Susan Fisher is a consultant for Novo Nordisk. All other authors declare no competing interests.

References

Baczyk, D., Drewlo, S., Proctor, L., Dunk, C., Lye, S., & Kingdom, J. (2009). Glial cell missing-1 transcription factor is required for the differentiation of the human trophoblast. *Cell Death and Differentiation*, *16*(5), 719–727. https://doi.org/10.1038/cdd.2009.1

Bailey, C. C., Zhong, G., Huang, I. C., & Farzan, M. (2014). IFITM-family proteins: The cell's first line of antiviral defense. *Annual Review of Virology*, *1*(1), 261–283. https://doi.org/10.1146/annurev-virology-031413-085537

Bartles, H., & Wang, T. (1983). Intercellular Junctions in the Human Fetal Membranes. *Anatomy and Embryology*, 103–120.

Benirschke, K., Kaufmann, P., & Baergen, R. (2006). Pathology of the Human Placenta. In *Pathology* (Vol. 38, Issue 2). https://doi.org/10.1016/s0031-3025(16)39684-2

Bergen, V., Lange, M., Peidli, S., Wolf, F. A., & Theis, F. J. (2020). Generalizing RNA velocity to transient cell states through dynamical modeling. *Nature Biotechnology*, *38*(12), 1408–1414. https://doi.org/10.1038/s41587-020-0591-3

Blaise, S., De Parseval, N., Bénit, L., & Heidmann, T. (2003). Genome wide screening for fusogenic human endogenous retrovirus envelopes identifies syncytin 2, a gene conserved on primate evolution. *Proceedings of the National Academy of Sciences of the United States of America*, *100*(22), 13013–13018. https://doi.org/10.1073/pnas.2132646100

Boyd, J. D., & Hamilton, W. J. (1967). Development and Structure of the Human Placenta From the End of the 3Rd Month of Gestation. *BJOG: An International Journal of Obstetrics & Gynaecology*, *74*(2), 161–226. https://doi.org/10.1111/j.1471-0528.1967.tb14864.x

Buchrieser, J., Degrelle, S. A., Couderc, T., Nevers, Q., Disson, O., Manet, C., Donahue, D. A., Porrot, F., Hillion, K. H., Perthame, E., Arroyo, M. V., Souquere, S., Ruigrok, K., Dupressoir, A., Heidmann, T., Montagutelli, X., Fournier, T., Lecuit, M., & Schwartz, O. (2019). IFITM proteins inhibit placental syncytiotrophoblast formation and promote fetal demise. *Science*, *365*(6449), 176–180. https://doi.org/10.1126/science.aaw7733

Del Peso, L., Castellanos, M. C., Temes, E., Martín-Puig, S., Cuevas, Y., Olmos, G., & Landázuri, M. O. (2003). The von Hippel Lindau/hypoxia-inducible factor (HIF) pathway regulates the transcription of the HIF-proline hydroxylase genes in response to low oxygen. *Journal of Biological Chemistry*, *278*(49), 48690–48695. https://doi.org/10.1074/jbc.M308862200

Dokras, A., Gardner, L. M. G., Seftor, E. A., & Hendrix, M. J. C. (2001). Regulation of human cytotrophoblast morphogenesis by hepatocyte growth factor/scatter factor. *Biology of Reproduction*, *65*(4), 1278–1288. https://doi.org/10.1095/biolreprod65.4.1278

Ferreira, L. M. R., Meissner, T. B., Mikkelsen, T. S., Mallard, W., O'Donnell, C. W., Tilburgs, T., Gomes, H. A. B., Camahort, R., Sherwood, R. I., Gifford, D. K., Rinn,

J. L., Cowan, C. A., & Strominger, J. L. (2016). A distant trophoblast-specific enhancer controls HLA-G expression at the maternal-fetal interface. *Proceedings of the National Academy of Sciences of the United States of America*, *113*(19), 5364–5369. https://doi.org/10.1073/pnas.1602886113

Fisher, S. J., Cui, T., Zhang, L., Hartman, L., Grahl, K., Guo-Yang, Z., Tarpey, J., & Damsky, C. H. (1989). Adhesive and degradative properties of human placental cytotrophoblast cells in vitro. *Journal of Cell Biology*, *109*(2), 891–902. https://doi.org/10.1083/jcb.109.2.891

Garrido-Gomez, T., Ona, K., Kapidzic, M., Gormley, M., Simón, C., Genbacev, O., & Fisher, S. J. (2017). Severe pre-eclampsia is associated with alterations in cytotrophoblasts of the smooth chorion. In *Development (Cambridge)* (Vol. 144, Issue 5, pp. 767–777). https://doi.org/10.1242/dev.146100

Genbacev, O., Larocque, N., Ona, K., Prakobphol, A., Garrido-Gomez, T., Kapidzic, M., Bárcena, A., Gormley, M., & Fisher, S. J. (2016). Integrin α4-positive human trophoblast progenitors: Functional characterization and transcriptional regulation. *Human Reproduction*, *31*(6), 1300–1314. https://doi.org/10.1093/humrep/dew077

Genbačev, O., Vićovac, L., & Larocque, N. (2015). The role of chorionic cytotrophoblasts in the smooth chorion fusion with parietal decidua. In *Placenta* (Vol. 36, Issue 7, pp. 716–722). https://doi.org/10.1016/j.placenta.2015.05.002

Genbacev, O., Zhou, Y., Ludlow, J. W., & Fisher, S. J. (1997). Regulation of human placental development by oxygen tension. *Science*, *277*(5332), 1669–1672. https://doi.org/10.1126/science.277.5332.1669

Haider, S., Meinhardt, G., Saleh, L., Kunihs, V., Gamperl, M., Kaindl, U., Ellinger, A., Burkard, T. R., Fiala, C., Pollheimer, J., Mendjan, S., Latos, P. A., & Knöfler, M. (2018). Self-Renewing Trophoblast Organoids Recapitulate the Developmental Program of the Early Human Placenta. *Stem Cell Reports*, *11*(2), 537–551. https://doi.org/10.1016/j.stemcr.2018.07.004

Hamilton, W. J., & Boyd, J. D. (1960). Development of the human placenta in the first three months of gestation. *Journal of Anatomy*, *94*, 297–328. http://www.ncbi.nlm.nih.gov/pubmed/14399291%0Ahttp://www.pubmedcentral.nih.gov/articlerender.fcgi?artid=PMC1244370

Harris, L. K., Jones, C. J. P., & Aplin, J. D. (2009). Adhesion Molecules in Human Trophoblast - A Review. II. Extravillous Trophoblast. *Placenta*, *30*(4), 299–304. https://doi.org/10.1016/j.placenta.2008.12.003

Harvey, K. F., Zhang, X., & Thomas, D. M. (2013). The Hippo pathway and human cancer. *Nature Reviews Cancer*, *13*(4), 246–257. https://doi.org/10.1038/nrc3458

Karantza, V. (2011). Keratins in health and cancer: More than mere epithelial cell markers. *Oncogene*, *30*(2), 127–138. https://doi.org/10.1038/onc.2010.456

Kliman, H. J., & Feinbergt, R. F. (1990). Human trophoblast-extracellular matrix (ECM) interactions in vitro: ECM thickness modulates morphology and proteolytic activity (invasion/placenta/choriocarcinoma/Matrigel/cyclic AMP). *Proc. Nat. Acad. Sci. USA*, *87*(April), 3057–3061.

Knöfler, M., Haider, S., Saleh, L., Pollheimer, J., Gamage, T. K. J. B., & James, J. (2019). Human placenta and trophoblast development: key molecular mechanisms and model systems. In *Cellular and Molecular Life Sciences*. https://doi.org/10.1007/s00018-019-03104-6

Lala, P. K., & Graham, C. H. (1990). Mechanisms of trophoblast invasiveness and their control: the role of proteases and protease inhibitors. *Cancer and Metastasis Review*, *9*(4), 369–379. https://doi.org/10.1007/BF00049525

Lee, C. Q. E., Gardner, L., Turco, M., Zhao, N., Murray, M. J., Coleman, N., Rossant, J., Hemberger, M., & Moffett, A. (2016). What Is Trophoblast? A Combination of Criteria Define Human First-Trimester Trophoblast. *Stem Cell Reports*, *6*(2), 257–272. https://doi.org/10.1016/j.stemcr.2016.01.006

Liu, X.-Y., Chen, W., Wei, B., Shan, Y.-F., & Wang, C. (2011). IFN-Induced TPR Protein IFIT3 Potentiates Antiviral Signaling by Bridging MAVS and TBK1. *The Journal of Immunology*, *187*(5), 2559–2568. https://doi.org/10.4049/jimmunol.1100963

Liu, Y., Fan, X., Wang, R., Lu, X., Dang, Y. L., Wang, H., Lin, H. Y., Zhu, C., Ge, H., Cross, J. C., & Wang, H. (2018). Single-cell RNA-seq reveals the diversity of

trophoblast subtypes and patterns of differentiation in the human placenta. *Cell Research*. https://doi.org/10.1038/s41422-018-0066-y

Lu, X., Wang, R., Zhu, C., Wang, H., Lin, H. Y., Gu, Y., Cross, J. C., & Wang, H. (2017). Fine-Tuned and Cell-Cycle-Restricted Expression of Fusogenic Protein Syncytin-2 Maintains Functional Placental Syncytia. *Cell Reports*, *21*(5), 1150–1159. https://doi.org/10.1016/j.celrep.2017.10.019

Maxwell, P. H., Dachs, G. U., Gleadle, J. M., Nicholls, L. G., Harris, A. L., Stratford, I. J., Hankinson, O., Pugh, C. W., & Ratcliffe, P. J. (1997). Hypoxia-inducible factor-1 modulates gene expression in solid tumors and influences both angiogenesis and tumor growth. *Proceedings of the National Academy of Sciences of the United States of America*, *94*(15), 8104–8109. https://doi.org/10.1073/pnas.94.15.8104

McGinnis, C. S., Murrow, L. M., & Gartner, Z. J. (2019). DoubletFinder: Doublet Detection in Single-Cell RNA Sequencing Data Using Artificial Nearest Neighbors. *Cell Systems*, *8*(4), 329-337.e4. https://doi.org/10.1016/j.cels.2019.03.003

McGowan, K. M., & Coulombe, P. A. (1998). Onset of keratin 17 expression coincides with the definition of major epithelial lineages during skin development. *Journal of Cell Biology*, *143*(2), 469–486. https://doi.org/10.1083/jcb.143.2.469

McMaster, M. T., Librach, C. L., Zhou, Y., Lim, K. H., Janatpour, M. J., DeMars, R., Kovats, S., Damsky, C., & Fisher, S. J. (1995). Human placental HLA-G expression is restricted to differentiated cytotrophoblasts. *Journal of Immunology (Baltimore, Md. : 1950)*, *154*(8), 3771–3778. http://www.ncbi.nlm.nih.gov/pubmed/7706718

Mi, S. (2000). *Syncytin is a captive retrovirus*. *403*(February), 785–789. www.nature.com

Moll, R., Franke, W. W., Schiller, D. L., Geiger, B., & Krepler, R. (1982). The catalog of human cytokeratins: Patterns of expression in normal epithelia, tumors and cultured cells. *Cell*, *31*(1), 11–24. https://doi.org/10.1016/0092-8674(82)90400-7

Nelson, W. G., & Sun, T. T. (1983). The 50- and 58-kdalton keratin classes as molecular markers for stratified squamous epithelia: Cell culture studies. *Journal of Cell Biology*, *97*(1), 244–251. https://doi.org/10.1083/jcb.97.1.244

Okae, H., Toh, H., Sato, T., Hiura, H., Takahashi, S., Shirane, K., Kabayama, Y., Suyama, M., Sasaki, H., & Arima, T. (2018). Derivation of Human Trophoblast Stem Cells. *Cell Stem Cell*, *22*(1), 50-63.e6. https://doi.org/10.1016/j.stem.2017.11.004

Otun, H. A., Lash, G. E., Innes, B. A., Bulmer, J. N., Naruse, K., Hannon, T., Searle, R. F., & Robson, S. C. (2011). Effect of tumour necrosis factor-α in combination with interferon-γ on first trimester extravillous trophoblast invasion. *Journal of Reproductive Immunology*, *88*(1), 1–11. https://doi.org/10.1016/j.jri.2010.10.003

Parry, S., & Strauss, J. (1998). Premature rupture of the fetal membranes. *The New England Journal of Medicine*, *338*(10), 663–670.

Red-Horse, K., Zhou, Y., Genbacev, O., Prakobphol, A., Foulk, R., McMaster, M., & Fisher, S. J. (2004). Trophoblast differentiation during embryo implantation and

formation of the maternal-fetal interface. *The Journal of Clinical Investigation*, *114*(6), 744–754. https://doi.org/10.1172/JCI22991

Rock, J. R., Gao, X., Xue, Y., Randell, S. H., Kong, Y. Y., & Hogan, B. L. M. (2011). Notch-dependent differentiation of adult airway basal stem cells. *Cell Stem Cell*, *8*(6), 639–648. https://doi.org/10.1016/j.stem.2011.04.003

Rock, J. R., Onaitis, M. W., Rawlins, E. L., Lu, Y., Clark, C. P., Xue, Y., Randell, S. H., & Hogan, B. L. M. (2009). Basal cells as stem cells of the mouse trachea and human airway epithelium. *Proceedings of the National Academy of Sciences of the United States of America*, *106*(31), 12771–12775. https://doi.org/10.1073/pnas.0906850106

Romero, R., Dey, S. K., & Fisher, S. J. (2014). Preterm labor: One syndrome, many causes. *Science*, *345*(6198), 760–765. https://doi.org/10.1126/science.1251816

Rotty, J. D., & Coulombe, P. A. (2012). A wound-induced keratin inhibits Src activity during keratinocyte migration and tissue repair. *Journal of Cell Biology*, *197*(3), 381–389. https://doi.org/10.1083/jcb.201107078

Segre, J. A., Bauer, C., & Fuchs, E. (1999). Klf4 is a transcription factor required for establishing the barrier function of the skin. *Nature Genetics*, *22*(4), 356–360. https://doi.org/10.1038/11926

Spence, J. S., He, R., Hoffmann, H. H., Das, T., Thinon, E., Rice, C. M., Peng, T., Chandran, K., & Hang, H. C. (2019). IFITM3 directly engages and shuttles

incoming virus particles to lysosomes. *Nature Chemical Biology*, *15*(3), 259–268. https://doi.org/10.1038/s41589-018-0213-2

Stuart, T., Butler, A., Hoffman, P., Hafemeister, C., Papalexi, E., Mauck, W. M., Hao, Y., Stoeckius, M., Smibert, P., & Satija, R. (2019). Comprehensive Integration of Single-Cell Data. *Cell*, *177*(7), 1888-1902.e21. https://doi.org/10.1016/j.cell.2019.05.031

Suryawanshi, H., Morozov, P., Straus, A., Sahasrabudhe, N., Max, K. E. A., Garzia, A., Kustagi, M., Tuschl, T., & Williams, Z. (2018). A single-cell survey of the human first-trimester placenta and decidua. *Science Advances*. https://doi.org/10.1126/sciadv.aau4788

Takahashi, K., Yan, B., Yamanishi, K., Imamura, S., & Coulombe, P. A. (1998). The two functional keratin 6 genes of mouse are differentially regulated and evolved independently from their human orthologs. *Genomics*, *53*(2), 170–183. https://doi.org/10.1006/geno.1998.5476

Thurman, J. M., & Holers, V. M. (2006). The Central Role of the Alternative Complement Pathway in Human Disease. *The Journal of Immunology*, *176*(3), 1305–1310. https://doi.org/10.4049/jimmunol.176.3.1305

Tilburgs, T., Crespo, Â. C., Van Der Zwan, A., Rybalov, B., Raj, T., Stranger, B., Gardner, L., Moffett, A., & Strominger, J. L. (2015). Human HLA-G+ extravillous trophoblasts: Immune-activating cells that interact with decidual leukocytes.

Proceedings of the National Academy of Sciences of the United States of America, *112*(23), 7219–7224. https://doi.org/10.1073/pnas.1507977112

Tirosh, I., Izar, B., Prakadan, S. M., Wadsworth, M. H., Treacy, D., Trombetta, J. J., Rotem, A., Rodman, C., Lian, C., Murphy, G., Fallahi-Sichani, M., Dutton-Regester, K., Lin, J. R., Cohen, O., Shah, P., Lu, D., Genshaft, A. S., Hughes, T. K., Ziegler, C. G. K., … Garraway, L. A. (2016). Dissecting the multicellular ecosystem of metastatic melanoma by single-cell RNA-seq. *Science*, *352*(6282), 189–196. https://doi.org/10.1126/science.aad0501

Vento-Tormo, R., Efremova, M., Botting, R. A., Turco, M. Y., Vento-Tormo, M., Meyer, K. B., Park, J. E., Stephenson, E., Polański, K., Goncalves, A., Gardner, L., Holmqvist, S., Henriksson, J., Zou, A., Sharkey, A. M., Millar, B., Innes, B., Wood, L., Wilbrey-Clark, A., … Teichmann, S. A. (2018). Single-cell reconstruction of the early maternal–fetal interface in humans. *Nature*. https://doi.org/10.1038/s41586-018-0698-6

Wang, F., Chen, S., Liu, H. B., Parent, C. A., & Coulombe, P. A. (2018). Keratin 6 regulates collective keratinocyte migration by altering cell–cell and cell–matrix adhesion. *Journal of Cell Biology*, *217*(12), 4314–4330. https://doi.org/10.1083/jcb.201712130

Wong, P., & Coulombe, P. A. (2003). Loss of keratin 6 (K6) proteins reveals a function for intermediate filaments during wound repair. *Journal of Cell Biology*, *163*(2), 327–337. https://doi.org/10.1083/jcb.200305032

Xu, B., Nakhla, S., Makris, A., & Hennessy, A. (2011). TNF-α inhibits trophoblast integration into endothelial cellular networks. *Placenta*, *32*(3), 241–246. https://doi.org/10.1016/j.placenta.2010.12.005

Yabe, S., Alexenko, A. P., Amita, M., Yang, Y., Schust, D. J., Sadovsky, Y., Ezashi, T., & Roberts, R. M. (2016). Comparison of syncytiotrophoblast generated from human embryonic stem cells and from term placentas. *Proceedings of the National Academy of Sciences of the United States of America*, *113*(19), E2598–E2607. https://doi.org/10.1073/pnas.1601630113

Yang, L., Jin, L., Ke, Y., Fan, X., Zhang, T., Zhang, C., Bian, H., & Wang, G. (2018). E3 Ligase Trim21 Ubiquitylates and Stabilizes Keratin 17 to Induce STAT3 Activation in Psoriasis. *Journal of Investigative Dermatology*, *138*(12), 2568–2577. https://doi.org/10.1016/j.jid.2018.05.016

Yeh, I. T., O'Connor, D. M., & Kurman, R. J. (1989). Vacuolated Cytotrophoblast: A subpopulation of trophoblast in the chorion laeve. *Placenta*, *10*(5), 429–438. https://doi.org/10.1016/0143-4004(89)90053-2

Yu, G., Wang, L. G., Han, Y., & He, Q. Y. (2012). ClusterProfiler: An R package for comparing biological themes among gene clusters. *OMICS A Journal of Integrative Biology*, *16*(5), 284–287. https://doi.org/10.1089/omi.2011.0118

Yuan, B., Ohyama, K., Bessho, T., & Toyoda, H. (2006). Contribution of inducible nitric oxide synthase and cyclooxygenase-2 to apoptosis induction in smooth chorion trophoblast cells of human fetal membrane tissues. *Biochemical and Biophysical*

Research Communications, *341*(3), 822–827. https://doi.org/10.1016/j.bbrc.2006.01.042

Yuan, B., Ohyama, K., Bessho, T., Uchide, N., & Toyoda, H. (2008). Imbalance between ROS production and elimination results in apoptosis induction in primary smooth chorion trophoblast cells prepared from human fetal membrane tissues. *Life Sciences*, *82*(11–12), 623–630. https://doi.org/10.1016/j.lfs.2007.12.016

Yuan, B., Ohyama, K., Takeichi, M., & Toyoda, H. (2009). Direct contribution of inducible nitric oxide synthase expression to apoptosis induction in primary smooth chorion trophoblast cells of human fetal membrane tissues. *International Journal of Biochemistry and Cell Biology*, *41*(5), 1062–1069. https://doi.org/10.1016/j.biocel.2008.09.031

Zhou, Y., McMaster, M., Woo, K., Janatpour, M., Perry, J., Karpanen, T., Alitalo, K., Damsky, C., & Fisher, S. J. (2002). Vascular endothelial growth factor ligands and receptors that regulate human cytotrophoblast survival are dysregulated in severe preeclampsia and hemolysis, elevated liver enzymes, and low platelets syndrome. *American Journal of Pathology*, *160*(4), 1405–1423. https://doi.org/10.1016/S0002-9440(10)62567-9

Zhu, J.-Y., Pang, Z.-J., & Yu, Y.-H. (2012). Regulation of trophoblast invasion: the role of matrix metalloproteinases. *Reviews in Obstetrics & Gynecology*, *5*(3–4), e137-43. https://doi.org/10.3909/riog0196

Chapter 4: Conclusions and Future Directions

The projects presented in this thesis provide novel insights into the cellular ontology, identity, behavior, and interactions of mouse and human trophoblasts. In Chapter 2, we established snRNA-seq technology in the mouse placenta to conduct a cellular and molecular census of trophoblasts in the developing placental labyrinth. We performed the first separate transcriptomic analyses of SynTI, SynTII, and S-TGC, which identified regulators of distinct differentiation trajectories for the common progenitor populations of each lineage. In Chapter 3, we applied scRNA-seq to the human placenta to understand differences in the cellular composition and transcriptional programs between the villous chorion and the smooth chorion. We characterized novel smooth chorion-specific CTBs (SC-CTBs) with an epidermal-like transcriptional program that likely protects the fetus from mechanical and pathogenic insults. Additionally, we showed that factors secreted by SC-CTBs restrict EVT invasion. These projects resolve the trophoblast of the developing mouse and human placenta at unprecedented resolution but, as is the case with all profiling studies, these explorations raise myriad questions and future research directions.

What are the developmental origins of the LaTP and LaTP2 populations?

LaTPs give rise to all trophoblasts of the labyrinth (Ueno et al., 2013, Chapter 2). LaTPs are derived from the extraembryonic ectoderm and arise after chorioallantoic fusion at E8.5 (Ueno et al., 2013; Maltepe and Fisher, 2015). However, how LaTP are specified from extraembryonic ectoderm is unknown. Additionally, how LaTP specification is coordinated with chorioallantoic fusion is an open question. Since the LaTP are the

progenitors for the entirety of the gas exchange interface in the mouse placenta, understanding how these cells are specified and maintained is central to understanding proper placental (and subsequently fetal) development. Future single cell profiling experiments spanning E7.5-E9.5 will identify the cell states and molecular changes present during this dynamic process. Incorporation of recently developed CRISPR-based lineage tracers will provide a definitive record of the lineage progression from extraembryonic ectoderm to each terminally differentiated labyrinth population (Chan et al., 2019). Our data demonstrates transcriptional and spatial distinctions between labyrinth progenitor populations, LaTP and LaTP2. They separate by E9.5, but their temporal emergence and the relationship between them, remains unclear. Our work suggests a bias in developmental potency; LaTP are more closely related to SynTII and LaTP2 are more closely related to SynTI and S-TGC. These findings are supported by genetic data. The earliest progenitors are Gcm1+ and Gcm1 is required for SynTII, but deletion of *Gcm1* does not eliminate SynTI and S-TGC (Simmons et al., 2008). These data suggest multiple progenitor populations exist by E8.5. Examination of existing Vcam1 and Itga4 null embryos, in which the allantois fails to fuse with the chorion, may help to identify if fusion is necessary for LaTP specification (Gurtner et al., 1995; Yang et al., 1995). Understanding when this heterogeneity arises and how it is established and maintained is necessary to understand the genesis of the labyrinth.

How are cell fate and spatial organization coordinated in the labyrinth?

Efficient gas and nutrient exchange between maternal and fetal blood requires rigid organization of multiple cell types, each of which arises from the same progenitor pool.

LaTP reside in clusters throughout developing labyrinth. Upon differentiation they organize into the stereotypical trilaminar gas exchange interface. We identified specific signaling pathways associated with differentiation of each lineage, but if and how these signals are spatially directed and/or restricted to ensure cells differentiating along each lineage end up in the correct orientation is not known. Our data suggest that local signaling cues are an important driver of fate specification. In this model, location is determined by proximity to maternal blood or to fetal vasculature through morphogen gradients and cell sorting molecules. However, an alternative hypothesis, the specification of cell fate followed by migration, cannot be ruled out. *In vitro* derivation of SynTII yields migratory cells and our data demonstrate that S-TGC are enriched for genes that regulate this process (Zhu et al., 2017; Figure 2.9 and 2.10), suggesting an analogous function *in vivo*. Defining the interaction between cell fate and location is the forte of spatial transcriptomic technologies (Rao et al., 2021). However, single cell resolution remains a challenge for most image based transcriptional profiling methodologies, though techniques with up to 10μm resolution have been recently developed (Rodriques et al., 2019). The labyrinth presents an even greater challenge as the entire trilaminar interface is mere microns thin.

What is the developmental potency of progenitor CTBs from the VC and SC?

A surprising finding of this thesis was the presence of proliferative progenitor trophoblasts in the SC that are analogous to those of the VC (Figure 3.11 and 3.13). However, these progenitors give rise to different lineages depending on their location (Figure 3.9). Whether the progenitor trophoblasts in each region have the same

developmental potential is not clear. Culturing progenitor trophoblasts from the SC in STB differentiation conditions could help answer this question (Okae et al., 2018; Knöfler et al., 2019). The converse experiment, coaxing VC cells to become SC-CTB, will be much more challenging as it entails determining the culture conditions necessary for producing SC-CTB *in vitro*. Understanding the developmental potency and/or plasticity of these progenitors is important for answering questions concerning the timing and mechanisms of lineage restriction and also for understanding how disease states can influence cell fates.

How do SC-CTBs regulate EVT invasion?

Our data demonstrate that CTBs isolated from the SC secrete soluble factors that restrict the invasion of EVTs isolated from the VC (Figure 3.20d). From careful examination of SC-CTB enriched transcripts and the existing literature, we can hypothesize about the candidates that might mediate this phenomenon (e.g., TNFα, SERPINE1, TIMPs – see Chapter 3 discussion). Immediate next steps include testing the contribution of these molecules in gain of function (using agonists or recombinant proteins) or loss of function assays (using blocking antibodies or small molecule inhibitors). However, secreted factors are likely only one component of how SC-CTB modulate EVT behavior. Frequent SC-CTB and EVT cell-cell interactions occur in the SC (Figure 3.20b). Membrane bound factors that may regulate EVT behavior include ECM modulators, adhesion molecules, and signaling receptors. One intriguing candidate is EphrinB2, which directs VC-derived EVTs to decidual arteries (Red-Horse et al., 2005). However, in the SC, EphrinB2 is expressed by neighboring CTBs,

eliminating this distal migratory signal from the decidua. Identification of additional membrane-bound regulators could be achieved by subjecting SC-CTBs to protein profiling experiments (arrays or relative quantitation mass spectrometry), which has already been done for the analogous cells of the VC (Chen et al., 2021). Finally, overlaying spatial information with transcript expression will provide much needed insight into how both secreted and contact-mediated signals functions in the SC. Either genome wide or targeted spatial transcriptomic methods will help to correlate cell identity with invasive potential, understand how SC-CTB interactions with EVTs changes transcriptional programs, and the cellular composition of the niche surrounding either more or less invasive EVTs.

What is the role of SC-CTBs in placental disease?

The SC is likely to have central roles in both severe pre-eclampsia (sPE) and chorioamnionitis, which often result in either therapeutic induction of labor or preterm labor, respectively. Pre-eclampsia is a heterogenous condition typically presenting with the new and sudden onset of maternal hypertension. This syndrome is accepted as having a placental trophoblast component and a maternal vascular contribution (Redman and Sargent, et al., 2005). Garrido-Gomez et al., demonstrate increased thickening of the SC in sPE as compared to non-infected preterm labor cases that were matched for gestational age. They also identify disease dependent transcriptional changes such as the upregulation of CSH1, a key hormone differentially expressed between VC and SC EVT (Figure 3.16). Together, these data demonstrate expansion of the SC in response to sPE and suggest a potential compensatory adoption of VC-like

characteristics. Decreased EVT invasion and failed remodeling of maternal decidual arteries is a common placental feature of severe pre-eclampsia (Redman and Sargent, et al., 2005). Investigating how invasion and arterial remodeling are regulated across placental regions may provide clues as to how these processes go awry in disease. Future scRNA-seq studies of sPE and non-infected preterm labor cases could identify disease-related alterations in cellular composition and transcriptional profiles.

Chorioamnionitis, an infection of the chorion and amnion, is estimated to be present in one-quarter of preterm labor cases. In this condition, the SC epithelium is infiltrated by large numbers of immune cells that produce cytokines and proinflammatory molecules, which may trigger early parturition (Romero et al., 2015). The molecular effects on the SC epithelium are unknown. Understanding how this influx of immune cells and the signals they generate change the SC epithelial barrier has great translational potential. This information could be used to devise new preventive and treatment strategies aimed at strengthening barrier function.

Future directions for placental biology

The projects presented in this thesis are studies of cell identity and, in the case of SC-CTBs, function in the placenta. Building on these data and recent technological advances, future work could include the manipulation and engineering of cell identity and behavior to explore basic placental biology during normal pregnancy and develop novel therapeutics for disease states that involve the placenta. The preponderance single cell transcriptional profiling has produced a dictionary of cell types and states,

complete with molecular definitions, ontological etymologies, and cell type synonyms and homonyms. These resources hold the promise of designing cells, systems, and tissues through the writing of cell fate and behavior and the printing of tissues and organ niches (Todhunter et al., 2016; Zheng et al., 2020). While this describes myriad future projects in the cell engineering and synthetic biology space, I will briefly touch on two direct applications here.

Culture of placental cells of any species remains a challenge. In mouse, trophoblast stem cells can be maintained in a self-renewing state but differentiation is restricted to specific lineages (Tanaka et al., 1998; Zhu et al., 2017). Differentiation of cultured human trophoblasts has progressed slightly more rapidly as there are now multiple published protocols that are coming into wider usage (Okae et al., 2018). Also, several organoid models have been developed (Turco et al., 2018; Haider et al., 2018). There is ample space for translating expression-based studies into cell culture protocols for the derivation of either heterogenous populations or specific lineages. This will be particularly useful for differentiating STBs *in vitro*, as many protocols yield multinuclear hormone producing cells but lack the polarization, apical microvilli and other mature features of that characterize these highly specialized cells *in vivo*. The methods for culturing human trophoblasts could be applied to other species (Bourdon et al., 2021). Expansion beyond traditional model organisms will benefit evolutionary studies and enhance efforts toward artificial placentation, a topic of great interest for the agriculture industry.

Finally, placental studies often lack functional assessments due to the ethical and practical challenges of *in vivo* manipulation, tissue availability, and *in vitro* culture. Recent successes in direct (*in situ*) *in vivo* CRISPR screening through injection of lentiviral sgRNA into Cas9 expressing mice are likely applicable to tissues beyond the brain and liver (Knouse and Keys, 2021; Jin et al., 2020). While this approach is limited to the mouse and other animal models such as nonhuman primates, it could play a valuable role in validating the functions of candidate regulatory genes identified in expression profiling studies such as those described here. Although more challenging, forward screening for complex phenotypes such as syncytiotrophoblast cell fusion could be achieved using a combination of *in situ* sequencing to identify guide RNAs and imaging-based readouts of cell fate or fusion (Feldman et al., 2019). Another potential method for functional genotype-phenotype screening is through the reprogramming of human induced pluripotent stem cells to trophoblast stem cells, and subsequently, differentiated placental lineages (Liu et al., 2020). Using human fibroblasts or other adult cells as the starting material, reduces ethical concerns and provides an easier to implement platform that is amenable to genome engineering and high throughput screening.

References

Bourdon, G., Cadoret, V., Charpigny, G., Couturier-Tarrade, A., Dalbies-Tran, R., Flores, M. J., Froment, P., Raliou, M., Reynaud, K., Saint-Dizier, M., & Jouneau, A. (2021). Progress and challenges in developing organoids in farm animal species for the study of reproduction and their applications to reproductive biotechnologies. *Veterinary Research*, *52*(1), 1–20. https://doi.org/10.1186/s13567-020-00891-w

Chen, H., Williams, K. E., Kwan, E. Y., Kapidzic, M., Puckett, K. A., Aburajab, R. K., Robinson, J. F., & Fisher, S. J. (2021). Global proteomic analyses of human cytotrophoblast differentiation/invasion. *Development (Cambridge)*, *148*(13), 1–11. https://doi.org/10.1242/DEV.199561

Feldman, D., Singh, A., Schmid-Burgk, J. L., Carlson, R. J., Mezger, A., Garrity, A. J., Zhang, F., & Blainey, P. C. (2019). Optical Pooled Screens in Human Cells. *Cell*, *179*(3), 787-799.e17. https://doi.org/10.1016/j.cell.2019.09.016

Garrido-Gomez, T., Ona, K., Kapidzic, M., Gormley, M., Simón, C., Genbacev, O., & Fisher, S. J. (2017). Severe pre-eclampsia is associated with alterations in cytotrophoblasts of the smooth chorion. *Development (Cambridge)*, *144*(5), 767–777. https://doi.org/10.1242/dev.146100

Gurtner, G. C., Davis, V., Li, H., McCoy, M. J., Sharpe, A., & Cybulsky, M. I. (1995). Targeted disruption of the murine VCAM1 gene: Essential role of VCAM-1 in chorioallantoic fusion and placentation. *Genes and Development*, *9*(1), 1–14. https://doi.org/10.1101/gad.9.1.1

Haider, S., Meinhardt, G., Saleh, L., Kunihs, V., Gamperl, M., Kaindl, U., Ellinger, A., Burkard, T. R., Fiala, C., Pollheimer, J., Mendjan, S., Latos, P. A., & Knöfler, M. (2018). Self-Renewing Trophoblast Organoids Recapitulate the Developmental Program of the Early Human Placenta. *Stem Cell Reports*, *11*(2), 537–551. https://doi.org/10.1016/j.stemcr.2018.07.004

Jin, X., Simmons, S. K., Guo, A., Shetty, A. S., Ko, M., Nguyen, L., Jokhi, V., Robinson, E., Oyler, P., Curry, N., Deangeli, G., Lodato, S., Levin, J. Z., Regev, A., Zhang, F., & Arlotta, P. (2020). In vivo Perturb-Seq reveals neuronal and glial abnormalities associated with autism risk genes. *Science*, *370*(6520). https://doi.org/10.1126/science.aaz6063

Knöfler, M., Haider, S., Saleh, L., Pollheimer, J., Gamage, T. K. J. B., & James, J. (2019). Human placenta and trophoblast development: key molecular mechanisms and model systems. In *Cellular and Molecular Life Sciences*. https://doi.org/10.1007/s00018-019-03104-6

Knouse, K., & Keys, H. (2021). A genome-wide screen in the mouse liver reveals sex-specific and cell non-autonomous regulation of cell fitness. *BioRxiv*, *29*(1), 2–6.

Liu, X., Ouyang, J. F., Rossello, F. J., Tan, J. P., Davidson, K. C., Valdes, D. S., Schröder, J., Sun, Y. B. Y., Chen, J., Knaupp, A. S., Sun, G., Chy, H. S., Huang, Z., Pflueger, J., Firas, J., Tano, V., Buckberry, S., Paynter, J. M., Larcombe, M. R., … Polo, J. M. (2020). Reprogramming roadmap reveals route to human induced

trophoblast stem cells. *Nature*, *586*(7827), 101–107. https://doi.org/10.1038/s41586-020-2734-6

Maltepe, E., & Fisher, S. J. (2015). Placenta: The Forgotten Organ. *Annual Review of Cell and Developmental Biology*, *31*, 523–552. https://doi.org/10.1146/annurev-cellbio-100814-125620

Maltepe, E., & Fisher, S. J. (2015). Placenta: The Forgotten Organ. *Annual Review of Cell and Developmental Biology*. https://doi.org/10.1146/annurev-cellbio-100814-125620

Okae, H., Toh, H., Sato, T., Hiura, H., Takahashi, S., Shirane, K., Kabayama, Y., Suyama, M., Sasaki, H., & Arima, T. (2018). Derivation of Human Trophoblast Stem Cells. *Cell Stem Cell*, *22*(1), 50-63.e6. https://doi.org/10.1016/j.stem.2017.11.004

Rao, A., Barkley, D., França, G. S., & Yanai, I. (2021). Exploring tissue architecture using spatial transcriptomics. *Nature*, *596*(7871), 211–220. https://doi.org/10.1038/s41586-021-03634-9

Red-Horse, K., Kapidzic, M., Zhou, Y., Feng, K. T., Singh, H., & Fisher, S. J. (2005). EPHB4 regulates chemokine-evoked trophoblast responses: A mechanism for incorporating the human placenta into the maternal circulation. *Development*, *132*(18), 4097–4106. https://doi.org/10.1242/dev.01971

Red-Horse, K., Kapidzic, M., Zhou, Y., Feng, K. T., Singh, H., & Fisher, S. J. (2005). EPHB4 regulates chemokine-evoked trophoblast responses: A mechanism for incorporating the human placenta into the maternal circulation. *Development*, *132*(18), 4097–4106. https://doi.org/10.1242/dev.01971

Redman, C. W., & Sargent, I. L. (2005). Latest advances in understanding preeclampsia. *Science*, *308*(5728), 1592–1594. https://doi.org/10.1126/science.1111726

Rodriques, S. G., Stickels, R. R., Goeva, A., Martin, C. A., Murray, E., Vanderburg, C. R., Welch, J., Chen, L. M., Chen, F., & Macosko, E. Z. (2019). Slide-seq: A scalable technology for measuring genome-wide expression at high spatial resolution. *Science*, *363*(6434), 1463–1467. https://doi.org/10.1126/science.aaw1219

Romero, R., Dey, S. K., & Fisher, S. J. (2014). *Preterm labor: One syndrome, many causes*. *345*(6198).

Simmons, D. G., Natale, D. R. C., Begay, V., Hughes, M., Leutz, A., & Cross, J. C. (2008). Early patterning of the chorion leads to the trilaminar trophoblast cell structure in the placental labyrinth. *Development*. https://doi.org/10.1242/dev.020099

Tanaka, S., Kunath, T., Hadjantonakis, A. K., Nagy, A., & Rossant, J. (1998). Promotion to trophoblast stem cell proliferation by FGF4. *Science*, *282*(5396), 2072–2075. https://doi.org/10.1126/science.282.5396.2072

Todhunter, M. E., Weber, R. J., Farlow, J., Jee, N. Y., Cerchiari, A. E., & Gartner, Z. J. (2016). Fabrication of 3-D Reconstituted Organoid Arrays by DNA-Programmed Assembly of Cells (DPAC). *Current Protocols in Chemical Biology*, *8*(3), 147–178. https://doi.org/10.1002/cpch.8

Turco, M. Y., Gardner, L., Kay, R. G., Hamilton, R. S., Prater, M., Hollinshead, M. S., McWhinnie, A., Esposito, L., Fernando, R., Skelton, H., Reimann, F., Gribble, F. M., Sharkey, A., Marsh, S. G. E., O'rahilly, S., Hemberger, M., Burton, G. J., & Moffett, A. (2018). Trophoblast organoids as a model for maternal–fetal interactions during human placentation. *Nature*, *564*(7735), 263–281. https://doi.org/10.1038/s41586-018-0753-3

Ueno, M., Lee, L. K., Chhabra, A., Kim, Y. J., Sasidharan, R., VanHandel, B., Wang, Y., Kamata, M., Kamran, P., Sereti, K. I., Ardehali, R., Jiang, M., & Mikkola, H. K. A. (2013). C-Met-Dependent Multipotent Labyrinth Trophoblast Progenitors Establish Placental Exchange Interface. *Developmental Cell*, *27*(4), 373–386. https://doi.org/10.1016/j.devcel.2013.10.019

Yang, J. T., Rayburn, H., & Hynes, R. O. (1995). <*Yang-Integrinko4.Pdf*>. *560*, 549–560.

Zhang, P., & Abate, A. R. (2020). High-Definition Single-Cell Printing: Cell-by-Cell Fabrication of Biological Structures. *Advanced Materials*, *32*(52). https://doi.org/10.1002/adma.202005346

Zhu, D., Gong, X., Miao, L., Fang, J., & Zhang, J. (2017). Efficient Induction of Syncytiotrophoblast Layer II Cells from Trophoblast Stem Cells by Canonical Wnt Signaling Activation. *Stem Cell Reports*, *9*(6), 2034–2049. https://doi.org/10.1016/j.stemcr.2017.10.014

Zhu, D., Gong, X., Miao, L., Fang, J., & Zhang, J. (2017). Efficient Induction of Syncytiotrophoblast Layer II Cells from Trophoblast Stem Cells by Canonical Wnt Signaling Activation. *Stem Cell Reports*. https://doi.org/10.1016/j.stemcr.2017.10.014

Publishing Agreement

It is the policy of the University to encourage open access and broad distribution of all theses, dissertations, and manuscripts. The Graduate Division will facilitate the distribution of UCSF theses, dissertations, and manuscripts to the UCSF Library for open access and distribution. UCSF will make such theses, dissertations, and manuscripts accessible to the public and will take reasonable steps to preserve these works in perpetuity.

I hereby grant the non-exclusive, perpetual right to The Regents of the University of California to reproduce, publicly display, distribute, preserve, and publish copies of my thesis, dissertation, or manuscript in any form or media, now existing or later derived, including access online for teaching, research, and public service purposes.

DocuSigned by:
Bryan Marsh
786A750335234BF...
Author Signature

4/22/2022
Date